SOLID CONTACT POTENTIOMETRIC SENSORS BASED ON CARBON NANOMATERIALS

Rafael Hernández Malo

ADVERTIMENT. L'accés als continguts d'aquesta tesi doctoral i la seva utilització ha de respectar els drets de la persona autora. Pot ser utilitzada per a consulta o estudi personal, així com en activitats o materials d'investigació i docència en els termes establerts a l'art. 32 del Text Refós de la Llei de Propietat Intel·lectual (RDL 1/1996). Per altres utilitzacions es requereix l'autorització prèvia i expressa de la persona autora. En qualsevol cas, en la utilització dels seus continguts caldrà indicar de forma clara el nom i cognoms de la persona autora i el títol de la tesi doctoral. No s'autoritza la seva reproducció o altres formes d'explotació efectuades amb finalitats de lucre ni la seva comunicació pública des d'un lloc aliè al servei TDX. Tampoc s'autoritza la presentació del seu contingut en una finestra o marc aliè a TDX (framing). Aquesta reserva de drets afecta tant als continguts de la tesi com als seus resums i índexs.

ADVERTENCIA. El acceso a los contenidos de esta tesis doctoral y su utilización debe respetar los derechos de la persona autora. Puede ser utilizada para consulta o estudio personal, así como en actividades o materiales de investigación y docencia en los términos establecidos en el art. 32 del Texto Refundido de la Ley de Propiedad Intelectual (RDL 1/1996). Para otros usos se requiere la autorización previa y expresa de la persona autora. En cualquier caso, en la utilización de sus contenidos se deberá indicar de forma clara el nombre y apellidos de la persona autora y el título de la tesis doctoral. No se autoriza su reproducción u otras formas de explotación efectuadas con fines lucrativos ni su comunicación pública desde un sitio ajeno al servicio TDR. Tampoco se autoriza la presentación de su contenido en una ventana o marco ajeno a TDR (framing). Esta reserva de derechos afecta tanto al contenido de la tesis como a sus resúmenes e índices.

WARNING. Access to the contents of this doctoral thesis and its use must respect the rights of the author. It can be used for reference or private study, as well as research and learning activities or materials in the terms established by the 32nd article of the Spanish Consolidated Copyright Act (RDL 1/1996). Express and previous authorization of the author is required for any other uses. In any case, when using its content, full name of the author and title of the thesis must be clearly indicated. Reproduction or other forms of for profit use or public communication from outside TDX service is not allowed. Presentation of its content in a window or frame external to TDX (framing) is not authorized either. These rights affect both the content of the thesis and its abstracts and indexes.

UNIVERSITAT ROVIRA I VIRGILI
SOLID CONTACT POTENTIOMETRIC SENSORS BASED ON CARBON NANOMATERIALS
Rafael Hernández Malo

UNIVERSITAT ROVIRA I VIRGILI
SOLID CONTACT POTENTIOMETRIC SENSORS BASED ON CARBON NANOMATERIALS
Rafael Hernández Malo

Doctoral thesis

Solid Contact Potentiometric Sensors Based on Carbon Nanomaterials

Report submitted by

Rafael Hernández Malo

To receive the degree of Doctor with the mention of International Doctorate by the Universitat Rovira i Virgili

UNIVERSITAT ROVIRA I VIRGILI

Department of Analytical Chemistry and Organic Chemistry

Tarragona. Spain 2014

UNIVERSITAT ROVIRA I VIRGILI
SOLID CONTACT POTENTIOMETRIC SENSORS BASED ON CARBON NANOMATERIALS
Rafael Hernández Malo

Doctoral thesis

Solid Contact Potentiometric Sensors Based on Carbon Nanomaterials

Supervised by: Dr. Jordi Riu Rusell

UNIVERSITAT ROVIRA I VIRGILI

Department of Analytical Chemistry and Organic Chemistry

Tarragona. Spain 2014

UNIVERSITAT ROVIRA I VIRGILI
SOLID CONTACT POTENTIOMETRIC SENSORS BASED ON CARBON NANOMATERIALS
Rafael Hernández Malo

Doctoral thesis

Solid Contact Potentiometric Sensors Based on Carbon Nanomaterials

Tribunal members:

Prof. Xavier Rius Ferrús.
Department of Analytical Chemistry and Organic Chemistry, Universitat Rovira i Virgili. Tarragona (Spain)

Prof. Wolfgang Maser.
Department of Nanotechnology. Institute of Carbochemistry- Consejo Superior de Investigaciones Científicas (ICB-CSIC). Zaragoza (Spain)

Dr. Maria Goreti Ferreira Sales
Department of Chemical Engineering, Instituto Superior de Engenharia do Porto (ISEP/IPP). Porto (Portugal)

External examiners:

Maître de Conférence Alicia Maroto Sánchez.
UFR Sciences et Techniques. Université de Bretagne Occidentale (UBO). Brest (France)

Assoc. Prof. Tom Petri Mikael Lindfors.
Laboratory of Analytical Chemistry, Process Chemistry Centre, Faculty of Chemical Engineering, Åbo Akademi University. Åbo (Finland)

Department of Analytical Chemistry and Organic Chemistry

Tarragona. Spain 2014

UNIVERSITAT ROVIRA I VIRGILI
SOLID CONTACT POTENTIOMETRIC SENSORS BASED ON CARBON NANOMATERIALS
Rafael Hernández Malo

UNIVERSITAT ROVIRA I VIRGILI
Departament de Química Analítica i Química Orgànica
Campus Sescelades
Marcel·lí Domingo, s/n
43007 Tarragona

Jordi Riu Rusell, Associate Professor of Analytical Chemistry at the Department of Analytical Chemistry and Organic Chemistry at the Universitat Rovira i Virgili,

CERTIFY

That the Doctoral Thesis entitled: 'Solid Contact Potentiometric Sensors Based on Carbon Nanomaterials', submitted by Rafael Hernández Malo to obtain the degree of Doctor by the Universitat Rovira i Virgili, in the Doctorate Program in Nanoscience and Nanotechnology, has been carried out under my supervision, in the Department of Analytical Chemistry and Organic Chemistry at the Universitat Rovira i Virgili. All the results presented in this thesis were obtained in experiments conducted by the above mentioned student, and meets the requirements to qualify for the International Doctorate mention.

Tarragona, September 2014

Dr. Jordi Riu Rusell

UNIVERSITAT ROVIRA I VIRGILI
SOLID CONTACT POTENTIOMETRIC SENSORS BASED ON CARBON NANOMATERIALS
Rafael Hernández Malo

"I have walked that long road to freedom. I have tried not to falter; I have made missteps along the way. But I have discovered the secret that after climbing a great hill, one only finds that there are many more hills to climb. I have taken a moment here to rest, to steal a view of the glorious vista that surrounds me, to look back on the distance I have come. But I can rest only for a moment, for with freedom comes responsibilities, and I dare not linger, for my long walk is not yet ended."

(Nelson Mandela)

UNIVERSITAT ROVIRA I VIRGILI
SOLID CONTACT POTENTIOMETRIC SENSORS BASED ON CARBON NANOMATERIALS
Rafael Hernández Malo

Agradecimientos

Después de un largo y a veces complicado camino, después de zarpar desde la seguridad de un puerto en busca de quién sabe qué, esta travesía llega a su fin. En este viaje, he podido conocer a gente maravillosa y vivir experiencias que nunca hubiera pensado, a crecer en todos los sentidos y en definitiva a forjarme un poco mas como grumete en esta vida.

En primer lugar, quisiera expresar mi gran gratitud al profesor *F. Xavier Rius* por permitirme enrolarme en este barco que ha sido esta tesis doctoral. Por explicarme en qué consistía la investigación aquella tarde en su despacho cuando me acerqué a ver que era aquello de los nanotubos de carbono. Por su increíble calidad tanto profesional como humana. Por permitirme que esto sea una realidad.

Al mismo nivel, al Dr. *Jordi Riu*, capitán de esta nave. No tengo suficientes palabras para agradecer todo lo que has hecho por mí. Por tu enorme paciencia al timón, por tener claro en todo momento el rumbo que debíamos seguir, por tener siempre cargados los cien cañones por banda, viento en popa a toda vela, porque por fin podemos gritar, tierra a al vista!! Mil gracias,

Agradecer especialmente a *Santiago Macho* por toda su ayuda que me ha brindado durante estos años. A *Pancho* y *Pascal* por ofrecerme su visión científica, y por vuestro afán por descrubrir. Mi más sincera gratitud para *Alicia Maroto*, por tu inocencia siempre tan entrañable y a *Tom Lindfors*, por tus conversaciones científicas con un té entre las manos mientras fuera nevaba. gracias por revisar esta tesis, me habéis ayudado muchísimo.

A mis compañeros durante estos años que ha durado mi andadura. A *Gustavo* por tener siempre una sonrisa en la cara y ayudarme en las visicitudes de la microbiología. A *Enrique*, porque he pasado muy agradables momentos chamo, gracias por esos ratos codo con codo en el laboratorio. A *Vane*, por que siempre has estado ahí en los momentos buenos y en los malos, gracias por tu apoyo. A *Idoia*, por ser la alegría de la huerta en todo momento y alegrarnos los días. A *Xavi*, por tu capacidad de comprender y ayudar, por esas conversaciones

científicas delante del rotavapor esperando a tener una membrana. A *Giselle*, *Laura*, *Zayda*, *Cris F*. *Joe* por compartir este camino conmigo y en especial a *Cris B*. por todo lo que vivimos juntos, por nuestros proyectos fallidos, por todo tu apoyo incondicional y sobretodo por estar a mi lado en los malos momentos, gracias por estar siempre ahí. Gracias.

A los técnicos del *servei de recursos científics i tècnics* de la URV, *Mercè Moncusí* y *Mariana Stefanova* por su inestimable ayuda a la hora de enfrentarme a los equipos de microscopía, a la técnico de laboratorio *Teresa Codera*, siempre dispuesta a ayudarme con los problemas logísticos que iban surgiendo y *Avelina*, *Olga* y *Eulalia* por vuestra ayuda 'burocrática'. Gracias a todos por tener siempre el barco preparado para cualquier contratiempo.

Al profesor *Wolfgang Maser* y todo su equipo, por que sin ellos no hubiéramos podido realizar esta tesis. Por mostrarse en todo momento receptivo a las ideas que teníamos, aun cuando fueran difíciles de realizar y por llevar a cabo tan buen trabajo con nuestros electrodos.

Quisiera agradecer al profesor *Ari Ivaska* por permitirme realizar una inolvidable estancia en el Departamento de Ingenieria Química de la Åbo Akademi University, así como al profesor *Johan Bobacka*, por aportarme parte de su conocimiento científico.

No podría olvidar a los integrantes del grupo del laboratorio de química analítica de la Åbo Akademi University, muy en especial a *Anna* y *Lotta Österholm*, quienes me ayudaron a integrarme en este increíble país, gracias por permitirme vivir una experiencia inolvidable que siempre llevaré muy cerca de mi corazón. A *Justyna Kupis*, por sus inolvidables charlas e inestimable compañía, siempre te las agradeceré y tendré presentes. A toda la gente que compartió conmigo momentos que nunca olvidaré. A *Jiayi*, *Marcin*, *Tingting*, *Michal*, *Grzegorz*, *Ning*, *Ulriika* y *Maija*. Siempre os tendré en una parte de mi corazón a todos.

No quisiera dejarme a nadie, gracias a todos los que habéis formado parte de este proyecto. En especial a aquellas personas que han estado más en lo personal que el lo científico porque sin ellas, el camino habría sido más duro.

A todos mis compañeros del GELSTO, por transmitirme unos valores que siempre me acompañarán y por todas esas tardes de juegos y diversión entre peques, en las que aprendíamos enseñando y por los campamentos de verano disfrutando de la naturaleza entre otras muchas cosas.

A mis compañeros durante la licenciatura, porque pasé muy buenos momentos a vuestro lado de los que todavía tengo un bonito recuerdo que siempre tenré conmigo.

A los amigos del barrio, mis amigos de toda la vida. A *Merche*, *Carmelo*, *Guada*, *Jose*, *Sergio*, *Tere* y al recién llegado *Quim*, porque lleváis acompañándome en este camino mucho tiempo, por vuestro apoyo incondicional y ayudarme en los tropiezos que ha habido durante el trayecto. Por todas las vivencias que hemos compartido y seguiremos comprrtiendo por todo el mundo. Os quiero muchísimo.

A mis amigos de ese lugar de la Mancha de cuyo nombre no quiero acordarme (aunque lo lleve dentro de mi corazón en todo momento), *Hector*, *Luis Juan*, *Victor e Iván* y especialmente a *Ruth* y *David* por su increíble calidad como personas, porque sé que siempre estaréis allí donde os necesite. Por esos ratos a la orilla del mar y por todos los que vendrán.

A *Juanjo*, porque hemos pasado unos momentos inceibles juntos, compartido experiencias que siempre tendré presente, por las risas y de vez en cuando por las lágrimas, por los viajes a Zaragoza, por las fiestas de Tordesilos, por esas llamadas en las que no entiendo nada pero que me hacen saber que estás ahí. Porque una amistad así es un verdadero tesoro.

A toda mi familia, a mis tíos y primos porque han sabido crear un entorno en el que hemos crecido con unas convicciones y unos valores inmejorables. Por todas las risas que hemos compartido y por todas las que vendrán, os quiero mucho

A mis abuelos *Ramón* y *Emiliana*, porque estoy orgulloso de tener unos abuelos como vosotros, porque nos lo habéis dado todo, porque sin vosotros todo hubiera sido muy difícil. Sé que estaréis contentos el día que me veáis presentar esto. A mi abuela *Brigida* y mi abuelo *Laureano*, porque sé que allá donde estéis, estaréis orgullosos de que haya llegado a este punto.

A mis padres *Rafael* y *Pilar*, porque me habéis ayudado a crecer en el mejor de los ambientes, por vuestra paciencia, cariño y amor incondicional. Por estar en cada momento importante de mi vida, por preocuparos por mi tanto. Todo lo que soy y que veis, os lo debo a vosotros. Gracias, gracias, gracias. Os quiero muchísimo.

A mi hermana *Pily*. Gracias por compartir tu vida conmigo, porque aunque te haga rabiar de vez en cuando, eres de las personas más importantes en mi vida. Por estar siempre que he necesitado de tu ayuda y comprenderme en todo momento. Te quiero mucho gordi.

A *Lucía* por ser dueña de una parcela de mi corazón muy grande y compartir el resto que queda de él, con todas las personas que he ido agradeciendo anteriormente. Por estar a mi lado y quererme tanto como yo la quiero a ella. Porque sé que no ha sido fácil este camino, por ayudarme a levantarme cuando me he caído y por apoyarme siempre que lo he necesitado. Te quiero.

To my family, my friends and my love

UNIVERSITAT ROVIRA I VIRGILI
SOLID CONTACT POTENTIOMETRIC SENSORS BASED ON CARBON NANOMATERIALS
Rafael Hernández Malo

Table of contents

Chapter 3. Experimental part / 45

Resumen

El principal objetivo de esta tesis es desarrollar electrodos potenciométricos de estado sólido basados en una capa transductora formada por materiales nanoestructurados de carbono como los nanotubos de carbono de capa simple (SWCNTs) y grafeno quimicamente modificado.

Los electrodos potenciométricos pertenecen a una de las clases de sensores electroquímicos más interesantes. Son capaces de detectar con fiabilidad, de forma sencilla y en pocos segundos gran cantidad de iones, así como algunos gases, pequeñas moléculas orgánicas y hasta pequeñas formas de vida como bacterias. Su fácil utilización junto a la posibilidad de miniaturización, bajo consumo energético y su reducido coste hacen de este tipo de sensores unos candidatos idóneos para producir en masa dispositivos portátiles con una gran variedad de analitos a determinar

La investigación en el campo de los materiales nanoestructurados de carbono se ha incrementado considerablemente en las dos últimas décadas con la introducción de los nanotubos de carbono (CNT) y recientemente del grafeno. Aprovechando estos avances, esta tesis pretende aportar al conocimiento científico la utilización de nanotubos de carbono en la construcción de sensores potenciométricos para la detección de iones en muestras reales complejas y la inserción de materiales basados en grafeno en sensores potenciométricos para la detección de bacterias.

Esta tesis está estructurada en 7 capítulos.

Capítulo I. Introducción y objetivos. Este capítulo ofrece una introducción a los electrodos potenciométricos de estado sólido, desde sus inicios hasta la actualidad, así como una breve introducción a la tesis y sus objetivos.

Capítulo II. Principios. En este capítulo se describen los aspectos teóricos necesarios para comprender mejor la tesis y situarse en el contexto de los sensores potenciométricos. Se profundiza en las bases de los electrodos selectivos de iones (ISEs) y los aptasensores, en los componentes de éstos, así como su mecanismo de detección.

Capítulo III. Parte experimental. En este capítulo se describen los métodos y procedimientos experimentales utilizados a lo largo de la tesis para obtener los resultados que se proporcionan y discuten en los capítulos siguientes

Capítulo IV. Electrodos selectivos de iones basados en nanotubos de carbono. Aplicación en muestras reales. Este capítulo explica la preparación de un electrodo selectivo de iones, utilizando SWCNTs como elemento transductor, para la detección de calcio en muestras reales complejas como la savia vegetal. Los resultados indican una muy buena sensibilidad y estabilidad del sensor con límites de detección bajos, capaces de detectar calcio a niveles muy inferiores a los encontrados en la savia, con lo que presenta un primer paso para su utilización en la industria agrícola en dispositivos miniaturizados para detección de analitos de interés *in situ* y de forma rápida.

Capítulo V. Electrodos selectivos de iones basados en grafeno químicamente modificado. La introducción del grafeno como material transductor en electrodos selectivos de iones (ISEs) es un campo que no ha sido extensamente desarrollado. El grafeno, material de recién descubrimiento y por el que Andre Geim y Konstantin Novoselov han obtenido el premio Nobel en física de 2010, posee unas notables propiedades que lo hacen un excelente candidato como material transductor en ISEs. Con la publicación del artículo "Reduced Graphene Oxide Films as Solid Transducers in Potentiometric All-Solid-State Ion-Selective Electrodes", se ha comprobado en este tipo de electrodos una mejora en la estabilidad de la respuesta respecto al sensor estudiado en el artículo previo basado en SWCNTs.

Capítulo VI. Aptasensores basados en grafeno químicamente modificado. Este último capítulo experimental se centra en el estudio de la aplicación del óxido de grafeno (GO) y del óxido de grafeno reducido (RGO) en la detección de bacterias basándonos en aptámeros específicos para la detección de *Stahylococcus aureus*. Los excelentes resultados muestran límites de detección de tan solo una unidad formadora de colonias (CFU) de forma selectiva, haciendo posible la detección de la presencia de la bacteria en pocos segundos. Además, se lleva a cabo una comparación entre dos tipos diferentes de unión del aptámero a la capa transductora razonando las ventajas y desventajas de cada una. Esta investigación podría suponer un gran avance en la detección de agentes patógenos y una considerable reducción de costes en este campo.

Capítulo VII. Conclusiones generales. Finalmente se aportan en este apartado las conclusiones generales de la tesis y se ofrece una visión del futuro que los materiales nanoestructurados de carbono pueden ofrecer dentro del campo de la potenciometría.

UNIVERSITAT ROVIRA I VIRGILI
SOLID CONTACT POTENTIOMETRIC SENSORS BASED ON CARBON NANOMATERIALS
Rafael Hernández Malo

Summary

The main objective of this thesis is to develop solid-state potentiometric electrodes based on a transducer layer formed by nanostructured carbon materials such as carbon nanotubes single layer (SWCNTs) and chemically modified graphene.

The potentiometric electrodes belong to a very interesting class of electrochemical sensors. They are able to detect reliably, easily and in a few seconds large amount of ions, as well as certain gases, small organic molecules and small life forms such as bacteria. Its ease of use, with the possibility of miniaturization, low power consumption and low cost make this type of sensors a suitable candidates to mass produce portable devices with a variety of analytes to be determined.

Research in the field of nanostructured carbon materials has increased considerably in the past two decades with the introduction of carbon nanotubes (CNT) and recently the graphene. Building on these advances, this thesis seeks to contribute to scientific knowledge the use of carbon nanotubes in the construction of potentiometric sensors for the detection of ions in real complex samples and the introduction of graphene based on potentiometric detection of bacteria sensor materials.

This thesis is structured in 7 chapters.

Chapter I. Introduction and objectives. This chapter provides an introduction to solid-state potentiometric electrodes, from its beginnings to the present, as well as a brief introduction to the thesis and its objectives.

Chapter II. The principles. Theoretical aspects needed to better understand the thesis and placed in the context of potentiometric sensors are described in this chapter. It delves into the basics of ion-selective electrodes (ISEs) and aptasensores in these components, as well as its detection mechanism.

Chapter III. Experimental part. Experimental methods and procedures used throughout the thesis are described to obtain the results that are provided in this chapter and discussed in the following chapters

Chapter IV. Carbon nanotubes-based ion-selective electrodes. Application to real samples. This chapter explains the preparation of an ion selective electrode using SWCNTs as transducer for the detection of calcium in real complex samples such as plant sap. The results indicate a very good sensitivity and stability of the sensor with low limits of detection, which can detect calcium at much lower levels than those found in the sap, which presents a first step for use in agricultural industry in miniaturized devices for detection of analytes of interest in situ and quickly .

Chapter V. Chemically modified graphene-based ion-selective electrodes. The introduction of the transducer material chemically modified graphene as ion-selective electrodes (ISEs) is a field that has not been extensively developed. Graphene, discovery and new material by Andre Geim and Konstantin Novoselov were awarded the Nobel Prize in Physics 2010, has some remarkable properties that make it an excellent candidate as a transducer material ISEs. With the publication of the article "Reduced Graphene Oxide Films as Solid Potentiometric Transducers in All- Solid - State Ion -Selective Electrodes", have been found in this type of electrodes improved stability compared to the response studied in the previous paper sensor based on SWCNTs.

Chapter VI. Chemically modified graphene-based aptasensors. This final experimental chapter focuses on the study of the application of graphene oxide (GO) and reduced graphene oxide (RGO) in the detection of bacteria based on specific aptamers for detecting *Stahylococcus aureus*. The excellent results show detection limits of only one colony forming unit (CFU) for selectively enabling the detection of the presence of bacteria in a few seconds. It is slso carried out a comparison between two different types of binding of the aptamer to the transducer layer reasoning the advantages and disadvantages of each. This research could lead to a breakthrough in the detection of pathogens and a significant cost reduction in this area.

Chapter VII. General conclusions. Finally in this section provide the general conclusions of the thesis and a vision of the future that nanostructured carbon materials can offer in the field of potentiometry is offered.

UNIVERSITAT ROVIRA I VIRGILI
SOLID CONTACT POTENTIOMETRIC SENSORS BASED ON CARBON NANOMATERIALS
Rafael Hernández Malo

UNIVERSITAT ROVIRA I VIRGILI
SOLID CONTACT POTENTIOMETRIC SENSORS BASED ON CARBON NANOMATERIALS
Rafael Hernández Malo

1.1. State of the art

Daily life, industrial processes, science and technology are characterized by the need to generate and measure information accurately and reliably. This gathering of information is carried out using chemical sensors. A chemical sensor is an instrument that allows us to transform chemical information (composition, presence of a particular element or ion, concentration, chemical activity, etc.) into an analytically useful signal. The IUPAC definition of a chemical sensor is a "*self-contained integrated device, which is capable of providing specific quantitative or semi-quantitative chemical information using a recognition element which is retained in direct spatial contact with a transduction element"* **[1]**.

Chemical sensors are composed of two basic functional units: the receptor part (which transforms chemical information into a measurable form of energy via a chemical recognition event) and the transducer part (which transforms this chemical recognition event into a useful analytical signal). Chemical sensors may be classified, for instance, according to the operating principle of the transducer, into optical, electrochemical, electrical, mass sensitive, magnetic and thermometric devices **[2,3]**. A similar definition applies to biochemical sensors, where the target would be a biochemical analyte such as proteins, microorganisms, etc.

Electrochemical sensors are the oldest and largest group of chemical sensors. They are devices that extract information from the measurement of certain electrical parameters deriving from analyte-sensor interaction. Depending on the electrical parameter measured, electrochemical sensors can be classified as amperometric sensors (measurement of current), conductometric sensors (measurement of conductivity) and potentiometric sensors (measurement of voltage).

Potentiometry measures voltage under conditions of no current flow to determine the analytical quantity of certain components in the analyte solution. The first analytical use of potentiometry was in Nernst's laboratory after he had published his well-known equation that relates ion activity and electrode potential **[4]**.
In 1906, Cremer determined that the electric potential established between the two sides of a glass membrane immersed in a fluid is proportional to the hydrogen ion concentration **[5]**, but it was not until 1909 that Haber and Klemensiewicz developed

the first pH electrode **[6]**. Although Haber and Klemensiewicz were the first to develop an electrode for the selective detection of hydrogen ions, pH determination was also improved and made more popular by Sorensen in the same year **[7]**. In the 1930s glass electrodes were incorporated into pHmeters, and this kind of electrode is still the most used pH electrode today. The evolution of potentiometry then saw a significant increase in the construction of ion-selective electrodes (ISEs) in one of the most interesting chapters of electrochemistry.

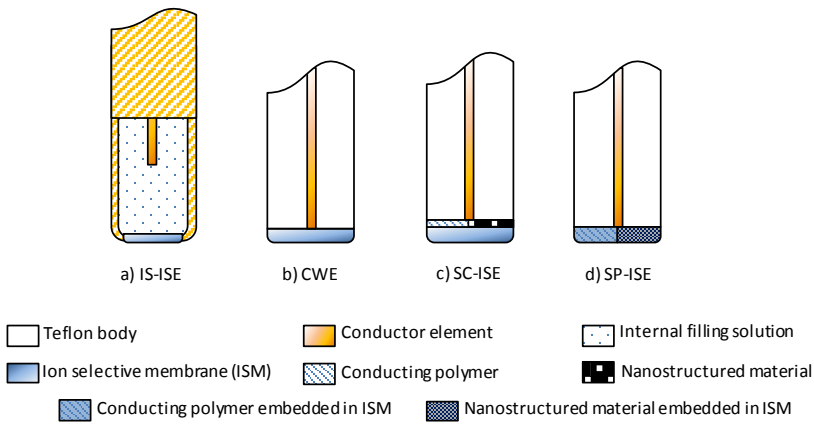

Figure 1.1. Evolution of ion-selective electrode manufacture. a) Internal solution ion-selective electrode. b) Coated wire electrode. c) Solid contact ion-selective electrode. d) single-piece ion-selective electrode. *Note*: Figure 1.1.c and 1.1.d represent two different configurations depending on the material used (conducting polymers or nanostructured materials).

Potentiometric electrodes developed slowly but surely over the decades subsequent to their discovery, but it was not until the 1960s that some important theoretical work by Nikolskii **[8]** and Eismann **[9]** describing modern ISE theory and several ion-selective membranes (ISM) was incorporated. ISM is the sensing part of ISEs. Figure 1.1 shows the evolution of ion-selective electrode manufacture from the use of an internal solution to the use of transducer material included in the membrane

One of the milestones in the development of ISM concerns the discovery of the specific and selective electrochemical behaviour of certain antibiotics towards selected ions **[10]** and the accidental discovery of crown ethers by Pedersen **[11]**. Their discovery and the study of their properties paved the way for a new chemistry discipline:

supramolecular chemistry. The founding fathers of supramolecular chemistry, Pedersen and two other researchers, Lehn **[12]** and Cram **[13]**, won the Nobel Prize for Chemistry in 1987. The introduction of host-guest chemistry in ISM led to the first liquid ion-exchanger membrane being constructed by Ross **[14]**, probably the greatest breakthrough in the development of ISEs. Soon after this, poly(vinyl chloride) (PVC)-based matrices were also incorporated **[15,16]** as an inert support for ISEs.

In 1970 Moody et al. developed a practical procedure for constructing liquid membrane ISEs based on plasticized PVC **[17]**, and PVC is still today the most widely used matrix in ISE membranes. However, two new findings led to the investigation of new free-plasticizer matrices: the alteration of ISE performance parameters due to the uptake of water from the sample **[18]** and the release of plasticizers to the sample, capable of producing inflammation in *in vivo* measurements **[19,20]**. The most common free-plasticizer matrices used as an alternative to PVC matrices were based on poly(acrylates) and poly(methacrylates) **[21,22]** and silicon rubber **[23]**.

Before then, ISEs consisted of a glass body in which a silver/silver chloride wire was dipped into an internal solution (Figure 1.1.a). These electrodes, known as conventional ISEs or internal solution ion-selective electrodes (IS-ISEs), are still used but have a number of drawbacks that limit their performance. IS-ISEs can only be used in a vertical position to ensure contact between the internal solution and the redox couple of the internal wire for converting ionic current to electronic current. The other big drawback is that having a liquid phase within a glass body limits miniaturization. Removing this internal solution and substituting it with a solid internal contact seemed the best option for improving the electrodes' characteristics.

In 1971 Cattrall and Freiser constructed a coated wire electrode (CWE) by simply immersing a metal wire in a PVC membrane **[24]**. However, this new type of electrode still has its drawbacks (Figure 1.1.b). ISM permeability to O_2 and water causes the creation of a half-cell at the interface between the actual membrane and the conductor, causing drifts in measurements due to their low capacitance **[25]**. The interface between the ISM and the metal wire lacked a thermodynamically reversible equilibrium for the ion-to-electron transduction process **[26]**. Looking at these drawbacks, in 1985 Nikolskii described the three conditions necessary for obtaining a stable, reproducible potential response in solid contact electrodes:

- Having a reversible, stable equilibrium in ion-to-electron transduction.
- Having a high exchange current at equilibrium so that the interface does not get polarized by the EMF measurement.
- Having no side reactions apart from the main electrode reaction.

Solid contact ion-selective electrodes (SC-ISEs) consist basically of a selective membrane attached to a transducer element and an electrical conductor jacketed in an inert body so as to avoid parasitic noise (Figure 1.1.c). Conducting polymers (CP) seemed to be a promising solution for the drawbacks in CWEs mentioned above. The ability of conducting polymers to have ion transport-coupled redox reactions **[27]** makes them especially suited to eliminating CWE problems due to their electronic and ionic conductivity. In 1992 a group including Ivaska and Lewenstam **[28]** introduced electroactive polymers between the metal conductor and the ISM of a typical CWE. This procedure has a stabilizing effect on the electrode potential. They used several polymers including electroactive poly(3-octylthiophene) (POT) **[29]**, polyaniline (PANI) **[30]**, polypyrrole (PPy) **[31]** and poly (3,4-ethylenedioxithiophene) (PEDOT) **[32]**.

Another advantage is that CPs can be used in both the sensor part and the transducer part since they have both properties. Alternatively, they can be used with the ISM, thereby taking advantage of the CWE's simplicity of manufacture and the stability of the SC-ISE's electrode potential. This type of electrode (Figure 1.1.d), made in one piece and known as the single-piece ion-selective electrode (SP-ISE), was introduced in 1995 by Bobacka et al **[27]**.

Great advances in the field of new materials have led to the nanotechnology revolution we are undergoing today. The use of nanostructured materials in ion-selective electrodes has solved the problems suffered by CPs involving side reactions with interfering redox species and also high sensitivity to CO_2 and O_2 **[33]**.

ISEs based on nanostructured carbon materials were first used by the Rius group in 2008 **[34]**. Carbon nanotubes (CNTs), discovered in 1991 by Iijima **[35]**, have excellent properties that make them suitable as transducer elements, avoiding the problems previously associated with conducting polymers.

The introduction of CNTs into the ISM matrix provided a much faster, reproducible way to develop the electrodes in one step **[36-38]**. A similar strategy has led to the construction of potentiometric similar sensing devices, but for the detection of biomolecules. Ampurdanés et al. developed an ISE for the rapid detection of choline **[39],** while Zelada et al. developed a potentiometric aptasensor for the rapid detection of living bacteria using selective aptamers anchored to carbon nanotubes **[40]** in ISM-free potentiometric biosensors.

As will be shown throughout this thesis, nanostructured carbon materials can be integrated into sensors for the potentiometric detection of analytes even in real complex samples, working easily, rapidly and cheaply with a wide range of analytes from small ions to bacteria. The versatility of these materials and their excellent properties make them ideal for avoiding the various drawbacks mentioned above.

1.2. Objectives

The main objective of this doctoral thesis is to develop and characterize solid contact electrodes (SCE) using different carbon nanomaterials such as carbon nanotubes (CNTs) and chemically modified graphenes as transducer layers.

This general objective can be broken down into a number of specific objectives:

- To prove that an ion-selective electrode (ISE) based on carbon nanotubes as a transducer layer can be used in real complex samples. Vegetal sap has been chosen as a proof-of-concept.
- To prove that chemically modified graphene can successfully be used as an ion-to-electron transducer material with improved performance characteristics over other nanostructured materials in ion-selective electrodes.
- To study the transduction mechanism in solid contact electrodes based on reduced graphene oxide.
- To build a potentiometric biosensor to detect bacteria based on the attachment of aptamers to chemically modified graphene. *Staphylococcus aureus* has been chosen as a model target as a proof-of-concept.

1.3. References

[1] Thevenot, D. R.; Toth, K.; Durst, R. A.; Wilson, G. S., Electrochemical biosensors: Recommended definitions and classification - (Technical Report). *Pure and Applied Chemistry* **1999,** *71*, 2333-2348.

[2] Recomendations for nomenclature of ion-selective electrodes. *Pure Applied Chemistry* **1975,** *48*, 127-132.

[3] Janata, J., Chemical Sensors. *Analytical Chemistry* **1992,** *64*, 196-219.

[4] Nernst, W., *Die elektromotorische Wirksamkeit der Ionen*. s.n.: 1889.

[5] Cremer, M., The cause of the electromotor properties of tissue, and a contribution to the science of polyphasic electrolytes. *Zeitschrift Fur Biologie* **1906,** *29*, 562-608.

[6] Haber, F.; Klemensiewicz, Z., Concerning electrical phase boundary forces. *Zeitschrift Fur Physikalische Chemie-Stochiometrie Und Verwandtschaftslehre* **1909,** *67*, 385-431.

[7] Sorensen, S. P. L., Enzyme studies - Note II - The measurement and the significance of hydrogenic concentrate in enzymatic processes. *Biochemische Zeitschrift* **1909,** *21*, 131-304.

[8] Nikolskii, B. P.; Shults, M. M., Some aspects of glass electrode theory. *Zhurnal Fizicheskoi Khimii* **1962,** *36*, 1327-1330.

[9] Eisenman, G.; Rudin, D. O.; Casby, J. U., Glass electrode for measuring sodium ion. *Science* **1957,** *126*, 831-834.

[10] Stefanac, Z.; Simon, W., Ion specific electrochemical behaviour of macrotetrolides in membranes. *Microchemical Journal* **1967,** *12*, 125-132

[11] Pedersen, C. J., Cyclic polyethers and their complexes with metal salts. *Journal of the American Chemical Society* **1967,** *89*, 2495-2496.

[12] Lehn, J. M.; Sauvage, J. P., Cation and cavity selectivities of alkali and alkaline earth cryptates. *Journal of the Chemical Society D-Chemical Communications* **1971,** 440-441.

[13] Cram, D. J.; Cram, J. M., Host-guest chemistry. *Science* **1974,** *183*, 803-809.

[14] Ross, J. W., Calcium-selective electrode with liquid ion exchanger. *Science* **1967,** *156*, 1378-1379.

[15] Bloch, R.; Shatkay, A.; Saroff, H. A., Fabrication and evaluation of membranes as specific electrodes for calcium ions. *Biophysical Journal* **1967,** *7*, 865-877.

[16] Shatkay, A., Ion specific membranes as electrodes in determination of activity of calcium. *Analytical Chemistry* **1967,** *39*, 1056-1065.

[17] Moody, G. J.; Oke, R. B.; Thomas, J. D. R., Calcium-Sensitive Electrode Based on a Liquid Ion Exchanger in a Poly(Vinyl Chloride) Matrix. *Analyst* **1970**, 95, 910-918.

[18] Lindfors, T.; Sundfors, F.; Hofler, L.; Gyurcsanyi, R. E., The Water Uptake of Plasticized Poly(vinyl chloride) Solid-Contact Calcium-Selective Electrodes. *Electroanalysis* **2011**, 23, 2156-2163.

[19] Lindner, E.; Cosofret, V. V.; Ufer, S.; Johnson, T. A.; Ash, R. B.; Nagle, H. T.; Neuman, M. R.; Buck, R. P., In-vivo and in-vitro testing of microelectronically fabricated planar sensors designed for applications in cardiology. *Fresenius Journal of Analytical Chemistry* **1993,** 346, 584-588.

[20] Lindner, E.; Cosofret, V. V.; Ufer, S.; Buck, R. P.; Kao, W. J.; Neuman, M. R.; Anderson, J. M., Ion-selective membranes with low plasticizer content - Electroanaytical characterization and biocompatibility studies. *Journal of Biomedical Materials Research* **1994,** 28, 591-601.

[21] Mascini, M.; Pallozzi, F., Selectivity of neutral carrier-PVC membrane electrodes. *Analytica Chimica Acta* **1974,** 73, 375-382.

[22] Heng, L. Y.; Hall, E. A. H., Taking the plasticizer out of methacrylic-acrylic membranes for K+-selective electrodes. *Electroanalysis* **2000**, 12, 187-193.

[23] Fiedler, U.; Ruzicka, J., Selectrode-Universal Ion-selective electrode. 7. Valinomycin-based potassium electrode with nonporous polymer membrane and solid-state inner reference system. *Analytica Chimica Acta* **1973**, 67, 179-193.

[24] Cattrall, R. W.; Freiser, H., Coated Wire Ion Selective Electrodes. *Analytical Chemistry* **1971**, 43, 1905-1906.

[25] Hulanicki, A.; Trojanowicz, M., Calcium-Selective Electrodes with PVC Membranes and Solid Internal Contacts. *Analytica Chimica Acta* **1976,** 87, 411-417.

[26] Cattrall, R. W.; Drew, D. M.; Hamilton, I. C., Some alhylphosphoric acid-esters for use in coated-wire calcium-selective electrodes. 1. Response characteristics. *Analytica Chimica Acta* **1975,** 76, 269-277.

[27] Bobacka, J.; Lindfors, T.; McCarrick, M.; Ivaska, A.; Lewenstam, A., Single Piece All-Solid-State Ion Selective Electrode. *Analytical Chemistry* **1995,** 67, 3819-3823.

[28] Cadogan, A.; Gao, Z. Q.; Lewenstam, A.; Ivaska, A.; Diamond, D., All-Solid-State Sodium-Selective Electrode Based on a Calixarene Ionophore in a Poly(Vinyl Chloride) membrane with a Polypyrrole Solid Contact. *Analytical Chemistry* **1992,** 64, 2496-2501.

[29] Bobacka, J.; McCarrick, M.; Lewenstam, A.; Ivaska, A., All-solid-state poly(vynil chloride) membrane ion-selective electrodes with poly(3-octylthiophene) solid internal contact. *Analyst* **1994,** 119, 1985-1991.

[30] Han, W. S.; Park, M. Y.; Chung, K. C.; Cho, D. H.; Hong, T. K., All solid state hydrogen ion selective electrode based on a tribenzylamine neutral carrier in a poly(vinyl chloride) membrane with a poly(aniline) solid contact. *Electroanalysis* **2001,** 13, 955-959.

[31] Michalska, A.; Hulanicki, A.; Lewenstam, A., All-solid-state hydrogen ion-selective electrode based on a conducting poly(pyrrole) solid contact. *Analyst* **1994,** 119, 2417-2420.

[32] Vazquez, M.; Bobacka, J.; Ivaska, A.; Lewenstam, A., Influence of oxygen and carbon dioxide on the electrochemical stability of poly(3,4-ethylenedioxythiophene) used as ion-to-electron transducer in all-solid-state ion-selective electrodes. *Sensors and Actuators B-Chemical* **2002,** 82, 7-13.

[33] Bobacka, J.; Ivaska, A.; Lewenstam, A., Potentiometric ion sensors. *Chemical Reviews* **2008,** 108, 329-351.

[34] Crespo, G. A.; Macho, S.; Xavier Rius, F., Ion-selective electrodes using carbon nanotubes as ion-to-electron transducers. *Analytical Chemistry* **2008,** 80, 1316-1322.

[35] Iijima, S., Helical Microtubules of Graphitic Carbon. *Nature* **1991,** 354, 56-58.

[36] Zhu, J.; Qin, Y.; Zhang, Y., Preparation of all solid-state potentiometric ion sensors with polymer-CNT composites. *Electrochemistry Communications* **2009**, 11, 1684-1687.

[37] Zhu, J.; Li, X.; Qin, Y.; Zhang, Y., Single-piece solid-contact ion-selective electrodes with polymer-carbon nanotube composites. *Sensors and Actuators B-Chemical* **2010**, 148, 166-172.

[38] Parra, E. J.; Crespo, G. A.; Riu, J.; Ruiz, A.; Rius, F. X., Ion-selective electrodes using multi-walled carbon nanotubes as ion-to-electron transducers for the detection of perchlorate. *Analyst* **2009**, 134, 1905-1910.

[39] Ampurdanes, J.; Crespo, G. A.; Maroto, A.; Angeles Sarmentero, M.; Ballester, P.; Xavier Rius, F., Determination of choline and derivatives with a solid-contact ion-selective electrode based on octaamide cavitand and carbon nanotubes. *Biosensors & Bioelectronics* **2009**, 25, 344-349.

[40] Zelada-Guillen, G. A.; Riu, J.; Duezguen, A.; Rius, F. X., Immediate Detection of Living Bacteria at Ultralow Concentrations Using a Carbon Nanotube Based Potentiometric Aptasensor. *Angewandte Chemie-International Edition* **2009**, 48, 7334-7337.

UNIVERSITAT ROVIRA I VIRGILI
SOLID CONTACT POTENTIOMETRIC SENSORS BASED ON CARBON NANOMATERIALS
Rafael Hernández Malo

UNIVERSITAT ROVIRA I VIRGILI
SOLID CONTACT POTENTIOMETRIC SENSORS BASED ON CARBON NANOMATERIALS
Rafael Hernández Malo

UNIVERSITAT ROVIRA I VIRGILI
SOLID CONTACT POTENTIOMETRIC SENSORS BASED ON CARBON NANOMATERIALS
Rafael Hernández Malo

2.1. Introduction

The solid-contact electrodes described in this thesis are based on a transduction element that connects the recognition layer specific for each target with a conductor capable of transferring the electrical signal produced to the potentiometer. This chapter contains an extensive description of the different parts of the electrode, highlighting the new materials used to construct electrodes and the different recognition layers within them. We also carry out a review of the principles of ion-selective electrodes and aptasensors. Finally there is a description of the analytical performance parameters for electrode characterization.

2.2. Potentiometric sensors

Potentiometry is a technique based on measuring the electromotive force (EMF) between an indicator electrode (IE) and a reference electrode (RE) under zero-current conditions in a closed circuit. In the case of ion-selective electrodes (ISEs), the basis of the signal response is a change in activity in the target analyte sample which brings about a change in the membrane/sample interface, while the potential of the reference electrode remains constant in time. This response should be quick and selective for the target analyte.

Figure 2.1 shows a typical potentiometric cell, composed of an indicator electrode and a reference electrode connected to a high-input impedance potentiometer. IE and RE create two different half-cells that can be immersed in the same solution (as shown in Figure 2.1) or in two different solutions, in which case a bridge material has to be used to connect the different half-cells.

For this thesis, two different types of indicator electrode have been developed: ISEs for the selective determination of calcium in real samples (using different nanostructured materials as the transduction layer) and an aptasensor for the selective determination of *Staphylococcus aureus*. For notation purposes, in some parts of the text 'indicator electrodes' will also be referred to as 'sensors' or 'biosensors'.

One of the main differences between these two types of indicator electrode is the analyte to be determined, for which different recognition layers are needed: ion-selective membrane for ions and aptamers for microorganisms. Another variant has

also been introduced, the use of different transducer elements, where the results are compared in the different sensors. Two different types of nanomaterial - carbon nanotubes and chemically modified graphene - were used to determine the viability of this material as a transducer.

The following sections aim to provide a theoretical basis describing each component of the indicator electrodes and the working mechanism used for detecting each target analyte.

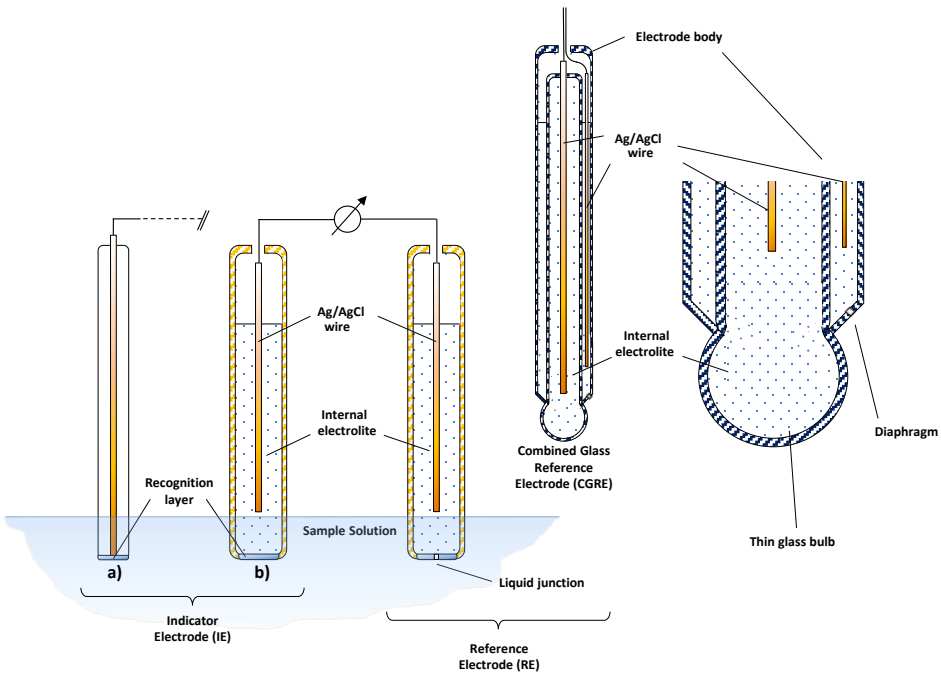

Ag | AgCl | KCl (3M) | Reference membrane|| Sample || Ion-selective membrane (ISM) |Internal solution | AgCl | Ag

Figure 2.1. Scheme of two different conventional electrochemical cells used in potentiometric measurements, composed of a reference electrode (right) and an indicator electrode (left). Two different indicator electrodes are shown: a) a solid contact electrode and b) an internal solution ion-selective electrode. The upper right part of the figure shows a combined glass reference electrode. Cell notation is given below the diagram, where interfaces are represented by | and liquid junctions by ||.

2.3. Recognition layer

The part responsible for the recognition event with the analyte is the recognition layer. This layer is able to interact with analyte molecules in several ways, such as selectively catalyzing a reaction **[1]**, participating in a chemical equilibrium **[2]** or transferring a charge **[3]**. These processes can take place via bulk interaction of the chemical species and the recognition layer or via surface interaction. In this thesis we have used both processes to detect different analytes depending on the specific electrode reported. In some cases the recognition layer was an ion-selective membrane (ISM) in ion-selective electrodes (ISEs), while in other cases we used aptamers as recognition layers to detect bacteria.

2.3.1. Ion-selective membranes (ISM)

The ion-selective membrane is the most important part of ion-selective electrodes. Parameters such as signal stability, selectivity and limit of detection depend on, among other things, the composition of the membrane.

Typical membrane components basically consist of a non-water-soluble polymeric matrix with an embedded ionophore. This uses host-guest chemistry to provide the membrane's selectivity to the target analyte **[4]**.

Depending on the specific membrane, other components such as lipophilic salts and plasticizers may also be required. Each component of the membrane plays an important role and the proportions of each component inside the membrane affect the final result. All the components are mixed in a so-called membrane cocktail dissolved in an organic solvent prior to being deposited in the substrate that forms the body of the ISE. This electrode preparation will be discussed in detail in Chapter 3.

2.3.1.1. Polymeric matrix

The main purpose of the polymeric matrix is to give support to the other components of the ion-selective membrane, providing the sensor with additional mechanical stability. It is lipophilic in character and is therefore usually prepared in organic solvents. The choice of polymer is very important and should not be considered simply as an inert support. It is involved in structural processes like bulk diffusion through the membrane,

influencing the limits of the response **[5]**. Apart from the necessary solubility, another important characteristic the matrix needs is a glass transition temperature (T_g) lower than room temperature. Polymers with a high T_g require the use of plasticizers, while those with a low T_g can be used without.

There are various matrices based on polymers such as silicone resins, polysiloxanes and polyurethanes, but the most commonly used are acrylic and poly(vinyl chloride) (PVC) matrices. The PVC membranes are typically composed of 33% PVC and 66% plasticizer. The most usual plasticizers are o-nitrophenyl octyl ether (o-NPOE with polar properties) and bis(2-ethylhexyl sebacate) (DOS with apolar properties) (Figure 2.2). Plasticizers in this type of matrix are used to provide a suitable glass transition temperature below room temperature, since this is one of the prerequisites for a working ISM **[6,7]**.

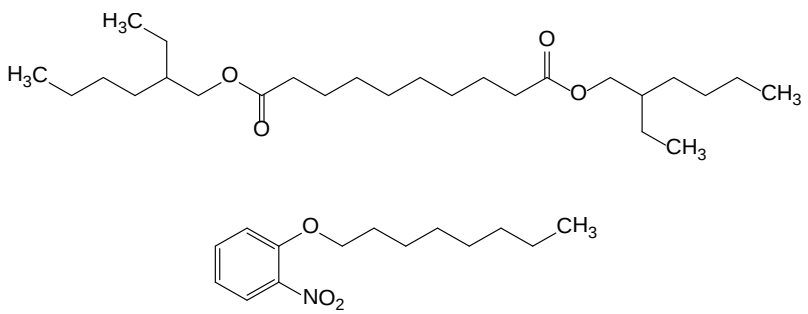

Figure 2.2. Chemical structure of the DOS (above) and o-NPOE (below) plasticizers.

The high ionic mobility of PVC-based membranes gives them a number of disadvantages, such as adhesion problems of the plasticizer **[8]**, the extraction of lipophilic compounds which impair the membrane's selectivity **[9]** and biocompatibility with tissues due to leaching of the plasticizer. This latter problem may even cause allergic reactions **[8]** when used in biological environments. Another typical problem is the insertion of a small water layer between the transducer material and the membrane, giving rise to instabilities in the analytical signals **[10]**. To overcome these problems, alternative membranes appeared with covalently-anchored plasticizer or plasticizer-free matrices, as in the case of acrylic membranes **[11]**.

The solution to these problems is to use polymeric matrices based on acrylate and methacrylate monomers. Early attempts used homopolymers of methacrylate (MMA) with a high T_g (378 K) **[12,13]**, but these did not give the desired result **[6]**. Therefore copolymers are used to decrease the T_g to below room temperature. Typical monomers used in conjunction with MMA are n-butyl acrylate (nBA) with a T_g of 218 K **[14-17]**, decyl methacrylate (DMA) with a T_g of 243 K **[18,19]** and isodecyl acrylate (IDA) with a T_g of 215 K **[20,21]**. The structures of monomers used in typical acrylate-based membranes are presented in Figure 2.3. These copolymers have good adhesive properties **[22,23]** and facilitate the covalent attachment of functional groups **[5,24]**. Also, ion mobility inside the acrylate membranes is 3 orders of magnitude lower than PVC with plasticizers, and therefore limits of detection are lower due to reduced ion fluxes **[25,26]** and the increased stability of the signal. However, these membranes do have a problem related to their ion mobility - high resistance **[5,17,24]** - and this leads to long conditioning times **[27,28]**.

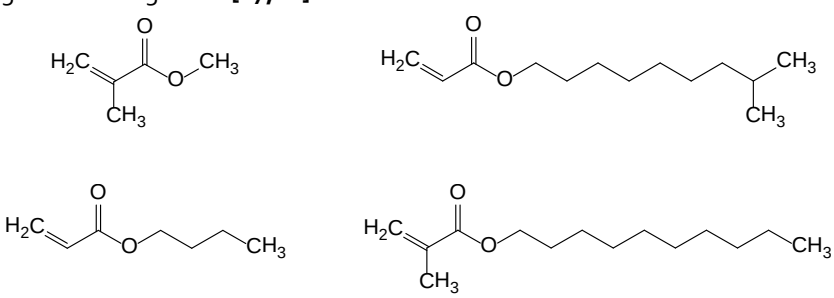

Figure 2.3. Chemical structures of commonly used monomers in acrylate-based membranes: (a) methyl methacrylate (MMA), (b) n-butyl acrylate (nBA), (c) decyl methacrylate (DMA) and (d) isodecyl acrylate (IDA).

2.3.1.2. Ionophores

The main components of the ISM are lipophilic/lipophobic complexing agents. These molecules, known as ionophores or ion carriers, can reversibly bind to ions due to their ability to form supramolecular interactions via Van der Waals forces, metal coordination or lipophilic/lipophobic interactions. The synthesis of ionophores is carried out according to the nature of the target analyte to be determined (primary ion), taking into account size, shape and charge. These molecules also need flexible structures

enabling conformational changes when the primary ion approaches the active site to form the ionophore-ion complex **[2]**.

Ionophores are the main component in the selectivity of the membranes. ISM selectivity is directly related to the equilibrium constant of the exchange reaction of the primary ion and the interfering ion from the aqueous phase and the organic phase at molecular level.

If a selective binding ionophore is incorporated into the ISM, it decreases the overall free energy for ion transfer in the organic phase for those ions bonded to the ionophore **[2]**. Furthermore, the effect on the ion's phase transfer equilibrium increases when the ionophore binds more strongly to an ion. The complexation process has to be kinetically fast, avoiding long time responses and deviations in the response slope **[29]**, but also without any large complex formation constant (β_{IL}) producing a kinetically irreversible complexation. In figure 2.4 it can be shown the ionophore used in this thesis for the selective detection of calcium (ETH129)

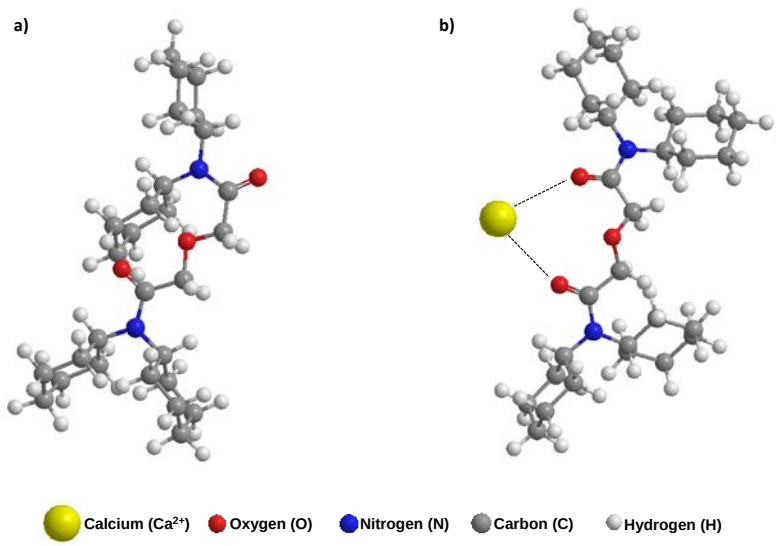

Figure 2.4. Ball-and-stick molecular model representations for N,N,N',N'-Tetracyclohexyl-3-oxapentanediamide (ETH129) a) without and b) with calcium interactions.

One of the requirements that limit the use of ionophores is that they need to have enough lipophilicity to ensure compatibility with the polymer membrane, thus avoiding the leaching of the compound into the aqueous phase over time. The addition of long alkyl chains or bulky organic groups imparting high lipophilicity helps to prevent the release of the ionophore. Ionophore (L) lipophilicity (P) is expressed by the following phase-transfer equilibrium expression (eq. 2.1), in which the higher the P factor, the lower the leaching-out rate.

$$P = \frac{[L(org)]}{[L(aq)]} \qquad \text{eq. 2.1}$$

To obtain membranes of an optimal working condition based on neutral ionophores, the addition of lipophilic ions with an opposite charge to the target analyte is beneficial.

2.3.1.3. Lipophilic salts

The use of lipophilic ions ensures the permselectivity of the membrane, achieving a Nernstian response due to the minimization of the co-extraction process **[2]**. The entry of ions into the membrane with a corresponding counter-ion from the solution is reduced, in theory leaving only the process of primary ion exchange.

If the same ionophore is a charged species, there is no need to add a lipophilic salt because the charged nature of the ionophore induces Donnan exclusion **[30]**.

Lipophilic salts do not drastically affect the selectivity of the ionophore, but they still have to be taken into account so as to carefully optimize the lipophilic salt/ionophore molar ratio **[31-33]**.

Due to their chemical stability and high lipophilicity, the salts most commonly used as anionic additives are generally tetraphenylborate derivatives such as sodium tetraphenylborate (NaTPB), potassium tetrakis(p-chlorophenyl)borate (KTpClPB), potassium tetrakis[3,5-bis(trifluoromethyl- phenyl]borate (KTFPB) and sodium tetrakis[3,5-bis(1,1,1,3,3,3-hexafluoro-2-methoxy-2-propyl)-phenyl] borate trihydrate (NaHFPB), while cationic lipophilic additives tend to be quaternary ammonium salts such as tridodecylmethylammonium (TDDMACl) and tetradodecylammonium chloride (TDDACl) (see figure 2.5).

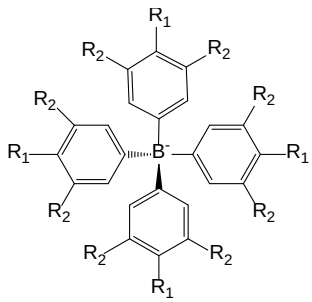

	R_1	R_2	Acronym
a)	H	H	TPB^-
b)	Cl	H	$TpClPB^-$
c)	H	CF_3	$TFPB^-$
d)	H	$C(CF_3)_2OCH_3$	$HFPB^-$

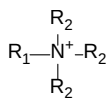

	R_1	R_2	Acronym
e)	CH_3	$(CH_2)_{11}CH_3$	$TDDMA^+$
f)	$(CH_2)_{11}CH_3$	$(CH_2)_{11}CH_3$	$TDDA^+$

Figure 2.5. Chemical structure of anionic and cationic sites currently used in ion-selective electrodes. Lipophilic anionic salts (R^-): a) tetraphenylborate (TPB^-), b) tetrakis(p-chlorophenyl)borate ($TpClPB^-$), c) tetrakis[3,5-bis(trifluoromethyl)-phenyl]borate ($TFPB^-$) and d) tetrakis-[3,5-bis(1,1,1,3,3,3-hexafluoro-2-methoxy-2-propyl)-phenyl]borate trihydrate ($HFPB^-$). Lipophilic cationic salts (R^+): e) tridodecylmethylammonium ($TDDMA^+$) and f) tetradodecylammonium ($TDDA^+$).

The addition of these salts favours the analytical performance parameters of the membrane, reducing response time, helping to decrease membrane resistance and avoiding undesirable signal instabilities. This is very positive, especially in polymer matrices based on acrylates with low ionic mobility, due to their greater resistance compared to PVC-based matrices.

2.3.2. Aptamers

Aptamers are small molecules made up of chains of oligonucleotides, peptides or nucleic acid bases with an extraordinary capacity for the selective binding of diverse targets. This wide variety of targets includes inorganic material such as ions and heavy metals **[34,35]**, ligands with low molecular weight **[36]**, organic materials such as drugs **[37]** and toxins **[38,39]**, and biological material such as whole cells **[40]**, viruses **[41]**, proteins **[42]**, peptides **[43]** and bacteria **[44,45]**.

These molecules have the ability to fold, adopting secondary and tertiary structural conformations, and to bind with high affinity and a higher specificity (dissociation

constant in the order of nano to picomolar) than antibody and biological ligands in some cases.

Aptamers are obtained by a method similar to natural selection called SELEX (systematic evolution of ligands by exponential enrichment) or by an in vitro evolution process carried out using a combinatorial chemistry technique for producing oligonucleotides (either ssDNA or RNA).

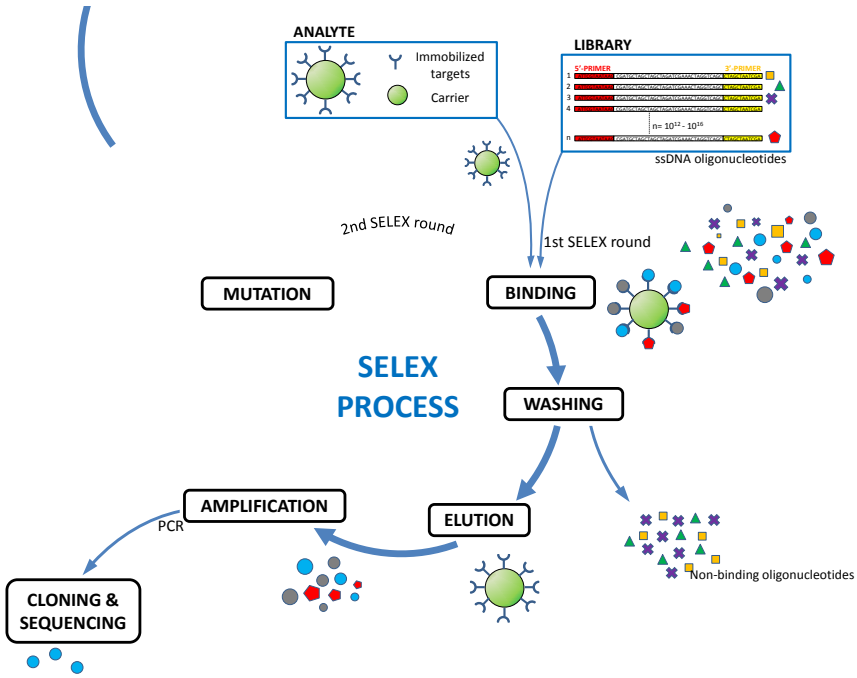

Figure 2.6. Schematic SELEX process.

As it is swhown in figure 2.6, in the first stage, an oligonucleotide library consisting of several randomly-generated sequences is synthesized. These sequences have a fixed length with constant 5′ and 3′ ends, which act as primers. The different possibilities given for a length n is determined by the relation 4^n (due to the position of each nucleic base A, T, C or G). These sequences are exposed to the target, where the chains with greater affinity bind. Those that do not bind with the analyte are eliminated, usually by affinity chromatography, whereas optimal sequences are eluted and amplified by PCR. This process is repeated for the next selection stages, in which the conditions are

stronger in each step. At the end of these interactions a sequence with an extraordinary affinity for the target analyte will be obtained

High specificity and sensitivity enable aptamers to distinguish between chiral molecules and recognize the different epitope of a target molecule **[46]**. Aptamers also offer a wide range of advantages such as stability, design flexibility, cost-effectiveness and target variety. These features make them desirable candidates for high-performance, fast analyses.

2.3.3. Conditioning and regeneration of electrodes

The conditioning process is essential in order to achieve low limits of detection. The procedure is carried out in two steps: a) a preconditioning step, where the electrode is submerged for 24 hours in a concentrated solution of the primary ion (10^{-2}M or 10^{-3}M), and b) a second step, where the electrode is rinsed with MilliQ distilled water and deposited for 48 hours in a diluted solution of the primary ion (10^{-8}M or 10^{-9}M). For common calibration curves where there is no need to obtain data for determining the limit of detection, the second conditioning step is reduced to 24 hours or less.

In the case of aptasensors, the conditioning process is performed by placing the electrode in a PBS solution overnight.

The regeneration of ISEs is done via the conditioning process, whereas the regeneration of aptasensors is done by incubating them in a 2M NaCl solution for 1 hour, then washing them in MilliQ distilled water for 90 min. The electrode is then reconstituted by conditioning it in PBS solution.

2.4. Transduction layer: Nanostructured carbon-based materials.

Nanomaterials and nanosensors are iconic words in modern science and technology. Nanomaterials offer new properties that improve the characteristics of the materials used so far as transducers. Their exceptional electrical properties, such as the high capacities generated at their interfaces and high charge transfers, along with their high surface-to-volume ratio makes them ideal for use as solid-contact transducers.

This thesis looks at two different carbon-based nanomaterials: single-walled carbon nanotubes and chemically modified graphene (graphene oxide and reduced graphene oxide

Carbon is considered to be a unique element in chemistry due to the high number of compounds it can form. The explanation for this lies in its electronic configuration. Carbon has the lowest atomic number of any element in column IV of the periodic table, having six electrons occupying $1s^2$, $2s^2$ and $2p^2$ atomic orbitals. In its crystalline phase, valence electrons give rise to $2s$, $2p_x$, $2p_y$ and $2p_z$ orbitals, which are very important in the formation of covalent bonds. It is relatively simple to combine the upper $2p$ energy levels and the lower 2s level due to the small energy difference between them.

Three possible hybridizations may occur in carbon - sp, sp^2 and sp^3 - generating different bonding states connected with certain structural arrangements. Hence sp bonding gives rise to chain structures, sp^2 to planar structures and sp^3 to tetrahedral structures, giving rise to the different forms present in nature.

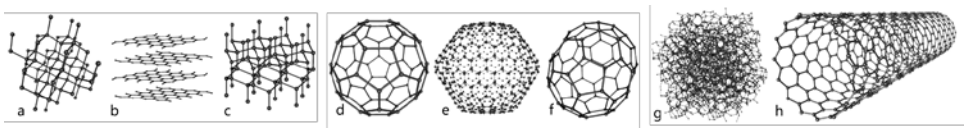

Figure 2.7. Structural arrangements of carbon allotropes: a) diamond, b) graphite, c) lonsdaleite, d) C60 (Buckminsterfullerene or buckyball), e) C540, f) C70, g) amorphous carbon and h) single-walled carbon nanotube.

There are 6 carbon allotropic forms: diamond, graphite, lonsdaleite, fullerenes, amorphous carbon and carbon nanotubes. The difference between these allotropic forms lies in the hybridization adopted by carbon and its disposition in space. Figure 2.7 shows the different allotropic forms of carbon and the final structures they adopt.

2.4.1. Graphene

When carbon atoms are combined with sp^2 hybridization, each atom in the structure is attached to 3 other carbon atoms, resulting in a flat structure called graphene. This arrangement of atoms produces a monolayer of carbon atoms arranged in hexagonal rings. Graphene is the basic structural element of certain carbon allotropes of other

dimensionalities. It can be wrapped up into zero-dimensional fullerenes, rolled up into one-dimensional nanotubes, or stacked into three-dimensional graphite by superimposing a huge number of graphene sheets one on top of another. The links between the graphene layers in graphite are stacked because of van der Waals forces and interactions between the π orbitals of carbon atoms. This arrangement can be carried out in different ways, giving rise to ABAB or ABCA forms (see figure 2.8)

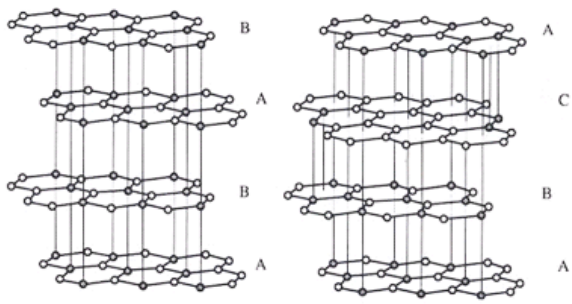

Figure 2.8. Different graphene monolayer arrangement models for graphite.

In any history of graphene, it is important to mention related materials such as graphite oxide (GO), graphite intercalation compounds (GICs) and reduced graphene oxide (RGO), which formed important steps in the investigation of graphene as we know it today.

Graphene has recently been attracting more interest, but the early years of its history date back to the 1840s, when Schafhaeutl reported the intercalation and exfoliation of graphite with sulphuric and nitric acids **[47]**. A few years later, in 1859, D.C. Brodie discovered a highly lamellar structure of thermally reduced graphite oxide **[48]** while trying to characterize the molecular weight of graphite by modifying some of the methods described by Schafhaeutl. Not only did he show the intercalation of the graphite layers but also the chemical oxidation of the surface, obtaining graphite oxide. Advances in instrumentation meant that in 1948, thanks to research by Ruess & Vogt, the number of layers present in lamellar graphite could be determined by electron microscopy, with isolated monolayers finally being detected **[49]**.

An important point in the history of graphene as we know it today was Boehm's discovery in 1962 of the chemical reduction of a dispersion of GO in an alkaline medium

with hydrazine and hydrogen sulphide **[50]**. Years later, in 1999, another type of approach was performed (micromechanically) to obtain thin lamellae of few-layered graphite. Unfortunately this was not completely exfoliated into monolayers, which could have sensed extraordinary electronic properties **[51]**.

The breakthrough in graphene research came in 2004 when two researchers from the University of Manchester, Andre Geim and Konstantin Novoselov, developed a simple, new and innovative method called micromechanical cleavage for isolating graphene from graphite **[52,53]**. This procedure consists of a top-down approach from three-dimensional graphite crystals, taking advantage of the weak interaction present between two different layers within the structure of the crystal. This simple approach easily produced large, high-quality graphene crystals with a room temperature quantum Hall effect and ballistic transport, properties that may mark out graphene as a promising candidate for electronic applications in the future.

Graphene has a large surface area (double that of SWCNTs), high mechanical strength (200 times greater than steel), and high elasticity and thermal conductivity **[54]**. It also presents high two-dimensional electrical conductivity, which makes it ideal for electrochemistry.

Current research into methods of preparing graphene is following bottom-up methodology in an attempt to form graphenic structures from polymeric reactions between small molecules such as polycyclic aromatic hydrocarbons (PAHs) **[55]**, polycyclic aryl halides on silver **[56]**, acetylenic coupling **[57]** and alkyne metathesis **[58,59]**.

2.4.2. Carbon nanotubes (CNTs)

The first evidence of the existence of carbon nanotubes dates from 1952, when L. Radushkevich and V. M. Lukyanovicha published clear images of carbon structures approximately 50 nm in diameter in the Soviet Journal of Physical Chemistry **[60]**. The fact that the publication was in Russian together with the prohibitions inherent to the Cold War meant that this discovery went unnoticed. In 1976, a paper by Oberlin, Endo & Koyama clearly showed hollow carbon fibres with nanometer-scale diameters using a vapour-growth technique **[61]**.

In 1981 a group of Soviet scientists published the results of a chemical and structural characterization of carbon nanoparticles produced by thermocatalytical disproportionation of carbon monoxide. Using TEM images and XRD patterns, the authors suggested that their 'carbon multi-layer tubular crystals' were formed by rolling graphene layers into cylinders. However, it was not until 1991 that carbon nanotubes attracted great interest after the publication of Iijima's paper in Nature **[62]**.

In figure 2.9 are represented 3 different structural arrangements of carbon allotropes: graphene and carbon nanotubes. Carbon nanotubes can be visualized as a graphene sheet of a certain size wrapped in a certain direction to form a cylinder. Depending on the number of walls in their molecular structure, CNTs are classified as single (SWCNTs) or multi-wall carbon nanotubes (MWCNTs).

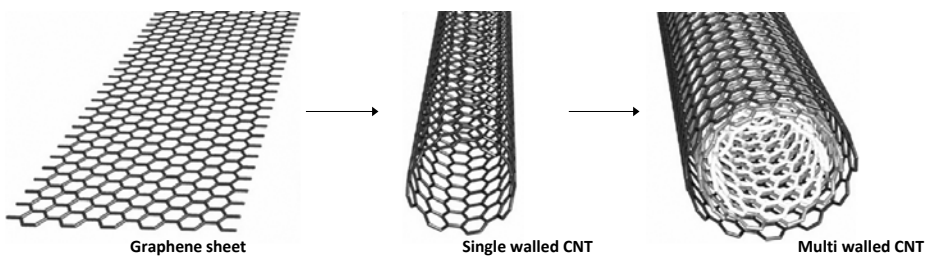

Figure 2.9. Graphical representations of ideal sheet, SWCNT and MWCNT.

To characterize this cylinder, two atoms of the graphene sheet are chosen, one as origin and the other as destination, to form a chiral vector (C_h), the so-called Hamada vector, $C_h=na_1+ma_2$ **[63]**, where a_1 and a_2 are the lattice vectors of the unitary hexagonal cell and (n,m) are two integers which determine the chirality and the diameter of a CNT. The chiral angle (θ) is formed between the Hamada vector and the unit lattice vector a_1. Depending on these variables, three types of nanotube can be described as shown in figure 2.10: *armchair* CNTs (m=n), *zigzag* CNTs (m=0, n=0) and *chiral* CNTs (m≠n).

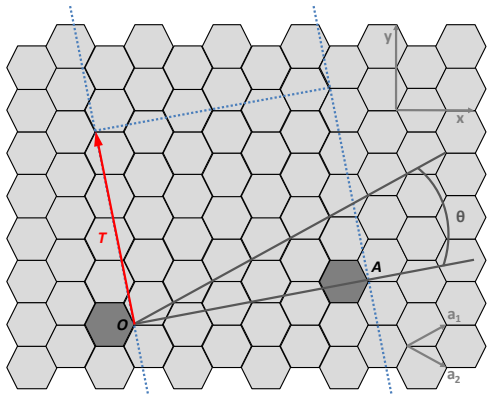

Figure 2.10. Cell unit for a single-walled carbon nanotube (4,2)

The properties of a carbon nanotube, such as optical activity, mechanical strength and electrical conductivity, depend on its chiral vector. A CNT is considered metallic if (n-m)=3i, where i is an integer. Otherwise the nanotube is considered to be a semiconductor **[64]** (see figure 2.11)

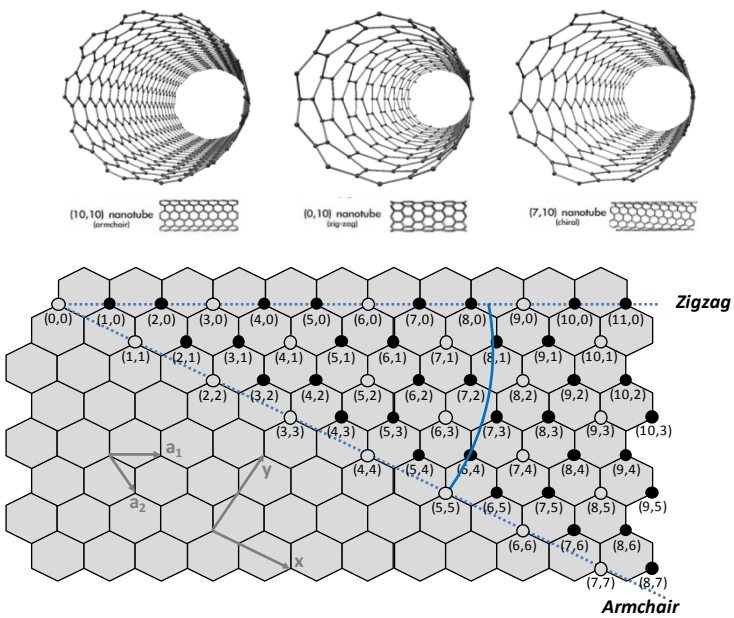

Figure 2.11. Chemical structures of (10,10) armchair, (0,10) zig-zag and (7,10) chiral SWCNTs, SWCNTs and representation of metallic/semi-metallic distribution of SWCNTs according to the Hamada vector.

Assuming this relationship, it is expected that two-thirds of nanotubes will be semi-conducting and one third metallic with random values of integers *n* and *m* **[65]**.

2.5. Working mechanism principles

2.5.1. ISE working mechanism

A typical scheme for potentiometric measurements was shown in figure 2.1. In the case of this thesis, the scheme includes an ISE, a reference electrode and a potentiometer. It can be considered as two galvanic half-cells represented by the ISE and the reference electrode and the electromotive force (EMF) produced as the sum of all the contributions from individual interfacial potentials, under zero-current conditions **[2]**

There are different models to explain the potential generated at the interface of the electrode. These are classified as total-equilibrium models (classical models), local-equilibrium models (diffusion-layer models) and advanced non-equilibrium models **[66]**, but here we will take into account only the generally accepted phase-boundary potential model (classical model) **[67]**.

A general working assumption is that most of the potential contributions are sample dependent. According to this **[66]**, the expression for the EMF can be simplified to:

$$\mathrm{EMF} = \mathrm{E_M} + \mathrm{E_J} + \mathrm{E_{const}} \qquad \text{eq. 2.2}$$

where E_M is the membrane potential, E_J is the liquid junction potential of the reference electrode and E_{const} can be described as the sum of all sample-independent potential contributions.

As regards liquid junction potential from reference electrode $(\mathrm{E_J})$, this appears due to the tendency of two different solutions (inner reference electrode|sample) to mix when they are kept in contact. Cations and anions from a more highly concentrated solution tend to spread into a less concentrated one so as to increase equilibrium. In order to prevent the solutions from mixing, a diaphragm (see figure 2.12) is placed at the interface of the sample solution and the internal filling solution of the reference electrode. This is a small ceramic or glass piece of the electrode, permeable to all the species, which prevents the solutions from mixing.

A potential difference is created because of charge separation due to different ion mobilities. The reference electrodes used in this thesis (Ag/AgCl reference electrodes) use a highly concentrated salt based on LiAcO or KCl solution, which have similar ion mobility, dominating the charge transfer at the liquid junction. This keeps the liquid junction potential rather small or at least constant, minimizing it from equation 2.2, and making the EMF independent of it. This can also be achieved using a salt bridge.
Membrane potential E_M can be considered as the sum of three different components:

$$E_M = E_{PB} + E_D + E_{PB'} \qquad \text{eq. 2.3}$$

Where E_{PB} is the boundary potential between the inner solution (or inner solid contact in the case of this thesis) and the membrane; E_D is the diffusion potential created inside the membrane; and $E_{PB'}$ is the boundary potential between the membrane and the sample solution.

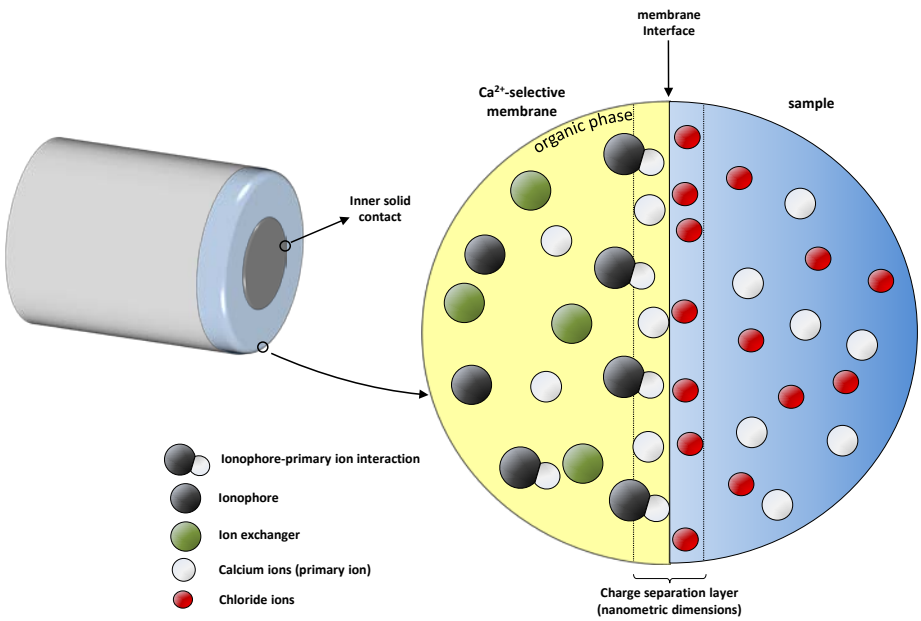

Figure 2.12. Phase-boundary sensing mechanism when the membrane is placed in contact with an aqueous solution containing a primary ion and a counterion. Charge separation in the membrane|sample solution interface generated due to the difference in the free hydration energies.

Different assumptions have to be considered in the phase boundary potential model to simplify it: i) Diffusion potential (E_D) may be neglected due to the fact that it is related to the kinetics of charged species in the ion-selective membrane. ii) E_{PB} can be considered as a constant because it is commonly considered to be sample independent, and so equation 2.3 is simplified to equation 2.4 assuming that the membrane potential is only dependent on the phase-boundary potential at the membrane|sample interface. iii) there exists an electrochemical equilibrium at the sample|membrane interface.

$$E_M = E_{PB'} \qquad \text{eq. 2.4}$$

Following all these assumptions, the potential cell under ideal conditions can be described by the well-known Nernst equation:

$$E = \Delta\emptyset = \emptyset^{org} - \emptyset^{aq} = \frac{\mu_i^o(aq) - \mu_i^o(org)}{z_i F} + \frac{RT}{z_i F} \ln \frac{a_i^{aq}}{a_i^{org}} \qquad \text{eq. 2.5}$$

where, $\emptyset$ is the electrical potential
z_i is the charge of species i
μ_i is the mobility of species 'i'
a_i is the activity of species 'i'
F is the Faraday constant (96485 C·mol-1).
R is the universal gas constant (8.314 J·K-1·mol-1)

The value of a_i^{org} in equation 2.5 remains constant, enabling the value of a_i^{aq} to be determined and making the total concentration of the primary ion in the membrane independent of the sample **[68,69]**. The Nernstian equation can then be simplified to:

$$E = E^o + \frac{59.16}{z_i} \ln a_i^{aq} \qquad \text{eq. 2.6}$$

2.5.2. Aptasensor working mechanism.

The mechanism of aptasensors is very different from the mechanisms of ISEs. This is partly caused by the structure of the target analyte: bacteria. Bacteria belong to the domain of prokaryotic organisms. These microorganisms have dimensions of a few

micrometers (typically 0.5-5.0 μm in length) and a variety of morphologies such as spirals, spheres and rods.

In figure 2.13 it is shown a representation of a bacteria and the different cell membrane components- A cytoplasmic membrane composed of lipids surrounds the cytoplasm. Like plant cells, most bacteria have a cell wall, composed of peptidoglycan (murein). Most of them also have a second lipid membrane (outer membrane) surrounding the cell wall. The bacterial cytoplasmic membrane is a lipid bilayer composed mainly of phospholipids with embedded protein molecules. Two different types of bacteria can be described depending on their bacterial cell wall: Gram-positive and Gram-negative.

In Gram-positive bacteria it is characteristic to detect a thick cell wall in which there are numerous layers of teichoic acid. Gram-negative bacteria, however, have a relatively thin wall consisting of a few layers of peptidoglycan, surrounded by a second lipid membrane (outer membrane) containing lipopolysaccharides and lipoproteins.

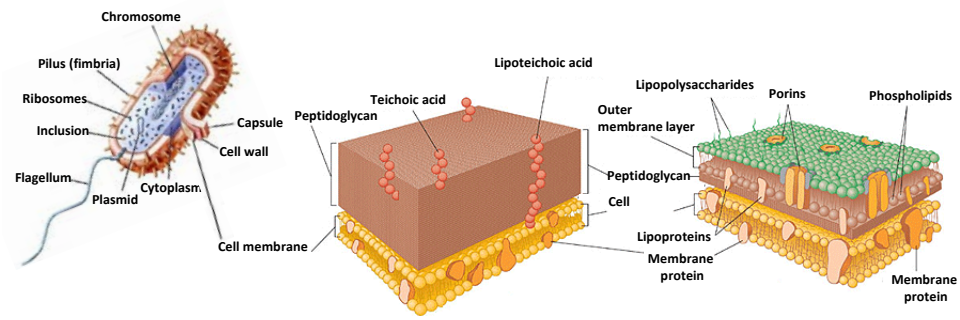

Figure 2.13. Bacteria representation parts with a cell membrane zoom for Gram-positive bacteria (left) and Gram-negative bacteria (right)

In the case of aptasensors, the working mechanism is not produced following a Nernstian response as in the previous case. Here the interaction comes about because of a biorecognition event between a DNA chain, which is anchored to the carbon nanomaterial, and the target analyte.

Johnson et al **[70]** revealed through studies on molecular dynamics that SWCNTs could induce single-stranded DNA (ssDNA) to achieve spontaneous conformational change in order to self-assemble. This interaction is possible due to the π–π stacking interaction between the aptamer bases and the carbon nanotube walls.

The interaction between aptamers and graphene-based materials takes place in a similar way **[71]**, and we used this feature for the detection of bacteria (see figure 2.14). When a particular bacterium that can be catched by the aptamer approaches the graphene/aptamer hybrid, a competitive equilibrium between the target bacteria and the graphene appears.

Negative charges from phosphate groups of the aptamers are largely ionized at pH 7.5. This negative charge is transferred to the carbon nanotubes, decreasing the standard potential of the sensor measured following functionalization of the graphene with the aptamers. When the target approaches the hybrid, this induces a conformational change in the aptamer that separates the phosphate negative charges from the graphene (or SWCNTs) **[71-73]**. This separation creates a change in the recorded potential detected by the potentiometer.

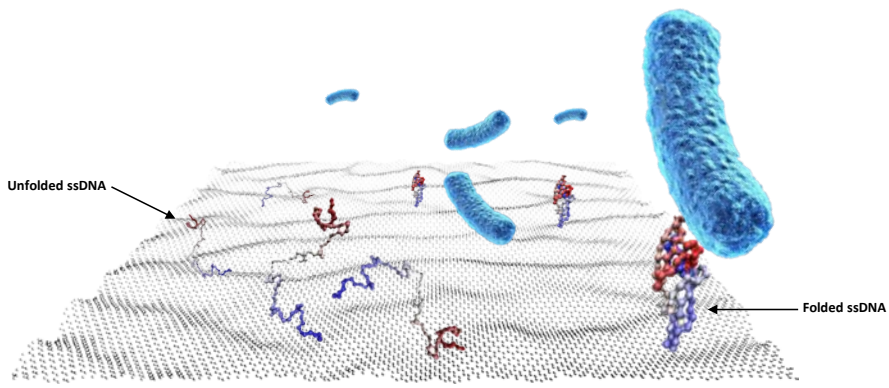

Figure 2.14. Schematic representation of aptamer sensing mechanism. The figure shows ssDNA but also RNA-aptamers can be used

2.6. Analytical performance parameters

The electrochemical section of the IUPAC Green Book contains a description of several parameters that define the analytical function of potentiometric sensors **[74]**. Figure 2.15 shows two different plots where all the parameters explained in this section can easily be viewed. Cell EMF is plotted on the abscissa axis versus the logarithm of the single ionic activity (Figure. 2.15.a) or versus time (Figure. 2.15.b).

2.6.1. Sensitivity

The sensitivity and linear concentration range of steady-state calibration curves can be determined directly from the sensor's response by plotting the instrumental signal versus logarithmic activity/concentration of the target analyte. In the case of ISEs, sensitivity is commonly described by the Nernstian slope and defined by RT/z_iF [$59.2/z_i$ $mV \cdot dec^{-1}$] at 25ºC, where z_i is the ion charge, R is the universal gas constant (8.314 $J \cdot K^{-1} \cdot mol^{-1}$), T is the absolute temperature and F is the Faraday constant (96485 $C \cdot mol^{-1}$). Deviations from this ideal behaviour can be brought about to obtain super and sub-Nernstian sensitivities, as in the case of biosensing by aptasensors.

2.6.2. Selectivity

Ideally, the potentiometric response of an electrode should be exclusively connected with the target analyte, i.e. the primary ion or bacteria in the case of this thesis. Unfortunately this interaction is not exclusive and the recognition layer responds to other analytes. This parameter together with the limit of detection is very important and sometimes determines whether an electrode can be used for a specific application.
The term selectivity has to be used in terms of quantitative characterization. Selectivity determines whether a reliable measurement of the target sample is possible, whether electrodes are able to differentiate between the target analyte and other analytes called interferences using the selectivity coefficients K_{ij}^{pot}.
In the case of ISEs, semiempirical extended Nikolskii-Eisenman formalism is used to describe the response to both primary and interfering ions:

$$\mathrm{EMF} = \mathrm{E_I^{0\prime}} + \frac{\mathrm{RT}}{\mathrm{z_i F}} \ln\left(\mathrm{a_i} + \sum_{\mathrm{i \neq j}}^{\mathrm{j}} \mathrm{K_{i,j}^{pot}} \mathrm{a_j}^{\mathrm{z_i/z_j}}\right) \qquad \text{eq. 2.8}$$

where, $E_I^{0\prime}$ is the standard potential
z_i is the charge number for primary ion 'i'
z_j is the charge number for ion 'j'
a_i is the activity of the primary ion
a_j is the activity of the interfering ions

Selectivity coefficients K_{ij}^{pot} can be determined using the equation:

$$\log K_{i,j}^{pot} = \frac{z_i F}{2.303\ RT}\left(E_J^{0\prime} - E_I^{0\prime}\right) = \frac{z_i F}{2.303\ RT}\left(E_J^{EMF} - E_I^{EMF}\right)\log\frac{a_i}{a_j^{z_i/z_j}} \qquad \text{eq. 2.9}$$

where, $E_I^{0\prime}$ is the standard potential of species 'i'
$E_J^{0\prime}$ is the standard potential of species 'j'
E_I^{EMF} is the measured potential of species 'i'
E_J^{EMF} is the measured potential of species 'j'

2.6.3. Limit of detection

In other analytical methods, the limit of detection is defined as three times the standard deviation of the background noise **[75]**. However, in the field of potentiometric measurements this definition for ion-selective electrodes has to be reconsidered because the typical noise is less than 0.1 mV, which would lead to very low limits of detection which would not correspond with reality.

In ISEs we can define the limit of detection (LOD) as the activity (or concentration) of a substance at the point of intersection of the extrapolated linear mid-range and final low-concentration-level segments of the calibration plot (see figure 2.15.a).

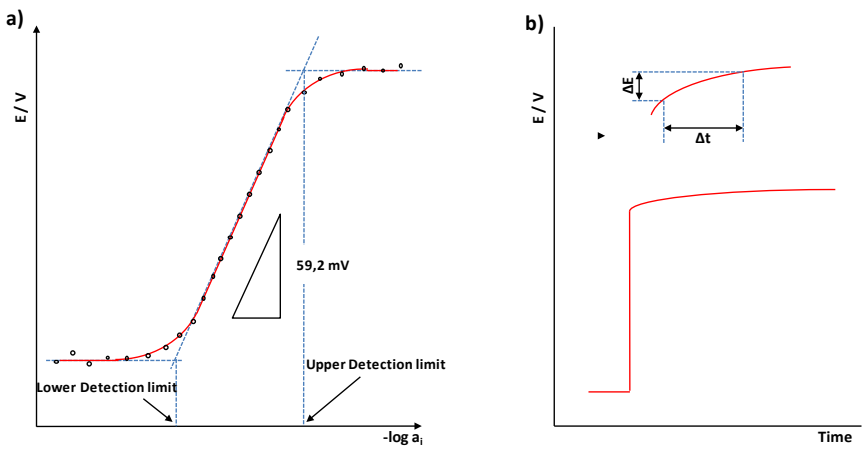

Figure 2.15. Main analytic performance parameters for an ISE.

When the concentration of primary ions is very high, electrodes become insensitive and an upper limit of detection can be defined. There is a loss of permselectivity in the membrane due to the coextraction of primary ions and counterions from the solution

sample to the ISM, typically through the presence of a high concentration of the primary ions in solution or the lipophilic behaviour of certain counterions.

In the case of aptasensors, which do not show a Nernstian response, the limit of detection has to be determined as the minimum quantity of bacteria that needs to be resolved from the instrumental limit of detection, delimited by the expression $3xSD_{noise}$. It is important in the case of bacteria to obtain very low limits of detection for simple positive/negative tests, assuring zero-tolerance conditions.

2.6.4. Linear concentration range

At high and low ionic activities there are deviations from linearity. These deviations are defined by the upper and lower limit of detection. Between those limits there is a part of the calibration curve in which the instrumental response follows a linear relationship with the logarithm of the activity.

Typically, the electrode calibration curve exhibits a linear response range between 10^{-1}M to 10^{-5}M for ISEs. This region contains useful analytical information and is ideally where calibration and measurement points can be determined.

2.6.5. Response time

Ideally, the response of an electrode to a change in activity or concentration should be instant. In practice this is impossible because there is an accommodation time for the host-guest complexation. Thus response time (t_R) can be considered as the time lapse between the instant at which the electrode comes into contact with the sample (or when there is a change in the activity of a solution) and the first moment at which the *emf* response is considered stable or becomes equal to a limiting value selected according to the experimental conditions established.

This parameter is usually concentration-dependent. For low-concentrated sample solutions the response time is usually long, while for relatively high concentrations of analyte the response time is usually short. A good ion-to-electron transduction can be denoted for time responses in the order of a few seconds.

2.6.6. Stability

Stability gives us information about the evaluation of the *emf* response in a short, medium and long-term range depending on experimental requirements. It can be expressed as a drift in terms of $\mu V \cdot h^{-1}$ or $mV \cdot h^{-1}$. A drift is a slow non-random change in the *emf* response of an electrode cell assembly kept in a solution of constant composition and temperature. Drifts can appear due to a variety of physical or chemical parameters such as temperature fluctuations, leaching of electroactive material from the membrane or sorption of interferents.

Good stability can be considered for electrode drifts of less than 0,5 $mV.h^{-1}$ in the long-term range. Drifts are usually detected at medium and long term, whereas in short terms any alterations of stability can be detected in the shape of *emf* jumps. Any type of drift in the output of a chemical sensor is undesirable. Short-term drift generally renders the sensor useless.

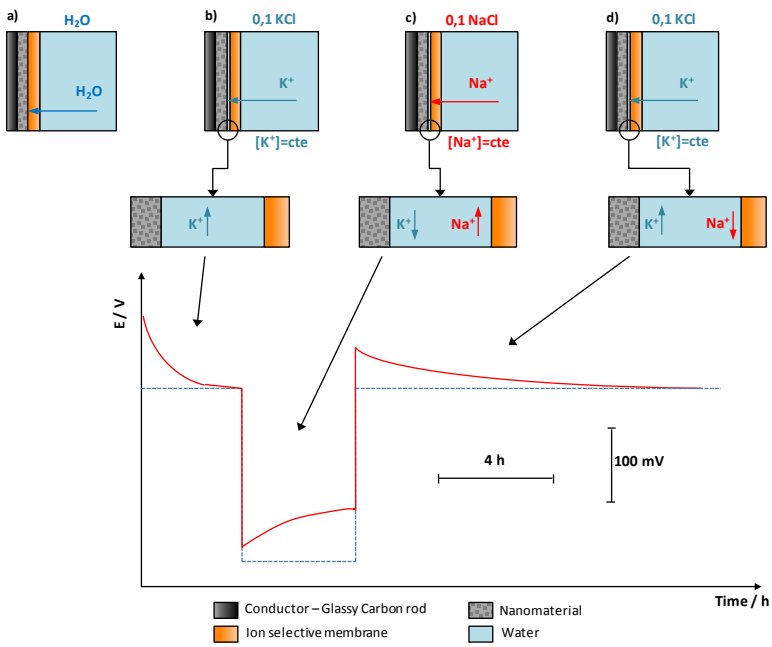

Figure 2.16. Water-layer test stages for a conventional SWCNT/K^+-ISE using nanomaterials as inner transducers

In terms of quality parameters, it is a good idea to check for the presence of a hypothetical small water layer between the membrane and the ion-to-electron transducer layer **[76]** due to the permeability of the membrane. This can give rise to drifts in the *emf* response (figure 2.16).

In a first step (figure 2.16.b), the behaviour of the electrodes is observed when they are exposed to a solution of the primary ion. In a second step (figure 2.16.c), the electrode is removed and rinsed with MilliQ distilled water and immersed for some hours in a solution of an interfering ion. Finally the solution is changed back to the initial one (figure 2.16.d).

2.7. References

[1] Lakshmi, D.; Bossi, A.; Whitcombe, M. J.; Chianella, I.; Fowler, S. A.; Subrahmanyam, S.; Piletska, E. V.; Piletsky, S. A., Electrochemical Sensor for Catechol and Dopamine Based on a Catalytic Molecularly Imprinted Polymer-Conducting Polymer Hybrid Recognition Element. *Analytical Chemistry* **2009,** *81*, 3576-3584.

[2] Bakker, E.; Buhlmann, P.; Pretsch, E., Carrier-based ion-selective electrodes and bulk optodes. 1. General characteristics. *Chemical Reviews* **1997,** *97*, 3083-3132.

[3] Liu, C.; Alwarappan, S.; Chen, Z.; Kong, X.; Li, C.-Z., Membraneless enzymatic biofuel cells based on graphene nanosheets. *Biosensors & Bioelectronics* **2010,** *25* (7), 1829-1833.Buhlmann, P.; Pretsch, E.; Bakker, E., Carrier-based ion-selective electrodes and bulk optodes. 2. Ionophores for potentiometric and optical sensors. *Chemical* Reviews 1998, 98, 1593-1687.

[4] Buhlmann, P.; Pretsch, E.; Bakker, E., Carrier-based ion-selective electrodes and bulk optodes. 2. Ionophores for potentiometric and optical sensors. *Chemical Reviews* **1998,** *98*, 1593-1687.

[5] Heng, L. Y.; Toth, K.; Hall, E. A. H., Ion-transport and diffusion coefficients of non-plasticised methacrylic-acrylic ion-selective membranes. *Talanta* **2004,** *63*, 73-87.

[6] Fiedler, U.; Ruzicka, J., Selectrode - Universal ion-selective electrode. 7. Valinomycin-based potassium electrode with nonporous polymer membrane and solid-state inner reference system. *Analytica Chimica Acta* **1973,** *67*, 179-193.

[7] Armstrong, R. D.; Horvai, G., Properties of PVC based membranes used in ion-selective electrodes. *Electrochimica Acta* **1990,** *35*, 1-7.

[8] Lindner, E.; Cosofret, V. V.; Ufer, S.; Buck, R. P.; Kao, W. J.; Neuman, M. R.; Anderson, J. M., Ion-selective membranes with low plasticizer content - Electroanalytical characterization and biocompatibility studies *Journal of Biomedical Materials Research* **1994,** *28*, 591-601.

[9] Buhlmann, P.; Hayakawa, M.; Ohshiro, T.; Amemiya, S.; Umezawa, Y., Influence of natural, electrically neutral lipids on the potentiometric responses of cation-selective polymeric membrane electrodes. *Analytical Chemistry* **2001,** *73*, 3199-3205.

[10] Hulanicki, A.; Trojanowicz, M., Calcium-selective electrodes with PVC membranes and solid internal contacts. *Analytica Chimica Acta* **1976,** *87*, 411-417.

[11] Veder, J.-P.; De Marco, R.; Clarke, G.; Chester, R.; Nelson, A.; Prince, K.; Pretsch, E.; Bakkert, E., Elimination of undesirable water layers in solid-contact polymeric ion-selective electrodes. *Analytical Chemistry* **2008,** *80*, 6731-6740.

[12] Heng, L. Y.; Hall, E. A. H., Methacrylic-acrylic polymers in ion-selective membranes: achieving the right polymer recipe. *Analytica Chimica Acta* **2000,** *403*, 77-89.

[13] Qin, Y.; Peper, S.; Bakker, E., Plasticizer-free polymer membrane ion-selective electrodes containing a methacrylic copolymer matrix. *Electroanalysis* **2002,** *14*, 1375-1381.

[14] Ceresa, A.; Sokalski, T.; Pretsch, E., Influence of key parameters on the lower detection limit and response function of solvent polymeric membrane ion-selective electrodes. *Journal of Electroanalytical Chemistry* **2001,** *501*, 70-76.

[15] Heng, L. Y.; Hall, E. A. H., One-step synthesis of K+-selective methacrylic-acrylic copolymers containing grafted ionophore and requiring no plasticizer. *Electroanalysis* **2000,** *12*, 178-186.

[16] Heng, L. Y.; Hall, E. A. H., Taking the plasticizer out of methacrylic-acrylic membranes for K+-selective electrodes. *Electroanalysis* **2000,** *12*, 187-193.

[17] Michalska, A. J.; Appaih-Kusi, C.; Heng, L. Y.; Walkiewicz, S.; Hall, E. A. H., An experimental study of membrane materials and inner contacting layers for ion-selective

K+ electrodes with a stable response and good dynamic range. *Analytical Chemistry* **2004,** *76*, 2031-2039.

[18] Peper, S.; Ceresa, A.; Qin, Y.; Bakker, E., Plasticizer-free microspheres for ionophore-based sensing and extraction based on a methyl methacrylate-decyl methacrylate copolymer matrix. *Analytica Chimica Acta* **2003,** *500*, 127-136.

[19] Qin, Y.; Bakker, E., A copolymerized dodecacarborane anion as covalently attached cation exchanger in ion-selective sensors. *Analytical Chemistry* **2003,** *75*, 6002-6010.

[20] Malinowska, E.; Gawart, L.; Parzuchowski, P.; Rokicki, G.; Brzozka, Z., Novel approach of immobilization of calix 4 arene type ionophore in 'self-plasticized' polymeric membrane. *Analytica Chimica Acta* **2000,** *421*, 93-101.

[21] Wydgladacz, K.; Durnas, M.; Parzuchowski, P.; Brzozka, Z.; Malinowska, E., Miniaturized sodium-selective sensors based on silicon back-side contact structure with novel self-plasticizing ion-selective membranes. *Sensors and Actuators B-Chemical* **2003,** *95*, 366-372.

[22] Moody, G. J.; Thomas, J. D. R.; Slater, J. M., Modified poly(vinyl chloride) matrix for ion-selective field-effect transistor sensors. *Analyst* **1988,** *113*, 1703-1707.

[23] Levichev, S. S.; Bratov, A. V.; Vlasov, Y. G., New photocurable composition for ISFET polymer membranes. *Sensors and Actuators B-Chemical* **1994,** *19*, 625-628.

[24] Rzewuska, A.; Wojciechowski, M.; Bulska, E.; Hall, E. A. H.; Maksymiuk, K.; Michalska, A., Composite polyacrylate - Poly(3,4-ethylenedioxythiophene) membranes for improved all-solid-state ion-selective sensors. *Analytical Chemistry* **2008,** *80*, 321-327.

[25] Szigeti, Z.; Vigassy, T.; Bakker, E.; Pretsch, E., Approaches to improving the lower detection limit of polymeric membrane ion-selective electrodes. *Electroanalysis* **2006,** *18*, 1254-1265.

[26] Sutter, J.; Radu, A.; Peper, S.; Bakker, E.; Pretsch, E., Solid-contact polymeric membrane electrodes with detection limits in the subnanomolar range. *Analytica Chimica Acta* **2004,** *523*, 53-59.

[27] Michalska, A.; Wojciechowski, M.; Bulska, E.; Mieczkowski, J.; Maksymiuk, K., Poly(n-butyl acrylate) based lead (II) selective electrodes. *Talanta* **2009,** *79*, 1247-1251.

[28] Lyczewska, M.; Wojciechowski, M.; Bulska, E.; Hall, E. A. H.; Maksymiuk, K.; Michalska, A., Chloride-selective electrodes with poly(n-butyl acrylate) based membranes. *Electroanalysis* **2007,** *19*, 393-397.

[29] Michalska, A.; Pyrzynska, K.; Maksymiuk, K., Method of achieving desired potentiometric responses of polyacrylate-based ion-selective membranes. *Analytical Chemistry* **2008,** *80*, 3921-3924.

[30] Grygolowicz-Pawlak, E.; Crespo, G. A.; Afshar, M. G.; Mistlberger, G.; Bakker, E., Potentiometric Sensors with Ion-Exchange Donnan Exclusion Membranes. *Analytical Chemistry* **2013,** *85*, 6208-6212.

[31] Bakker, E.; Xu, A. P.; Pretsch, E., Optimum composition of neutral carrier based pH electrodes. *Analytica Chimica Acta* **1994,** *295*, 253-262.

[32] Eugster, R.; Gehrig, P. M.; Morf, W. E.; Spichiger, U. E.; Simon, W., Selectivity-modifying influence of anionic sites in neutral-carrier-based membrane electrodes. *Analytical Chemistry* **1991,** *63*, 2285-2289.

[33] Meier, P. C.; Morf, W. E.; Laubli, M.; Simon, W., Evaluation of the optimum composition of neutral-carrier membrane electrodes with incorporated cation-exchanger sites. *Analytica Chimica Acta* **1984,** *156*, 1-8.

[34] Li, J.; Guo, S.; Zhai, Y.; Wang, E., Nafion-graphene nanocomposite film as enhanced sensing platform for ultrasensitive determination of cadmium. *Electrochemistry Communications* **2009,** *11*, 1085-1088.

[35] Helwa, Y.; Dave, N.; Froidevaux, R.; Samadi, A.; Liu, J., Aptamer-Functionalized Hydrogel Microparticles for Fast Visual Detection of Mercury(II) and Adenosine. *Acs Applied Materials & Interfaces* **2012,** *4*, 2228-2233.

[36] Famulok, M., Oligonucleotide aptamers that recognize small molecules. *Current Opinion in Structural Biology* **1999,** *9*, 324-329.

[37] Gallego, J.; Varani, G., Targeting RNA with small-molecule drugs: Therapeutic promise and chemical challenges. *Accounts of Chemical Research* **2001,** *34*, 836-843.

[38] Cruz-Aguado, J. A.; Penner, G., Determination of Ochratoxin A with a DNA Aptamer. *Journal of Agricultural and Food Chemistry* **2008,** *56*, 10456-10461.

[39] Kim, S.-E.; Su, W.; Cho, M.; Lee, Y.; Choe, W.-S., Harnessing aptamers for electrochemical detection of endotoxin. *Analytical Biochemistry* **2012,** *424*, 12-20.

[40] Famulok, M.; Mayer, G.; Blind, M., Nucleic acid aptamers - From selection in vitro to applications in vivo. *Accounts of Chemical Research* **2000,** *33*, 591-599.

[41] Tang, Z.; Parekh, P.; Turner, P.; Moyer, R. W.; Tan, W., Generating Aptamers for Recognition of Virus-Infected Cells. *Clinical Chemistry* **2009,** *55*, 813-822.

[42] McCauley, T. G.; Hamaguchi, N.; Stanton, M., Aptamer-based biosensor arrays for detection and quantification of biological macromolecules. *Analytical Biochemistry* **2003,** *319*, 244-250.

[43] Wilson, D. S.; Szostak, J. W., In vitro selection of functional nucleic acids. *Annual Review of Biochemistry* **1999,** *68*, 611-647.

[44] Ikanovic, M.; Rudzinski, W. E.; Bruno, J. G.; Allman, A.; Carrillo, M. P.; Dwarakanath, S.; Bhahdigadi, S.; Rao, P.; Kiel, J. L.; Andrews, C. J., Fluorescence assay based on aptamer-quantum dot binding to Bacillus thuringiensis spores. *Journal of Fluorescence* **2007,** *17*, 193-199.

[45] Zelada-Guillen, G. A.; Luis Sebastian-Avila, J.; Blondeau, P.; Riu, J.; Xavier Rius, F., Label-free detection of *Staphylococcus aureus* in skin using real-time potentiometric biosensors based on carbon nanotubes and aptamers. *Biosensors & Bioelectronics* **2012,** *31*, 226-232.

[46] Michaud, M.; Jourdan, E.; Villet, A.; Ravel, A.; Grosset, C.; Peyrin, E., A DNA aptamer as a new target-specific chiral selector for HPLC. *Journal of the American Chemical Society* **2003,** *125*, 8672-8679.

[47] Schafhaeutl, C., Ueber die Verbindungen des Kohlenstoffes mit Silicium, Eisen und anderen Metallen, welche die verschiedenen Gallungen von Roheisen, Stahl und Schmiedeeisen bilden. *Journal für Praktische Chemie* **1840,** *21*, 129-157.

[48] Brodie, B. C., On the Atomic Weight of Graphite. *Philosophical Transactions of the Royal Society of London* **1859,** *149*, 249-259.

[49] Ruess, G.; Vogt, F., *Hochstlamellarer kohlenstoff aus graphitoxyhydroxyd - Uber den ort aktiven eigenschafen am kohlenstoffkristall. *Monatshefte Fur Chemie* **1948,** *78*, 222-242.

[50] Boehm, H. P.; Clauss, A.; Fischer, G. O.; Hofmann, U., Das adsorptionsverhal sehr dunner kohlenstoff-folien. *Zeitschrift Fur Anorganische Und Allgemeine Chemie* **1962,** *316*, 119-127.

[51] Lu, X. K.; Yu, M. F.; Huang, H.; Ruoff, R. S., Tailoring graphite with the goal of achieving single sheets. *Nanotechnology* **1999,** *10*, 269-272.

[52] Novoselov, K. S.; Geim, A. K.; Morozov, S. V.; Jiang, D.; Zhang, Y.; Dubonos, S. V.; Grigorieva, I. V.; Firsov, A. A., Electric field effect in atomically thin carbon films. *Science* **2004,** *306*, 666-669.

[53] Novoselov, K. S.; Geim, A. K.; Morozov, S. V.; Jiang, D.; Katsnelson, M. I.; Grigorieva, I. V.; Dubonos, S. V.; Firsov, A. A., Two-dimensional gas of massless Dirac fermions in graphene. *Nature* **2005,** *438*, 197-200.

[54] Geim, A. K.; Novoselov, K. S., The rise of graphene. *Nature Materials* **2007,** *6*, 183-191.

[55] Wu, J.; Pisula, W.; Muellen, K., Graphenes as potential material for electronics. *Chemical Reviews* **2007,** *107*, 718-747.

[56] Bieri, M.; Treier, M.; Cai, J.; Ait-Mansour, K.; Ruffieux, P.; Groening, O.; Groening, P.; Kastler, M.; Rieger, R.; Feng, X.; Muellen, K.; Fasel, R., Porous graphenes: two-dimensional polymer synthesis with atomic precision. *Chemical Communications* **2009,** 6919-6921.

[57] Siemsen, P.; Livingston, R. C.; Diederich, F., Acetylenic coupling: A powerful tool in molecular construction. *Angewandte Chemie-International Edition* **2000,** *39*, 2633-2657.

[58] Zhang, W.; Moore, J. S., Alkyne metathesis: Catalysts and synthetic applications. *Advanced Synthesis & Catalysis* **2007,** *349*, 93-120.

[59] Schultz, M. J.; Zhang, X.; Unarunotai, S.; Khang, D.-Y.; Cao, Q.; Wang, C.; Lei, C.; MacLaren, S.; Soares, J. A. N. T.; Petrov, I.; Moore, J. S.; Rogers, J. A., Synthesis of linked carbon monolayers: Films, balloons, tubes, and pleated sheets. *Proceedings of the National Academy of Sciences of the United States of America* **2008,** *105*, 7353-7358.

[60] Radushkevick, L. V.; Lukyanovich, V. M. O strukture ugleroda, obrazujucegosja pri termiceskom razlozenii okisi ugleroda na zeleznom kontakte. **1952**,88-95.

[61] Oberlin, A.; Endo, M.; Koyama, T., Filamentous growth of carbon through benzene decomposition. *Journal of Crystal Growth* **1976,** *32*, 335-349.

[62] Iijima, S., Helical microtubules of graphitic carbon. *Nature* **1991,** *354*, 56-58.

[63] Kim, S. N.; Rusling, J. F.; Papadimitrakopoulos, F., Carbon nanotubes for electronic and electrochemical detection of biomolecules. *Advanced Materials* **2007,** *19*, 3214-3228.

[64] Dekker, C., Carbon nanotubes as molecular quantum wires. *Physics Today* **1999,** *52*, 22-28.

[65] Dai, H. J., Carbon nanotubes: Synthesis, integration, and properties. *Accounts of Chemical Research* **2002,** *35*, 1035-1044.

[66] Bobacka, J.; Ivaska, A.; Lewenstam, A., Potentiometric ion sensors. *Chemical Reviews* **2008,** *108*, 329-351.

[67] Bakker, E.; Buhlmann, P.; Pretsch, E., The phase-boundary potential model. *Talanta* **2004,** *63*, 3-20.

[68] Buhlmann, P.; Yajima, S.; Tohda, K.; Umezawa, Y., EMF response of neutral-carrier based ion-selective field-effect transistors with membranes free of ionic sites. *Electrochimica Acta* **1995,** *40*, 3021-3027.

[69] Bakker, E.; Pretsch, E., Lipophilicity of tetraphenylborate derivates as ionic sites in neutral carrier-based solvent polymeric membranes and lifetime of corresponding ion-selective electrochemical and optical sensors. *Analytica Chimica Acta* **1995,** *309*, 7-17.

[70] Johnson, R. R.; Johnson, A. T. C.; Klein, M. L., Probing the structure of DNA-carbon nanotube hybrids with molecular dynamics. *Nano Letters* **2008,** *8*, 69-75.

[71] Liu, J.; Li, Y.; Li, Y.; Li, J.; Deng, Z., Noncovalent DNA decorations of graphene oxide and reduced graphene oxide toward water-soluble metal-carbon hybrid nanostructures via self-assembly. *Journal of Materials Chemistry* **2010,** *20*, 900-906.

[72] Hong, Y.; Brown, D. G., Electrostatic behavior of the charge-regulated bacterial cell surface. *Langmuir* **2008,** *24*, 5003-5009.

[73] Currie, L. A., Nomenclature in evaluation of analytical methods including detection and quantification capabilities. *Pure and Applied Chemistry* **1995,** *67* , 1699-1723.

[74] E. R. Cohen; T. Cvitas; J. G. Frey; B. Holmström; K. Kuchitsu; R. Marquardt; I. Mills; F. Pavese; M. Quack; J. Stohner; H.L. Strauss; M. Takami; A.J. Thor, *Quantities, Units and Symbols in Physical Chemistry, IUPAC Green Book, 3rd Edition*. IUPAC & RSC Publishing: 2007.

[75] Bakker, E.; Pretsch, E., Potentiometric sensors for trace-level analysis. *Trac-Trends in Analytical Chemistry* **2005,** *24*, 199-207.

[76] Fibbioli, M.; Morf, W. E.; Badertscher, M.; de Rooij, N. F.; Pretsch, E., Potential drifts of solid-contacted ion-selective electrodes due to zero-current ion fluxes through the sensor membrane. *Electroanalysis* **2000,** *12*, 1286-1292.

UNIVERSITAT ROVIRA I VIRGILI
SOLID CONTACT POTENTIOMETRIC SENSORS BASED ON CARBON NANOMATERIALS
Rafael Hernández Malo

UNIVERSITAT ROVIRA I VIRGILI
SOLID CONTACT POTENTIOMETRIC SENSORS BASED ON CARBON NANOMATERIALS
Rafael Hernández Malo

3.1. Introduction.

A detailed vision of the steps to construct solid contact electrodes is given in Chapter three. This chapter contains information about the general experimental part of the thesis. It is mainly divided into three sections. The first section is focused on obtaining the carbon nanomaterials materials used (the transducer part of the electrodes), giving information about purifications and reactions involved. The second section defines the development and construction of the electrodes, and finally, the third section explains the principal microscopic and electrochemical techniques used to characterise the electrodes.

3.2. Reagents.

3.2.1. Carbon Nanomaterials.

The carbon nanomaterials used as transduction layer in this thesis were:

- Single-walled carbon nanotubes (SWCNTs), 95% purity (outer diameter: 1-2 nm, length: 10-20 μm) purchased from Carbolex Inc (Lexington, Kentuky, USA)
- Graphite powder, <45 μm, ≥99.99% purchased from Sigma Aldrich (Tres Cantos, Madrid, Spain)

Graphite powder was the starting point to obtain graphene oxide (GO) and reduced graphene oxide (RGO). The procedure for obtaining these nanomaterials is defined in section 3.3.2.2

3.2.2. Polymeric membranes.

3.2.2.1. Membrane matrices.

The backbone material used for membrane preparation in Ca^{2+}-ISEs in this thesis was plasticiser-free acrylic moisture based basically on a copolymer of n-butyl acrylate (*n*BA) and methyl methacrylate (MMA). The monomers were purchased from sigma Aldrich and mixed in a proportion of 1:10. A radical initiator was used to begin the copolymerization reaction, the 2,2-Azobis(2-methylpropionitrile) (AIBN) purchased from Fluka. Other reagents in this reaction were ethanol, dichloromethane and high boiling point petroleum ether (80-100ºC) purchased from Sigma Aldrich. Reagent grade benzene was purchased from Fluka.

3.2.2.2. Ion selective membrane components.

In addition to the acrylic polymeric matrix, the ionophore used in Ca^{2+}-ISEs was N,N,N'-N'-tetraciclohexyl-3-oxapentanediamide (ETH129, selectophore grade), and the lipophilic salt was potassium tetrakis[3,5-bis-(trifluoromethyl) phenyl]borate (KTFPB), both purchased from Fluka.

3.2.3. Culturing media and microorganisms.

In the case of the aptasensors, the used single strain DNA specific for *Staphylococcus aureus* were synthetic polynucleotides modified (see figure 3.1.) for the specific interaction with the graphene-based nanomaterials purchased from Eurogenetec S.A. (Liège, Belqium)

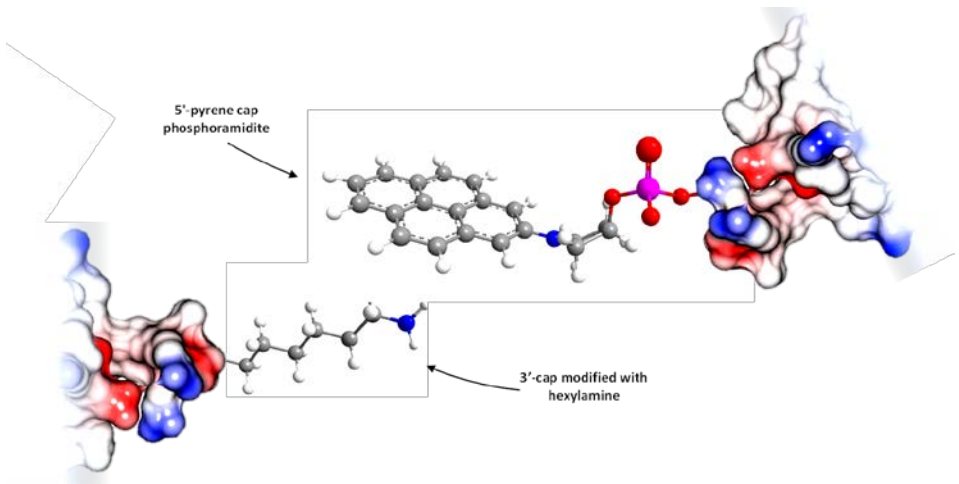

Figure 3.1. Details of 5'-pyrene cap phosphoramidite and 3'-cap modified with hexylamine functionalization for the aptamer used for the detection of *Staphylococcus aureus*.

- Single strain DNA 5'-cap modified with 5'-pyrene cap phosphoramidite for the non-covalent functionalisation of reduced graphene oxide.
  Sequence:
  5'GCAATGGTACGGTACTTCCGCGCCCTCTCACGTGGCACTCAGAGTGCCGG
  AAGTTCTGCGTTATCAAAAGTGCACGCTACTTTGCTAA-3'

- Single strain DNA 3'-cap modified with hexylamine for the covalent functionalisation of graphene oxide.
  Sequence:
  5'GCAATGGTACGGTACTTCCTCCCACGATCTCATTAGTCTGTGGATAAGCG
  TGGGACGTCTATGACAAAAGTGCACGCTACTTTGCTAA-3'

Lyophilized strains of *Salmonella Typhi* (CECT 409), *Lactobacillus casei* subsp. *casei* (CECT 4180), *Escherichia coli* (CECT 675), *Staphylococcus aureus* (CECT 4630) were purchased from Colección Española de Cultivos Tipo (Valencia, Spain).

The following culturing media were purchased from Becton, Dickinson and Company (Sparks, USA), prepared according to indications.

- Lactobacilli MRS (deMan, Rogosa and Sharpe) agar. This medium was used in the isolation, enumeration and cultivation of *Lactobacillus* species. **[1,2]**
- Lactobacilli MRS (deMan, Rogosa and Sharpe) broth. This medium was used in the isolation, enrichment and cultivation of *Lactobacillus* species. **[1,2]**
- Tryptic soy agar (TSA). This non-selective medium was used in the enumeration and cultivation of pure strains of *Salmonella typhi*, *Staphylococcus aureus* and *Escherichia coli*. **[2]**
- Tryptic soy broth (TSB). This non-selective medium was used in the enrichment and cultivation of pure strains of *Salmonella Typhi*, *Staphylococcus aureus* and *Escherichia coli*. **[2]**
- MacConkey agar. This medium was used for isolation, differentiation and confirmatory growth of *Escherichia coli*. **[2]**
- Lysogeny broth and agar (Luria-Bertani medium, LB). This medium was used for maintenance, enumeration and growth of *Escherichia coli* strains. **[2]**

All the bacteria strains were cultured following standard microbiological techniques, using adequately sterilized materials, solutions and culturing media.

Lyophilized pure strains of *Salmonella Typhi* (CECT 409), *Lactobacillus casei* subsp. casei (CECT 4180), *Escherichia coli* (CECT 675), *Staphylococcus aureus* (CECT 4630) were reactivated with NaCl 0.85 % and further incubated in broth for 24-48 h at 37 °C. The pellet was then transferred to selective agar medium and subcultured for 24-48 h at 37

°C in order to confirm the purity of the strains. The selective medium used in this latter step depended on the cultured bacteria. Characteristic colonies were transferred to non-selective broth and agar media and cultured for 24-48 h at 37 °C. Colonies obtained in agar cultures were then transferred to glycerol/TSB 20:80 and stored at -20 °C until needed and reactivated by inoculating the bacteria in 10 mL of sterile broth medium at 37 °C for 24 h. Bacteria grown in non-selective broth were used for testing of biosensors.

3.2.4. Other materials.

Other reagents used to prepare the different solutions for the calibration process were L-malic acid, ammonium citrate, potassium nitrate, potassium phosphate dibasic, magnesium citrate tribasic nonahydrate, L-arginine, ammonium tartrate dibasic and tetrahydrofuran, all purchased from Fluka.

Acetone, lithium acetate, potassium chloride, dimethylformamide (DMF), calcium nitrate, sodium nitrate, sulphuric acid, potassium permanganate, hydrazine monohydrate, N-(3-dimethylaminopropyl)-N'-ethyl-carbodiimide hydrochloride (EDC), N-hydroxysuccinimide (NHS), 2-(N-morpholino) ethannesulfonic acid (MES) and phosphate buffered saline (PBS) pH 7.4 were purchased from Sigma-Aldrich.

All the solutions prepared for performance tests were made with double deionised water (18.2 MΩ·cm specific resistance) using a MilliQ PLUS reagent grade water system (Millipore Corporation, Bedford, USA)

Abrasive paper (Carbimet 600/P1200) and alumina with different grain size (30, 5, 1 and 0.03 µm Micropolish II) were obtained from Buehler (Lake Bluff, Illinois, USA).

Euphorbia characias (figure 3.2.) sap exudates were collected during the autumn from the banks of the river Francolí in Tarragona, Spain. A small cut was made in plant specimens and allowed to bleed for a few seconds. Immediately following collection, the exudates were frozen at -20 °C.

Figure 3.2. *Euphorbia characias plants used in the tests performedin chapter 4.*

For the body construction of electrodes, glassy carbon rods Sigradur® G grade with a length of 50 mm and a diameter of 3 mm were purchased from Hochtemperatur-Werkstoffe GMBH, (Thierhaupten, Germany). Copper wires and teflon were purchased from RS Amidata (Madrid, Spain).

Materials, culturing media and solutions were sterilized by autoclaving at 121°C for 15 minutes in a J.P. Selecta autoclave model Med 12 (Barcelona, Spain). All the microbiological cultures were incubated in an incubator model 100-800, Memmert GmbH Co KG (Schwabach, Germany).

3.3. Development of solid-contact electrodes.

This section provides an extended description of the setting-up of the solid-contact electrodes developed in this thesis, from the body construction to the coupling joint between the sensing part and the transducer.

3.3.1. Obtaining the conductor substrates.

A glassy carbon rod with a length of 50 mm and a diameter of 3 mm (sigradur® G grade, Hochtemperatur-Werkstoffe GMBH, Germany) was used as a conducting core of the electrode. The glassy carbon (GC) rod was polished several times first with a sheet of abrasive paper (Buehler Carbimet 600/P1200) and then with different grain-sized alumina (30, 5, 1 and 0.5 µm) to obtain a glass-like surface

The polished GC rods were jacketed with a hard teflon body (40 mm in length, diameter 6mm) by mechanical pressure in order to prevent possible contact of the sample solution with the conductor element (GC rod) in membrane-free electrodes, which can promote instabilities in the electrical signal.

It is important to clean and polish the surface of the conducting wire in order to ensure the contact with the transduction part which enlarges the lifetime of the electrode. Poor contact between the transducer and conductive wire may cause drifts and signal interferences.

The steps used in this procedure were:

First, the glassy carbon rod is inserted in the teflon body by mechanical aid using a miller (Proxon FF 400, Niersbach, Germany). All polishing is carried out with the glassy carbon jacketed in order to reduce the edge effect.

A piece of Buehler Carbimet 600 abrasive paper is placed in a dry and clean glass plate, and the electrode is polished against the sandpaper, keeping the electrode surface parallel to the sandpaper surface. The small alumina particles are cleaned off of the electrode using distilled water and an ultrasonicaton bath. This step is repeated several times until a clear and homogenous surface is obtained.

Further on, a nylon polishing pad (white colour) is placed firmly in a new dry and clean glass plate with care to make sure no air bubbles are trapped between the pad and the glass plate. A small amount of 1 micron Alpha alumina powder is placed in the polishing pad and everything is wetted with distilled water. The electrode is held vertically and polished in the same way as the previous step against the alumina slurry using a circular motion while pressing firmly. After 10 minutes of polishing, the electrode is rinsed thoroughly with distilled water using an ultrasonication bath to remove the remaining alumina particles. This step is repeated on a new nylon polishing pad using a 0,3 micron Alpha alumina powder.

The last polishing step is repeated using a microcloth polishing pad (brown colour) with 0,05 micron Gamma alumina powder to obtain a mirror-like finish. The electrode is rinsed one more time with distilled water using an ultrasonication bath. It is important to remark that, before going to the next smaller size of alumina powder, one has to thoroughly rinse the electrode and hands with large quantity of water. If one is not

careful in the process and larger powder particles are carried to the smaller powder polishing pad, it will never get the mirror effect expected.

Finally, using a clean polishing cloth with the polished electrode face downwards, all the extra particles are removed.

In the same way, a similar procedure was used to construct copper electrodes. Copper wires (length 50 mm and diameter 1,13 mm, Amidata) were polished using abrasive paper (Carbimet 600/P1200, Buehler) and subsequently treated with alumina of different grain-size (30, 5, 1 and 0,03 µm Micropolish II, Buehler).

3.3.2. Obtaining carbon nanomaterials.

Three different carbon nanomaterials have been used in this thesis: SWCNTs, graphene oxide (GO) and reduced graphene oxide (RGO). In the case of SWCNTs, their only pretreatment was purification and oxidation to obtain the desired material. In the other part, graphene-based nanomaterials have been obtained in a redox process with exfoliation stages.

3.3.2.1. Purification of SWCNTs.

Commercial SWCNTs contain certain levels of impurities such as amorphous carbon and catalytic nanoparticles from their synthesis process. It is necessary to remove these nanoparticles that can influence the electrochemical behaviour of the electrodes. Figure 3.3 shows the schematic process of the raw material.

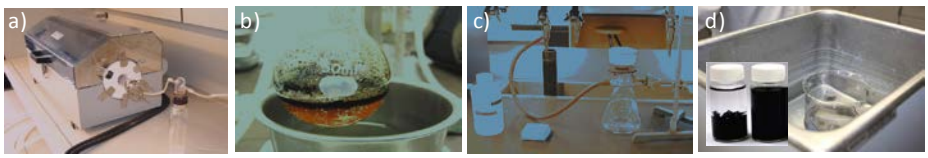

Figure 3.3. SWCNTs purification process scheme comprising a) dry oxydation of raw material, b) wet oxidation, c) vacuum filtration and d) low bath sonication. Inset in figure 3.3 d) shows the sonication effect after purification

A modified Furtado's method **[3]** for the purification and debundling of SWCNTs was followed. As a first step, a dry oxidation of the raw material was carried out in order to remove the amorphous carbon present in the material. A certain amount of SWCNTs

(250 mg) were deposited in a quartz tubular reactor (120 cm length x 4 cm diameter, Afora (Madrid, Spain)) and heated in a horizontal split tube furnace (HST/600, Carbolite) at 365 ºC for 90 min under a dry airflow current (100 $cm^3 \cdot min^{-1}$, Carburos Metálicos).

SWCNT growth needs metallic nanoparticles that act as a precursor, and could remain in the raw material affecting the electrochemical behaviour of SWCNTs **[4]**. SWCNTs obtained from the dry oxidation were refluxed in a 2.6M HNO_3 solution for 4 hours, obtaining a black-coloured solution. The solution is filtrated under vacuum in a 5 µm pore size polycarbonate membrane and washed with water. The resultant brown-coloured solution is neutralized with NaOH.

Finally, the SWCNTs are redispersed in N,N-dymethylformamide (DMF) and ultrasonicated for 4 hours in a low power bath. This method produces stable dispersions of SWCNTs in DMF, avoiding the use of surfactants to disperse the nanotubes, and eliminating washing steps to remove the surfactant.

3.3.2.2. Obtaining of graphene-based nanomaterials.

Graphite oxide was prepared using a modified Hummer's method from graphite powder using $NaNO_3$, H_2SO_4 and $KMnO_4$ in an ice bath **[5]**. Graphite powder (20 g) was put into cold (0 °C) concentrated H_2SO_4 (460 ml). $KMnO_4$ (60 g) was added gradually with stirring and cooling, so that the temperature of the mixture was not allowed to reach 20 °C. The mixture was then stirred at 35 °C for 2 h, and distilled water (920 ml) was added. In 15 min, the reaction was terminated by the addition of a large amount of distilled water (2.8 l) and 30% H_2O_2 solution (50ml), after which the colour of the mixture changed to bright yellow. The mixture was filtered and washed with 1:10 HCl solution (5 l) in order to remove metal ions. The GO product was suspended in distilled water to give a viscous, brown, 2% dispersion, which was centrifuged at a medium speed (4000 rpm) according to an experimental procedure described recently **[6]**, yielding a brown-coloured water solution homogeneous of exfoliated graphene oxide sheets (GO) with a final concentration of 0.45 mg/ml. Final exfoliation was achieved by dilution of the 0.45 mg/ml GO dispersion (1 ml) with deionized water (24 ml), followed by 15 min sonication. The resulting homogeneous yellow-brown solution, which contained 0.2 g/l GO, is stable for a period of months. GO dispersions of lower

concentrations were prepared diluting the mentioned 0.2 g/l dispersion with deionized water.

Reduction of deposited GO (see figure 3.4) was performed by a 24h exposure of electrodes to hydrazine hydrate vapours **[7]** (*caution*: hydrazine vapours are highly toxic). This reduction method allowed a complete reduction of graphene oxide sheets (RGO) while maintaining the smooth and homogeneous morphology of the deposited films.

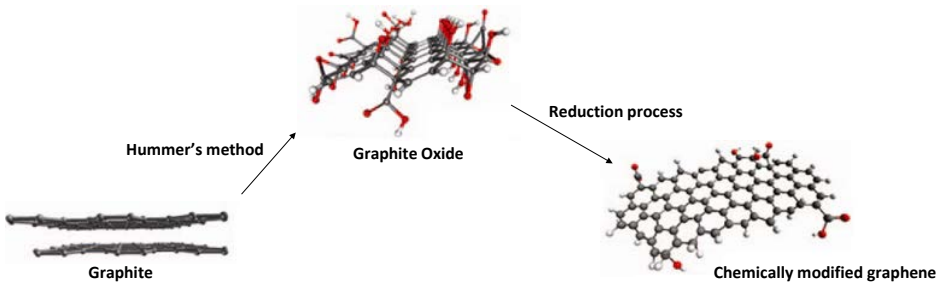

Figure 3.4. Graphite and graphene oxide schematic synthesis from graphite powder.

3.3.3. Deposition of carbon nanomaterials.

Three different methods have been used to deposit carbon nanomaterials onto the surface of the polished glassy carbon electrodes. SWCNTs were deposited by means of spraying, while drop casting and mechanical exfoliation were used to deposit graphene-based nanomaterials.

3.3.3.1. Spraying.

The deposition of SWCNTs was done using a spray technique where 10 mg of purified SWCNTs were dispersed in 10 ml of pure DMF and homogenised by ultrasonication in a tip sonicator for 30 min (amplitude 50%, cycle 0.5, Ultraschallprozessor UP200S, Dr. Hielscher).

The fresh SWCNT dispersion is then placed in an aerograph at a distance of approximately 30 cm from the electrode. A heat gun also is focused on the electrode in order to evaporate the solvent as soon as possible. The number of sprays and the time of addition are the representative variables to obtain different thicknesses of the

membrane. Typical sprays of 2 seconds of duration followed by dry steps with the heat gun produce 30 µm thicknesses on average for 30 repetitions of the process approximately (see figure 3.5).

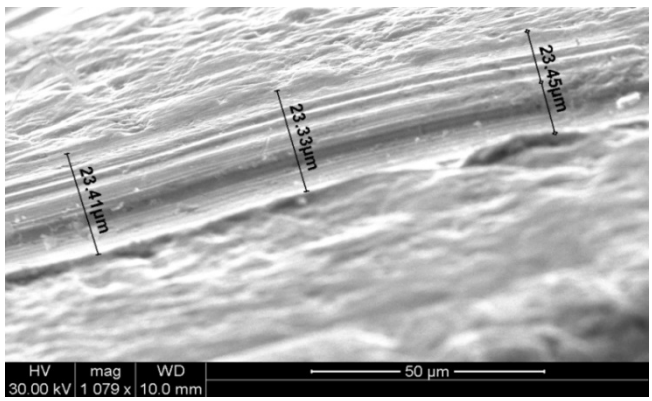

Figure 3.5. ESEM image for a deposition of SWCNTs (20 repetitions).

3.3.3.2. Drop casting

The drop casting method has been used for the deposition of graphene and graphene oxide, obtaining a high control of the thickness of the graphene-based materials layer. Depending of the desired thickness, the control of the amount of deposited material is done by diluting the initial graphene oxide dispersion. 15 µl of homogeneous graphene oxide dispersion were drop-casted and dried upside down at room temperature for 60 minutes obtaining a 125 nm layer thickness. This method was performed with several depositions in order to assure the linearity of the layer with the volume added (see appendix 8.2.2.1.2)

3.3.4. Preparation of the recognition layer.

Two different recognition layers have been used in this thesis, depending on the target analyte to detect. In the first part, calcium ions were the focus of our research, and calcium-selective membranes were prepared using acrylic matrix as a support (either using SWCNTs or graphene-based materials as solid transducers). For the detection of *Staphylococcus aureus*, the recognition layer was based on the aptamer bonding to the transduction layer (graphene-based material) by covalent and non-covalent interactions.

3.3.4.1. Ion selective membrane preparation.

The preparation of the acrylic-based ion-selective membrane (see figure 3.6) consists of two parts, the *acrylic membrane preparation* where the core of the membrane is synthetized, and the *proper ion-selective membrane formation* with the inclusion of the ionophore.

Acrylic membrane preparation. The method used in this thesis was solution polymerization initiated by free radicals, although other polymerization methods as photopolimerization can be used for acrylic matrices synthesis **[8]**.

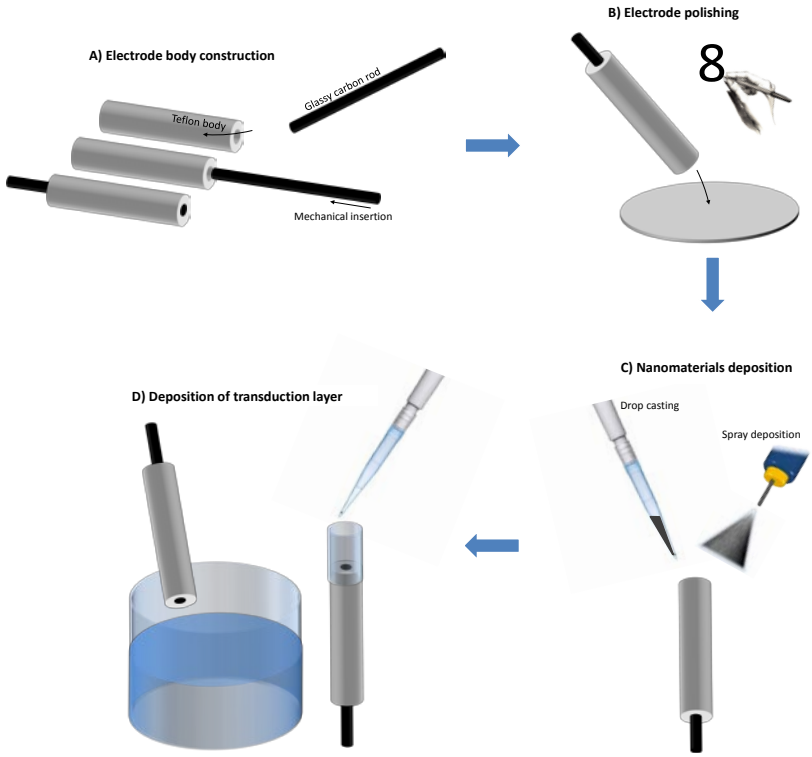

Figure 3.6. Image of the basic ISE-electrode construction including: a) mechanical electrode construction where a glassy carbon rod is jacketed in a teflon body, b) the electrode polishing simulating a writing number 8 in order to homogenize the surface as much as possible, c) deposition of transduction layer by drop coating or spray deposition depending on the material added and d) deposition of the sensing membrane by drop coating.)

This type of polymerization technique has the advantage of simplicity and introduces little or no ionic contaminants which may interfere with the ionic response of the polymer.

Several combinations of monomers can be used to construct an acrylic membrane (see figure 3.7). In this thesis, a combination of methylmetacrylate and n-butyl acrylate has been chosen in a 1:10 proportion. This selection has been chosen only for bibliographic reasons. A higher content of *n*BA helps to lower the T_g of membrane, producing a slightly better selectivity of the membrane **[8]**.

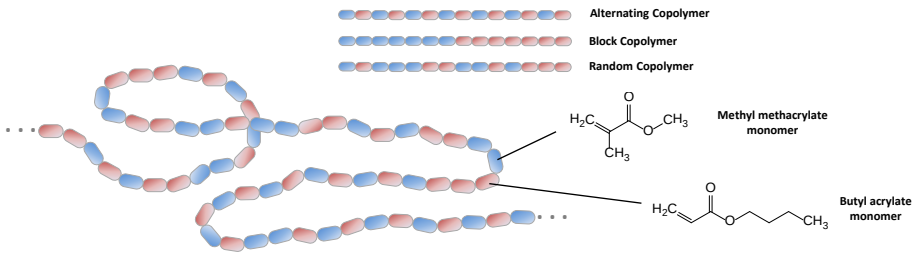

Figure 3.7. Schematic representation of the copolymer produced, based in nBA and MMA monomers. The upper part shows the different polymerizations depending on the disposition of monomers across the polymer chain.

Appropriate amounts of methylacrylate and n-butyl acrylate monomers are added to 100 ml of dry benzene (anhydrous 99,8%) in a flask. The solution is degassed for 15 minutes by bubbling with a stream of nitrogen gas. The polymerization reaction begins by adding a suitable amount of initiator and heating the solution to a constant temperature of 80ºC for 12 hours. The initiator used in this polymerization is 2,2-azobis(2-methylpropionitrile) commonly named AIBN. Its most common chemical reaction is one of decomposition, eliminating a molecule of nitrogen gas to form two 2-cyanoprop-2-yl radicals as described in figure 3.8.

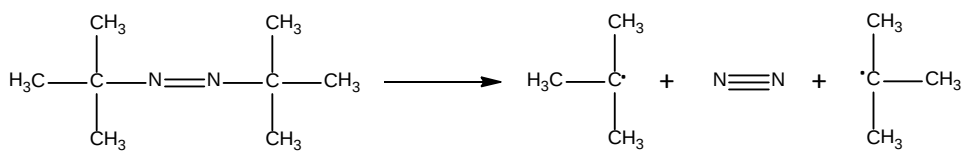

Figure 3.8. Radicalary decomposition reaction of AIBN.

Acrylic matrices synthesis. During this step, the solution becomes increasingly viscous. After this step, the polymer solution is cooled and high boiling point (80-100 ºC) petroleum ether is added in a proportion of ten times the volume of the polymer solution. It is then noted that white flaky precipitates appears depending of the amount of nBA used during the polymerization. The final precipitate is dried in a rotavapour under vacuum conditions for 2 hours. The composition of this membrane as well as the amount of petroleum ether necessary to obtain the polymeric precipitate is shown in the following table.

Table 3.1. Composition of a 1:10 acryclic membrane

Monomer composition				**Benzene**		**Initiator**		**Petroleum ether**
Monomer	*Mmol*	*g*	*ml*	*g*	*ml*	*mg/ml benzene*	*mg*	*ml*
MMA	4	0,40	0,42	2,62	3,0	0,96	2,88	≈ 100
nBA	43	5,54	6,10					

After this procedure, the polymer is removed from the flask and kept at room temperature in a desiccator. The use of a high *n*BA content in the solution results in sticky polymers, hindering the obtaining of the final polymer.

Preparation of the ion-selective membrane. The final ion-selective membrane selected in this thesis is a membrane with 2.0 wt% ionophore content with a 3.2:1.0 molar ratio of ionophore and ionic sites (equivalent to 31.2 mol% of lipophilic anion relative to the ionophore). For the preparation of the ion-selective membrane, 195 mg of the prepared acrylic membrane were deposited in an Eppendorf tube and dissolved in 2.0 ml of dichloromethane **[9-11]** with the suitable amount of ionophore and lipophilic salt and stirred in a vortex until the complete dissolution of the components. The composition of this is shown in the following table.

Table 3. 2. Composition of the Ca^{2+}-Ion selective membrane

Component	**Ammount**		**Fraction**
	mg (or ml)	*mol*	*%*
Polymeric matrix	195		
Ionophore (ETH129)	3,90	$8{,}47 \times 10^{-6}$	2% wt (related to polymeric matrix)
Lipophilic salt	1,31	$2{,}64 \times 10^{-6}$	31,2% mol related to the ionophore
Dichloromethane	2		

After preparing the ion-selective membrane, it is kept inside a freezer to avoid the evaporation of the dichloromethane. The Eppendorf tube, which contains the membrane, is covered with parafilm. Before drop casting the cocktail was degassed by sonication for 10 min **[12]**.

Deposition of the sensor part. A short piece of thermoplastic was placed in the polished cap (see figure 3.6) of the electrode and heated with a heat gun until it fit to the electrode body in order to hold the liquid membrane for the deposition. 150 µl (3x50 µl) of the cocktail membrane were dissolved in dichloromethane and placed on the electrode, ensuring a slow evaporation of the solvent and thus avoiding the formation of undesired bubbles.

3.3.4.2. Aptamer bonding.

Two different strategies (see figure 3.9) were used for the detection of *Staphylococcus aureus*: covalent bonding and non-covalent bonding of aptamers to the transducer layer of the aptasensor.

3.3.4.2.1. Covalent bonding

As has been shown in section 3.3.2.2, graphene oxide moieties contain carboxylic groups. In order to create active points of anchorage for the covalent bonding, an activation of these carboxylic acids is needed.

Graphene oxide electrodes were introduced in a solution of N-(3-dimethylamino-propyl)-N′-ethyl-carbodiimide (EDC, 100 nM) and H-hydroxysuccini-mide (NHS, 25 nM) in a 2-(N-morpholino) ethane sulfonic acid buffer (MES, 50 nM) at pH 5 for 30 min to activate the carboxylic groups.

Finally, electrodes were immersed overnight into 0.5 ml of a 1 µM 3′-cap modified with hexylamine binding aptamer solution dispersed in PBS pH 7.4 (1 mM) and conditioned for its use.

3.3.4.2.2. Non-covalent bonding

In the case of the RGO electrodes, non-covalent functionalization of the 5′-cap modified with 5'-pyrene cap phosphoramidite binding aptamer was carried out by depositing a drop of the 1 µM aptamer dispersed in PBS pH 7.4 (1 mM) and leaving overnight in a wet atmosphere.

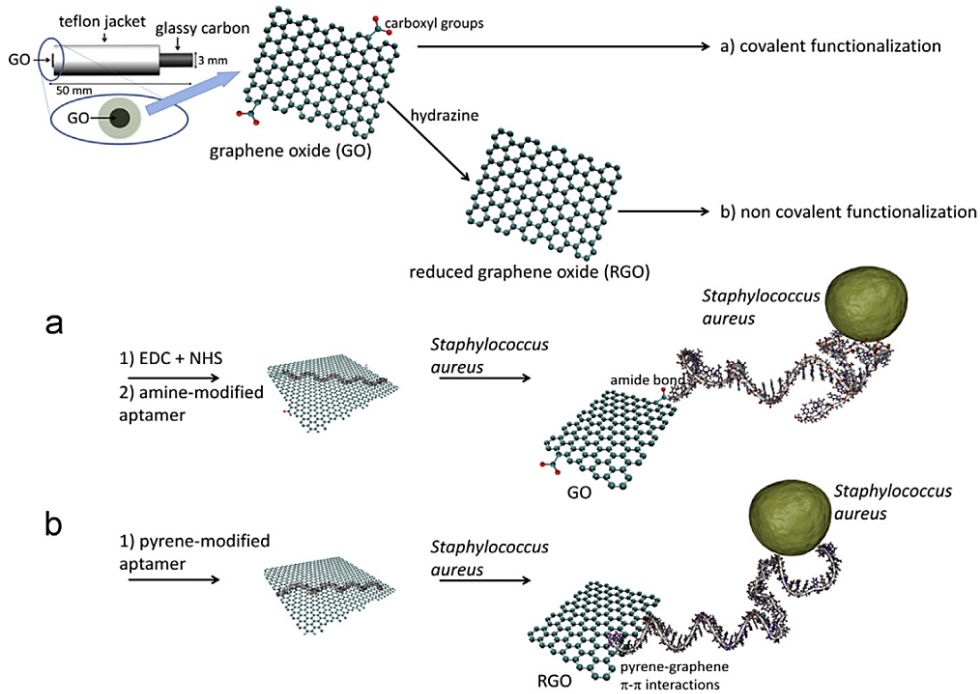

Figure 3.9. Schematic representation of the two strategies followed for the a) covalent and the b) non-covalent functionalization of graphene nanomaterials for the detection of bacteria.

3.3.5. Conditioning and regeneration of electrodes.

In the case of the ISEs, the conditioning process was performed in two steps in order to reach lower limits of detection. In the first stage, the electrodes were placed in a relatively concentrated solution of the primary ion ($CaCl_2$ 10^{-3} M) for one day in order to exchange all the interfering ions of the membrane for the target ion (Ca^{2+}). After this stage, the electrodes were rinsed with MilliQ water and then conditioned for two more days in a 10^{-9} M solution of $CaCl_2$ to completely clean the membrane of any interfering ions **[13,14]**.

Once the electrodes had been preconditioned, those are rinsed with MilliQ water and placed in a second solution in this case more diluted than the previous one (10^{-9} M) for 48 h.

In the case of aptasensors, the conditioning process is performed by depositing the electrodes in an autoclaved PBS solution overnight inside a Biosafety level II cabinet in order to assure no contamination of the solution from the environment.

Regeneration of ISEs can be done by a common conditioning process, but in the case of aptasensors, bacteria that have been caught by the aptamers have to be detached from the aptamers. This regeneration is done by incubating the electrodes in a 2 M NaCl solution by 1 hour, followed by a washing step in MilliQ water for 90 min. After this, the electrode is reconstituted by conditioning in PBS buffer.

3.4. Electrode characterisation.

In this section the electrochemical, microscopic and spectroscopic techniques employed for the characterization of the electrodes will be briefly described, detailing the equipment used and the variables at which the data has been recorded.

3.4.1. Microscopic characterisation.

3.4.1.1. Atomic Force Microscopy (AFM) and confocal microscopy.

A Multimode 8 with control electronics Nanoscope V (Bruker Corporation, Karlsruhe, Germany) AFM was used in order to obtain information about morphology of carbon nanotubes and its disposition over the electrodes and also to measure the thickness of the graphene layer deposited. Confocal microscopy LEICA Dual Core 3D measuring Microscope 3D equipment was used to control the thickness of graphene depositions.

3.4.1.2. Transmission Electron Microscopy (TEM)

The transmission electron microscopy used was a JEM 1011 (Jeol Ltd., Japan) and all the samples were imaged by depositing a drop solution in a copper grid and leaving the solvent to evaporate. This technique is applied to very thin materials or solutions, and in the case of this thesis has been applied to characterize these purification steps of SWCNTs and ensure that all the carbonaceous matter and catalytic impurities have been removed and to observe the interaction between bacteria and graphene sheets. 100 kV voltage and 20-200K increase were the typical conditions used.

3.4.1.3. Scanning Electron Microscopy (SEM)

Two different scanning electron microscopies were used in this thesis. An environmental scanning electron microscopy (E-SEM, Quanta 600, FEI, Hillsboro) was used to characterize the SWCNT layer deposited onto the electrodes by the spraying technique, the graphene layer deposited by drop coating and the ion-selective membrane.

Experimental parameters were determined in each case to obtain the maximum resolution but normal values were high vacuum ($6x10^{-4}$) 30 kV voltage and 10 mm working distance. Ion-selective membranes were also checked by E-SEM inspection. The thickness of the membranes was measured in the same way.

Scanning Electron Microscopy (SEM, JSM 6400 Jeol) was used to characterize the CNT layer deposited onto the electrodes by the spraying technique onto copper wires.

3.4.2. Electrochemical characterisation.

3.4.2.1. Electrochemical Impedance Spectroscopy (EIS)

All the electrochemical measurements were performed in a one-compartment, three-electrode glass electrochemical cell, schematically described in figure 3.10

All the impedance measurements performed to characterise the electrodes used in this thesis were been done using a silver/silver chloride single junction reference electrode (Ag/AgCl/KCl (3M)) model 6.0733.100 (Metrohm, Switzerland). The counter electrode was a glassy carbon rod (GC) polished and the working electrodes are the different electrodes used.

All the impedance spectra were recorded in the frequency range from 100 KHz to 10 mHz using an Autolab frequency response analyzer system AUT20.FRA2 AUTOLAB, Eco chemie, B.V) and an electrochemical- Analyzer Workstation model 600 Series (CH Instruments). All the solutions used, were prepared with high concentrations ranging from 10-1 to 10-3 of the primary ion in presence of oxygen or argon/nitrogen in order to purge the oxygen present in solution, depending on the experiment.

3.4.2.2. Cyclic Voltammetry (CV)

Five cycles in the potential range -0.5 V to 0.5 V at a scan rate of 0.1 V/s were performed in each case in a 0.1 M $CaCl_2$ solution of the primary both with and without the presence of oxygen depending of the parameters required for the experiment.

3.4.2.3. Chronopotentiometry

The instrumentation to carry out the constant-current chronopotentiometric measurements was the same as the electrochemical impedance technique. Each measurement was performed using a constant current of -1 nA during 50 s followed by an inverse current of the same value for the same time (1 nA). All the measurements were made at room temperature using a 0.1 M $CaCl_2$ solution of the primary ion.

3.4.2.4. Potentiometry

A Keithley 6514 electrometer and Lawson multichannel high input impedance electrometer (10^{15} Ω) were used to record the EMF.

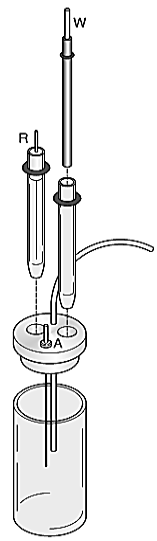

Figure 3.10. Schematic representation of a glass cell with a reference electrode (R), a working electrode (W), and a counter electrode (A) with a secondary hole for the entrance of gases like nitrogen or argon.

In the case of potentiometric measurements, a double-junction Ag/AgCl/ 3 M KCl reference electrode (type 6.0729.100, Methrom AG) containing a 1 M LiAcO electrolyte bridge was used. A commercial Ca^{2+} ion-selective electrode (Crison Instruments, ref 96 60) was used in order to compare the results obtained of the working electrode from chapter 4.

All measurements were recorded using a water-jacketed glass cell (figure 3.9) in stirred condition at room temperature (22±2 ºC) or at isothermal conditions (22±0.5 ºC) depending on the requirements of the experiment. The same cell was used for the measurements in all the experiments in order to ensure that each experiment was carried out under the same conditions.

The electrolyte used in the electrochemical cell for potentiometric measurements was typically different concentrations of aqueous Ca^{2+} solutions (Chapter 4 and 5) and PBS 1.7 mM pH 7.4 in the case of bacteria detection (Chapter 6)

3.4.3. Spectroscopic characterisation.

3.4.3.1. X-ray photoelectron spectroscopy (XPS)

X-Ray photoelectron spectroscopy was carried out on an ESCAPlus Omicron spectrometer using a monochromatized Mg X-ray source (1253.6 eV). XPS data were analyzed using the CasaXPS software in order to obtain the chemical composition of the prepared RGO material.

3.5. References.

[1] De Man, J. C.; Rogosa, M.; Sharpe, M. E., A medium for the cultivation of *lactobacilli*. *Journal of Applied Bacteriology* **1960,** *23*, 130-135.

[2] Gerhardt, P.; Murray, R. G. E.; Costillow, R. N.; Nester, E. W.; Wood, W. A.; Krieg, G. B., *Manual of methods for general bacteriology*. 1981.

[3] Furtado, C. A.; Kim, U. J.; Gutierrez, H. R.; Pan, L.; Dickey, E. C.; Eklund, P. C., Debundling and dissolution of single-walled carbon nanotubes in amide solvents. *Journal of the American Chemical Society* **2004,** *126*, 6095-6105.

[4] Heng, L. Y.; Hall, E. A. H., One-step synthesis of K+-selective methacrylic-acrylic copolymers containing grafted ionophore and requiring no plasticizer. *Electroanalysis* **2000,** *12*, 178-186.

[5] Stankovich, S.; Dikin, D. A.; Piner, R. D.; Kohlhaas, K. A.; Kleinhammes, A.; Jia, Y.; Wu, Y.; Nguyen, S. T.; Ruoff, R. S., Synthesis of graphene-based nanosheets via chemical reduction of exfoliated graphite oxide. *Carbon* **2007,** *45*, 1558-1565.

[6] Zhang, T.; Zhang, D.; Shen, M., A low-cost method for preliminary separation of reduced graphene oxide nanosheets. *Materials Letters* **2009,** *63*, 2051-2054.

[7] Robinson, J. T.; Perkins, F. K.; Snow, E. S.; Wei, Z.; Sheehan, P. E., Reduced Graphene Oxide Molecular Sensors. *Nano Letters* **2008,** *8*, 3137-3140.

[8] Heng, L. Y.; Hall, E. A. H., Taking the plasticizer out of methacrylic-acrylic membrananes for K+-selective electrodes. *Electroanalysis* **2000,** *12*, 187-193.

[9] Craggs, A.; Moody, G. J.; Thomas, J. D. R., PVC matrix membrane ion-selective electrodes - Construction and laboratory experiments. *Journal of Chemical Education* **1974,** *51*, 541-544.

[10] Michalska, A. J.; Appaih-Kusi, C.; Heng, L. Y.; Walkiewicz, S.; Hall, E. A. H., An experimental study of membrane materials and inner contacting layers for ion-selective K+ electrodes with a stable response and good dynamic range. *Analytical Chemistry* **2004,** *76*, 2031-2039.

[11] Lai, C.-Z.; Joyer, M. M.; Fierke, M. A.; Petkovich, N. D.; Stein, A.; Buhlmann, P., Subnanomolar detection limit application of ion-selective electrodes with three-dimensionally ordered macroporous (3DOM) carbon solid contacts. *Journal of Solid State Electrochemistry* **2009,** *13*, 123-128.

[12] Sutter, J.; Radu, A.; Peper, S.; Bakker, E.; Pretsch, E., Solid-contact polymeric membrane electrodes with detection limits in the subnanomolar range. *Analytica Chimica Acta* **2004,** *523*, 53-59.

[14] Lindner, E.; Umezawa, Y., Performance evaluation criteria for preparation and measurement of macro- and microfabricated ion-selective electrodes. Pure and Applied Chemistry **2008**, 80, 85-104.

UNIVERSITAT ROVIRA I VIRGILI
SOLID CONTACT POTENTIOMETRIC SENSORS BASED ON CARBON NANOMATERIALS
Rafael Hernández Malo

UNIVERSITAT ROVIRA I VIRGILI
SOLID CONTACT POTENTIOMETRIC SENSORS BASED ON CARBON NANOMATERIALS
Rafael Hernández Malo

4.1. Introduction.

Our research group showed the use of carbon nanotubes as transducer element in ion-selective electrodes. The main conclusion of these studies was that carbon nanotubes had excellent properties for use them as transducers but also how this material can overcome problems found using other materials such as sensitivity to light or CO_2. Another advantage of using carbon nanotubes is their lipophilicity prevents the formation of thin layers of water between the conductive suport and the transducer element, which layers can cause instability in the signal and decreasing the life of the electrodes.

This article shows the use of single-walled carbon nanotubes as a transducer material for the selective detection of calcium ions in complex samples such as sap plants. Sap is a fluid transported in specialized cells called xylem cells. These cells are responsable of the ransport of wáter and nutrients from roots to the leaves. Xylemathic sap consists basically of a water solution of hormones, mineral elements and other nutrients.

Plants face similar problems to those of other multicellular organisms regarding lack or excess of components such as ions. For this reason it is important to know the concentrations of ions.

This approach is the first step in the use of such sensors directly in live plants causing minimal damage for the determination of calcium in situ. Further work on the miniaturization of this type of electrodes with different types of ion-selective membrane using microelectrodes and solid state reference electrodes, would enable the determination of any ion in plants and even a continous monitoring.

For the construction of the electrode we used very cheap materials, such as fine copper wires which have intrinsic large redox reactivity. These electrodes clearly show that carbon nanotubes effectively isolate the conductive support (i.e. copper wires) from the aqueous sample, since they did not show signs of oxidation after the determination of calcium.

The Content of this chapter has-been published in the journal Analyst, year 2010, volume 135, pages 1979-1985, and co-authored by Jordi Riu and F. Xavier Rius.

4.2. Article

PAPER www.rsc.org/analyst | Analyst

Determination of calcium ion in sap using carbon nanotube-based ion-selective electrodes

Rafael Hernández, Jordi Riu* and F. Xavier Rius

Received 15th March 2010, Accepted 17th May 2010
DOI: 10.1039/c0an00148a

4.2.1. Abstract

A new reduced-size solid-state electrode using carbon nanotubes as the transducing layer has been developed for the direct determination of Ca^{2+} in sap, overcoming problems encountered by commercial ISEs analysing real complex samples. We show that this solid-contact ISE, which can be easily miniaturized, can be used directly in diluted real samples without any other pretreatment. The performance parameters of the new ISE include a Nernstian slope and excellent stability, good coefficients of selectivity, range of linearity (10^{-5}-$10^{-2.5}$ M) and limit of detection ($10^{-6.2}$ M), thus making it an excellent tool for determining Ca^{2+} in a wide range of plant species.

Key words: Solid-contact ISE, carbon nanotubes, sap, calcium, potentiometry

4.2.2. Introduction

Ions are essential for plant growth. These nutrients are absorbed and transported within the flow of the sap that the plant needs in order to grow. Depending on their concentration in the plant, ionic nutrients can be classified as macronutrients (e.g. NO^{3-}, PO_4^{3-}, K^+, Ca^{2+}, Mg^{2+}, SO_4^{2-}) or micronutrients (e.g. Fe^{2+}, Zn^{2+}, Mn^{2+}, Cu^{2+}, etc), Regardless of this classification, all these ions are essential for the survival of the plant and any alteration in their concentrations in the sap can cause various diseases and even the eventual death of the specimen. For instance, excess in nitrogen concentrations produces excessive growth, deep green colour and forms weak plants with soft tissues, and therefore more prone to pests and diseases, wind, rain, hail, frost. Moreover, deficiency in nitrogen concentrations leads to loss of coloration and leaf fall

and thus prevents the plant from growing. Likewise, deficiency in potassium reduces the plant's ability to flower and bear fruit. Calcium is an essential nutrient in plants. It plays an important structural role in the cell wall and membrane, is a counter-cation for inorganic and organic anions, is a main intracellular messenger and helps harvest and process nitrates for protein metabolism. Nevertheless, calcium deficiency or excess **[1]** can cause several costly disorders in horticulture. By correctly analyzing sap we can determine the presence and extent of such alterations, identify whether the plant requires fertilizer or water and thus give the plant the most precise and suitable treatment.

However, the composition of sap can be very difficult to determine because, for example, of its high ionic strength, the complexity of its matrix and its low stability in contact with air. Sap is currently analyzed using different methods such as ion chromatography **[2]**, capillary electrophoresis **[3]** and atomic absorption spectroscopy (AAS) **[4]**. Although these techniques are very sensitive and selective, they all have a high instrumental cost. Furthermore, ion chromatography and capillary electrophoresis require a long analysis time, and atomic absorption spectroscopy only analyzes the total concentration of the analyte and is unable to determine the concentration of free ion. In order to obtain a suitable sample, these methodologies also require complex pretreatments such as ultrasound-assisted solubilisation **[5]**, acidic extraction **[6]** or heating to obtain dry matter, procedures which involve a large investment in time and reagents. Therefore, an analysis method needs to be developed that requires only minimum sample pretreatment and the lowest quantity of sap, thereby also keeping damage to the plant to a minimum.

Of all the electrochemical techniques potentiometry is probably the simplest. Despite the versatility of ion selective electrodes (ISEs), their direct application to real samples is limited mainly by their limited selectivity and because of the unstable signal produced by complex matrices. Several studies have applied ISEs to real samples; for instance, ISEs have been used by Eriksen et al. **[7]** to determine copper in natural water, by De Marco et al. **[8]** to determine mercury in seawater, and by Ceresa et al. **[9]** to determine lead in drinking water. Miller et al. **[10]** developed an ISE with internal solution for the direct measurement of Na^+ in plant cells. This type of electrode, as with

all classical ISEs with internal solution, is limited to taking vertical measurements, is difficult to miniaturize and leaks ions from the internal solution.

Using all-solid state ISEs, that is, electrodes with no internal solution, could overcome these drawbacks. Many authors have reported all-solid state ISEs whose transducer layer is made of electroactive polymers **[11-13]**. Several of these ISEs have been reported to the analysis of real samples, such as the detection of blood electrolytes **[14]**, environmental analysis **[15]**, or they have been used in other challenging and innovative applications such as its integration in scanning electrochemical microscopies **[16]**. However, these ISEs also exhibit a number of problems such as the presence of drifts caused by a change in the pH which in turn may be induced by CO_2 that has permeated through the polymeric sensing membrane.

Additionally, redox reactions such as that between oxygen and water **[17]** may also interfere with the analytical signal. However, from a practical point of view, the major drawback of many conducting polymers is their sensitivity to light. Other ion-to-electron transfer promoters have also been reported to act as transducers in solid state ISEs. These mainly use nanostructured materials such as three-dimensionally ordered macroporous carbon **[18]**, fullerenes **[19]**, platinized porous silica **[20]** and carbon nanotubes, either single-walled (SWCNTs) **[21]** or multi-walled (MWCNTs) **[22]**. Consequently, nanostructured materials can be considered as a good alternative to conducting polymers because they overcome most of the problems mentioned above. The main reason for a stable potentiometric signal is the large contact area between the ion-selective membrane and the electronically conducting nanostructured material. This contact area generates a large double-layer capacitance that stabilizes the potential **[18,23]**. The transduction mechanism of carbon nanotubes can be explained by the notable charge transfer capability between heterogeneous phases and the very large surface to volume ratio of carbon nanotubes together with their remarkable double-layer capacitance **[24]**. Furthermore carbon nanotubes are easily deposited over many surfaces, which make them ideal for solid contact electrodes.

This paper aims to move towards the direct, on-line determination of ions in plant sap by showing that ISEs can be used in complex real samples. Consequently, we report the development of the first solid-state robust ISE with an SWCNT transducing layer for the direct, sensitive and selective determination of Ca^{2+} ions in sap. This ISE can directly

determine calcium ions in diluted sap samples in a few seconds without any other pretreatment and with sample volumes of only a few microlitres. The electrode is built on top of a thin copper wire by depositing a layer of SWCNTs and a polymeric membrane selective to calcium ions. Copper wire (diameter 1.13 mm) is an inexpensive conductive electrode that is very easy to handle and its reduced area means that small electrodes can be developed. The concentration of Ca^{2+} in real sap samples has been assessed by comparing the results obtained using aqueous calibration and standard addition techniques.

4.2.3. Experimental Procedure

4.2.3.1. Reagents and samples

Fluka (Tres Cantos, Spain) provided Ca^{2+}-selective ionophore N,N,N′-N′-tetracyclohexyl-3-oxapentanediamide (ETH129), ammonium citrate, L-malic acid, potassium nitrate, potassium phosphate dibasic, magnesium citrate tribasic nonahydrate, L-arginine, ammonium tartrate dibasic, reagent grade benzene, tetrahydrofuran, petroleum ether (80–100 ºC), potassium tetrakis[3,5-bis-(trifluoromethyl)phenyl]borate and azobisisobutyro-nitrile initiator (AIBN). Sigma-Aldrich (Tres Cantos, Spain) provided methyl metacrylate (MMA), n-butyl acrylate (nBA), dichloromethane (DCM), ethanol, acetone and petroleum ether high boiling point (80–100 ºC), lithium acetate, potassium chloride, dimethylformamide (DMF), calcium nitrate and purified single-walled carbon nanotubes (>95 % purity, short, 1-2 nm diameter and 0.5-2 µm length).
Aqueous solutions were prepared with freshly deionized water (18.2 MΩ·cm specific resistance) obtained with a Milli-Q PLUS reagent-grade water system (Millipore, Madrid, Spain). Sandpapers and alumina were obtained from Buehler (Düsseldorf, Germany). Copper wire 1.13 mm diameter was purchased from RS Amidata (Madrid, Spain).

Sap exudates were collected during the autumn from *Euphorbia characias* grown on the banks of the river Francolí in Tarragona, Spain. A small cut was made on each plant specimen and allowed to bleed for a few seconds. Immediately following collection, the exudates were frozen at -20 ºC. Sap fluid was thawed to room temperature prior to chemical analysis. The stability in air of *Euphorbia characias* sap and, generally

speaking, that of any plant is very low because contact with air triggers many enzymatic reactions.

4.2.3.2. Apparatus and procedures

Environmental scanning electron microscope (ESEM) images were taken on a Quanta 600 (FEI Company, Inc.) A high input impedance electrometer 6514 from Keithley and an Autolab PGSTAT 128N from Eco Chemie, were used to obtain the corresponding potentiometric and impedance measurements.

All the experiments were done at room temperature (22±2 ºC) with the same double-junction Ag/AgCl/ 3 M KCl reference electrode (type 6.0729.100, Methrom AG) containing a 1 M LiAcO electrolyte bridge. The same cell was used for the measurements in all the experiments in order to ensure that each experiment was carried out under the same conditions. The auxiliary electrode used in impedance measurements was a glassy carbon rod and the working electrode was the SWCNT-based ISE for Ca^{2+} (area 1 mm^2).

4.2.3.3. Electrode preparation.

The solid-contact electrode was built on top of a copper wire (length 50 mm and diameter 1.13 mm) jacketed with a PVC layer. The surface of the electrode was polished first with a sheet of abrasive paper (Buehler Carbimet 600/P1200) and then with different grain-sized alumina (30, 5, 1 and 0.5 µm).

A dispersion of non carboxilated SWCNTs in DMF (1 % w/v) was homogenized using a tip-sonicator for 30 min (Ultraschallprozessor UP200S (Dr. Hielscher), amplitude 60 %, cycle 0.5) and spray-deposited on top of the polished copper surface. The SWCNTs were spray-deposited in successive steps of 1 s and then dried in air.

4.2.3.4. Preparation of the ion selective membrane for calcium.

An acrylic matrix was used as the base for the ion-selective membrane (ISM). The acrylic matrix (methyl butyl acrylate, MBA 1:10; one part of methyl acrylate for 10 parts of butyl acrylate) was synthesized according to the procedure described by Heng et al. **[25]**. A suitable amount of ETH129 (ionophore) and of the lipophilic anion (K^+-tetrakis) were added to the acrylic matrix following the procedure reported by Qin et al. **[26]**. A

total amount of 200 mg of cocktail (lipophilic anion, acrylic matrix and ionophore) dissolved in 2 mL of dichloromethane was used (96.5 % wt. acrylic matrix, 3 % wt. ionophore, 0.05 % wt.). 100 µL of the cocktail-membrane was deposited by drop casting over the PVC coated copper wire conductor that constitutes the electrode. The electrode was maintained under dry conditions for 1 day and was subsequently conditioned in the most appropriate solution depending on the measurement.

4.2.3.5. Electrode conditioning.

Conditioning the electrodes is a fundamental step for obtaining reliable results. In almost all the EMF measurements, the electrodes were first conditioned in a 10^{-3} M solution of $CaCl_2$ for one day in order to exchange all the interfering ions of the membrane for the target ion (Ca^{2+}) and then conditioned for two more days in a 10^{-9} M solution of $CaCl_2$ to completely clean the membrane of any interfering ions **[27]**.
To estimate the limit of detection, the electrodes were conditioned for one day in the same solution in which the measurements were taken (different initial solutions were tested according to the dilution method proposed by Lai et al. **[18]** Finally, for the water layer test, the electrodes were immersed overnight in a 10^{-2} M $CaCl_2$ solution.

4.2.4. Results and discussion

4.2.4.1. Electrode development and characterization

Images obtained using the environmental scanning electron microscope (ESEM) of the deposited SWCNT network show a layer of SWCNTs with an average thickness of 30 µm. This layer is homogeneously deposited over the entire electrode surface without leaving any part of the copper wire electrode in direct contact with the ion-selective membrane. Once the polymeric membrane had been deposited, ESEM measurements showed that the calcium selective membrane had an average thickness of 45 µm.

4.2.4.1.1. Electrochemical impedance measurements.

Figure 4.1.a shows the impedance plot of a system composed of a copper wire coated with SWCNTs. This impedance plot is very similar to that obtained by Crespo et al. for a similar system but using glassy carbon instead of copper **[24]**. Its capacitance line is principally located at low frequencies and only deviates slightly at higher frequencies,

these deviations being the product of a fast charge transfer between the copper and the SWCNTs, and the SWCNTs and the solution. Figure 4.1.b displays a typical behaviour observed for a Cu/SWCNTs/ISM electrode. At high frequencies the signal is mainly dominated by the parallel resistance and geometric capacitance of the membrane (shown as a depressed semicircle). At low frequencies, a diffusional component can be observed that is related to diffusion of the analyte from the solution into the selective membrane. The spectrum was recorded in a frequency range of 100 kHz - 1 mHz.

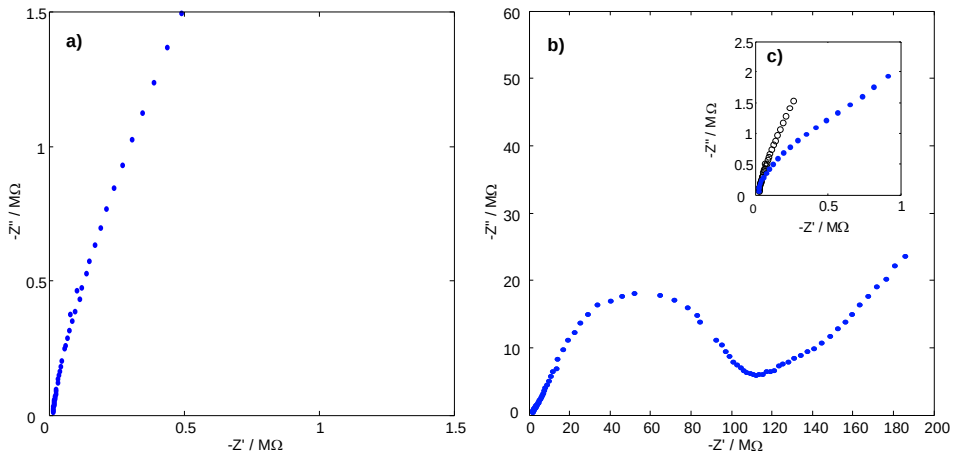

Figure 4.1. a) Impedance plot of the Cu/SWCNT electrode in 0.01 M NaCl. Frequency range = 100 kHz to 0.01 Hz, E_{dc} = 0.16 V, ΔE_{ac} = 10 mV. b) Impedance plot of the Cu/SWCNT/ISM electrode in 0.1 M $CaCl_2$. Frequency range = 1 mHz to 100 kHz, E_{dc} = 0.2 V, ΔE_{ac} = 10 mV. c) Zoom of the comparison of Cu/SWCNT (empty dots) and Cu/SWCNT/ISM (solid dots) electrodes at high frequencies.

Inset in figure 4.1.b shows a zoom at high frequencies comparing the behaviour of the two electrodes. The fast charge transfer of the electrode without membrane (empty dots) has been replaced for a moderate charge transfer produced by the resistance in the electrode with membrane (solid dots).

4.2.4.1.2. Chronopotentiometry.

Reversed chronopotentiometry has been used to evaluate the electrical behaviour and the short-term potential stability of the calcium selective solid-contact electrode.

Figure 4.2 shows a typical image recording the potential stability versus time while a current of -1 nA is applied to the electrode for 50 s followed by a current of +1 nA for the same period of time. A sudden potential shift is recorded when the current applied changes from -1 to +1 nA. This shift is related to the total resistance (*R*) according to Ohm's law $R = E/I$. The estimated total resistance was R = 120 MΩ (I = 1 nA). The short-term stability of the potential can be determined from the ratio $\Delta E/\Delta t$. This value corresponds to $\Delta E/\Delta t = 9.30 \times 10^{-4}$ V/s. Capacitance (C) of the system can be derived from the fundamental capacitor equation, $I = C \cdot dE/dt$. The value obtained for the capacitance was 5.37 μF.

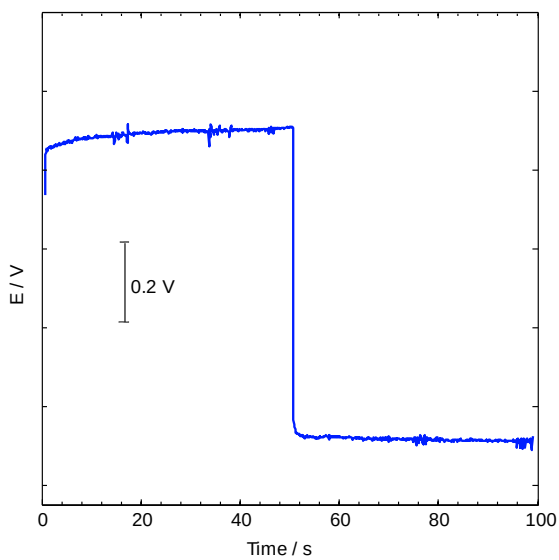

Figure 4.2. Chronopotentiometric results. Applied current -1 nA for 50s and 1 nA for 50s. Solution of 0.1 M $CaCl_2$

4.2.4.1.3. Water layer test.

The water layer test is applied to detect the presence of a hypothetical thin water layer between the membrane and the ion-to-electron transducer layer **[28]**. The water layer test consists of observing the behaviour of the electrode when a solution of the primary ion ($CaCl_2$ 0.1 M in our case) is exchanged for a solution of an interfering ion ($MgCl_2$ 0.1 M in our case), and then exchanged again for the initial solution of $CaCl_2$. Figure 4.3 shows the absence of a water layer at the interface between the membrane and the

SWCNT layer. A rapid shift is observed when the interfering ion replaces the primary ion (zone B), thus giving stable EMF readings. This fact suggests that the calcium is rapidly replaced by magnesium in the membrane. The water layer is deemed to be absent because there are no appreciable drifts in zone B due to the equilibrium of the interfering ion in the aqueous layer. Figure 4.3 also shows that the response signal to the primary ion has the same value before and after being exposed to the interfering ion (steps A and B respectively). The highly hydrophobic character of the SWCNTs could be the reason for the absence of the water layer.

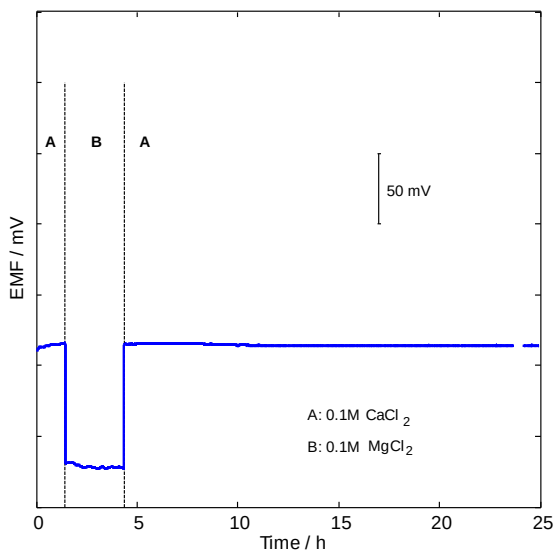

Figure 4.3. Water layer test. The electromotive force (EMF) was recorded successively in (A) 10^{-2} M $CaCl_2$, (B) 10^{-2} M $MgCl_2$ and (A) 10^{-2} M $CaCl_2$.

4.2.4.2. Performance parameters.

The sensitivity and linear range of the electrode were estimated by measuring the effect of the electromotive force on different concentrations of aqueous Ca^{2+} solutions ranging from 10^{-6} to $10^{-2.25}$ M. The parameters were calculated on the basis of 15 calibration curves with 5 different electrodes (3 measurements for each electrode) measured over 2 months. A typical calibration curve representing the electromotive force (EMF) versus time is shown in figure 4.4.a. Time responses of 5 minutes for the lowest concentrations of analyte (10^{-6} M) gradually decrease to time responses of 10

seconds for concentrations higher than 10^{-4} M (insets of figure 4.4.a). In figure 4.4.b, the error bars represent the range between the minimum and maximum value for the 15 measurements at each activity value. Thus, figure 4.4.b shows that a near Nernstian slope of 28.7 mV/decade (SD = $4.8x10^{-4}$ mV/decade, R^2 = 0.9998) and a linear range from 10^{-5} to $10^{-2.5}$ M were obtained.

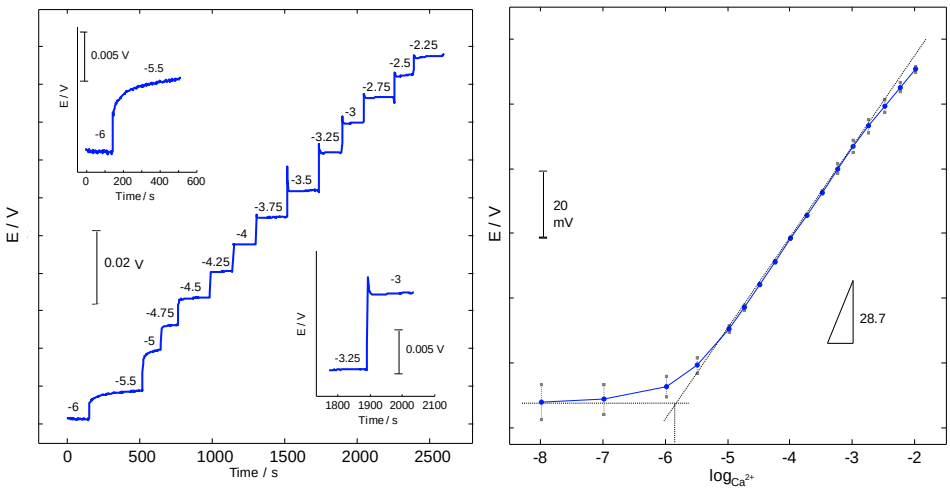

Figure 4.4. a) Electromotive force measurements recorded for increasing concentration values of Ca^{2+} in the solution. Logarithmic values are displayed on top of each segment. Insets: Response time at low and high activities of calcium. b) Calibration curve in aqueous standards of Ca^{2+} with error bars corresponding to 15 calibration curves recorded over 2 months.

Figure 4.5 shows the medium-term stability of the electrodes. It was evaluated by recording the potentiometric signal over a long time when using a concentration of 10^{-4} M of $CaCl_2$. The initial conditioning solution was 10^{-6} M and two further additions of Ca^{2+} were performed in order to reach the overall calcium concentrations of 10^{-5} M and 10^{-4} M **[27]**.

The drift of the potentiometric signal was calculated for 20 hours and gave a value of 493 µV/h. This value shows that the electrode has a very stable behaviour under intermediate-term conditions. We did not find any evidence of frequent redox reactions on the copper surface when using carbon nanotubes for the transducer layer. This is probably due to the absence of a water layer and the capacitive based mechanism that

operates when carbon nanotubes are used, rather than being caused by redox reactions with conducting polymers.

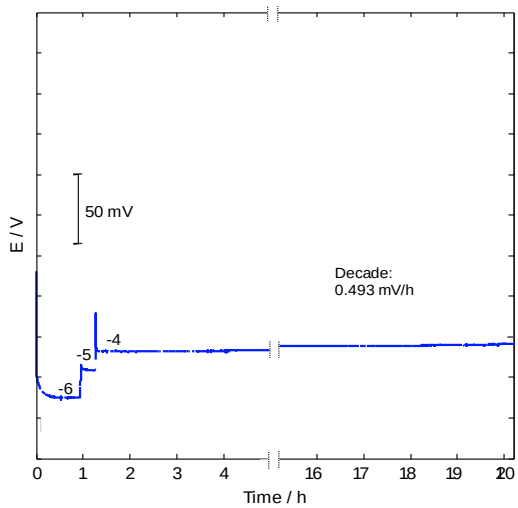

Figure 4.5. Long term potential stability of the Ca^{2+}-selective electrode over 20 hours for a 10^{-4} M solution of $CaCl_2$.

The limit of detection (LOD) was obtained using the dilution method proposed by Lai et al. **[18]** Figure 4.6 shows the LOD calculated using an initial concentration solution of 10^{-1} M. An LOD of $10^{-6.5}$ was estimated. The LOD obtained in this paper is lower than the one reported by Sodergard et al. **[29]** for similar calcium ISE. In any case, since the concentration of Ca^{2+} in plants is between 10^{-4} and 10^{-1} depending on the species, the season and the type of soil, the LOD obtained ensures that calcium is correctly determined in plants.

The selectivity of the electrodes has been performed using the separated solutions method **[22]**. The selectivity coefficients were determined measuring by duplicate the electromotive force of three different electrodes in different concentrations of interfering ions obtaining the following results: $log^{pot}_{Ca,Mg}$= -4,8 ± 0,2; $log^{pot}_{Ca,Ba}$= -5,5 ± 0,3; $log^{pot}_{Ca,K}$=- 2,2 ± 0,2; $log^{pot}_{Ca,Na}$= -3,1 ± 0,4; $log^{pot}_{Ca,Li}$= -2,5 ± 0,2.

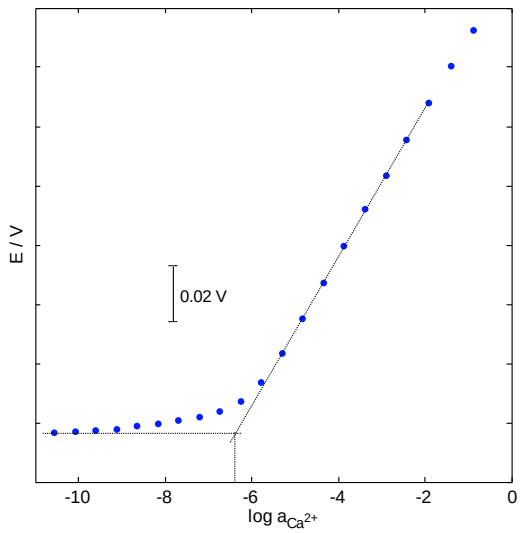

Figure 4.6. Limit of detection for calcium ion selective electrode, conditioned in 10^{-9} M $CaCl_2$ for 2 days.

4.2.4.3. Application to sap samples

The calcium in sap samples was quantified by showing the absence of proportional and constant errors when using sap samples. The absence of proportional errors is shown using the method of standard additions and the absence of constant errors is shown using the Youden calibration **[30]**. In absence of these errors, the calcium concentration in sap can be found simply using the calibration line based on aqueous standards. The goodness of the results obtained using a calcium-ISE mounted on SWCNTs was also shown by calculating the recovery factor when analyzing real sap samples. The calcium concentration in sap is quite high; therefore, the sap collected was diluted to 1:25 in Milli-Q water so that only a volume of 100 ml of sap was needed for each analysis, thus minimizing harm to the plant.

Table 1 shows the coefficients of the calibration curves using the standard additions method and aqueous standards. 24 different calibration curves in the linear range from 10^{-5} to 10^{-2} M were built using 6 different electrodes and 4 repetitions for each electrode. There is no statistically significant difference (using a *t*-test with a significant level of 5%) between the slopes of the calibration lines obtained using both methods. This information shows that there are no proportional errors in our measurements.

Table 4.1. Least-squares regression analysis of the three calibration graphs

	n[a]	*Slope* ± *s*[b]	*Intercept* ± *s*	*Correlation coefficient*[c], R^2
Aqueous standard	24	26,8 ± 0.3	88,8 ± 1,0	0,997
Standard additions	24	26,9 ± 0.1	82,9 ± 0,3	0,992
Youden Calibration	24	0,4 ± 0.1	75,5 ± 3,7	0,993

[a] Number of calibration data points (6 electrodes, 4 repetitions for each electrode)

[b] Standard deviation.

[c] Worst value for correlation coefficient.

A Youden test was applied to determine the presence/absence of constant errors. This method consists of analysing different quantities (volumes or masses) of the real sap sample. The intercept of the Youden calibration plot corresponds to the total Youden blank (TYB) and includes all the constant contributions to the analytical signal. These contributions do not change with the amount of sample analysed. A *t*-test with a significant level of 5% revealed no statistical differences between the intercepts of the standard calibration and the Youden calibration; therefore, we assessed the absence of constant errors and found the calcium concentration in sap by simply using the calibration line based on aqueous standards.

After showing that the newly developed ISE can be used for the direct determination of calcium in sap, the next step was to study the traceability of the results by comparing them with a suitable reference. We started by comparing the results of the real sap analysis with the results using a commercial Ca^{2+} ion-selective electrode (Crison Instruments, ref 96 60). The slope of the standard additions calibration curve obtained using the commercial ISE for diluted (1:25) samples of sap is super-Nernstian (34,7 ± 7,03x10^{-4} mV/decade) while the one obtained with the newly developed electrode is Nernstian (29,4 ± 6,57x10^{-4} mV/decade). The commercial ISE found a calcium concentration of 8x10^{-11} M, which is well outside the usual ranges for calcium in sap, whereas our ISE found a calcium concentration of 1,15x10^{-4} M, a response within the normal range of calcium concentrations in a typical sap. The electrical signal of the commercial ISE when measuring real sap was not stable, had many fluctuations and it was not possible to obtain a stable signal after hours and hours of measurement, what

shows the difficulty of using classical commercial ISEs in the measurement of real complex samples. The best response time we were able to obtain for the commercial electrode was very high (about 10-20 minutes) and residual stains of the real sample adhered permanently to the electrode. In contrast, our electrode remained clean after each measurement, thus providing short response times and high response stability.

Since the comparison between the calcium ISEs was not at all conclusive, we decided to assess the traceability using recovery factors in real sap samples. The standard additions method obtained recovery values of almost 100% for different concentration levels. The recovery factor of 4 different electrodes was evaluated for 2 different concentration levels under time-intermediate conditions for over a period of 3 weeks. Each level of concentration was repeated in duplicate. Table 2 displays the results for the recovery factor test.

Table 4.2. Recovery factor for Ca^{2+} in sap samples.

Sample concentration	*n*[a]	*Concentration added*	*Concentration found*	*Recovery factor ± s*[b]
0,2 mM	6	0,05 mM	0,2464 mM	92,8 ± 7,0
2 mM	6	0,5 mM	2,533mM	106,6 ± 0,8

[a] Number of calibration data points (3 electrodes, 2 repetitions each electrode)
[b] Standard deviation.

4.2.5. Conclusions

In this paper we show that a reduced-size solid-state ISE with a carbon nanotube transducer layer can be used to determine calcium ions in real sap samples. The electrode is built on top of a thin copper wire which is used as the conducting material. This copper wire shows no redox reactions probably because of the capacitive-based transduction mechanism of the SWCNTs. The tip of the electrode has an external diameter of 2,75 mm (inner diameter is 1,13 mm) which enables reduced volumes of test samples to be analyzed more easily. Additionally, the use of copper rather than other conductive materials such as glassy carbon **[21,22,31]** makes the electrode much cheaper and, therefore, large-scale manufacture much more affordable. The different

comparisons made using real sap samples and aqueous standards show the traceability of the results obtained with the newly developed ISE.

Carbon nanotubes add more stability to the electrical signal due to their excellent electronic and chemical properties: the fast ion-to-electron transduction allows obtaining short response times and the hydrophobic behaviour of carbon nanotubes avoids the formation of thin water layers. These water layers are the principal reason of redox reactions with O_2 and CO_2 that cause instabilities in the signal, so carbon nanotubes solve some of the problems encountered in ISEs where the transduction layer is a conducting polymer.

4.2.6. Future Trends.

A straightforward way to miniaturize this ISE would be to use screen printing, which is reported to be a reproducible and low-cost technique for constructing miniaturised planar solid-state thick-film sensors and which could also open the way to easier on-line measurements with minimal harm to plants. These miniaturized ISEs are aimed to be reliable and maintenance-free, and have fewer temperature and pressure range limitations than standard ISEs. Furthermore, the low cost of screen printing allows these miniaturised planar sensors to be disposable, which is very useful if the user wants to avoid cross-contamination between measurements when analysing a small volume of sample.

4.2.7. Acknowledgements

The authors would like to thank the Spanish Ministry of Science and Education (project CTQ2007-67570/BQU) for its financial support.

4.2.8. References

[1] White, P. J.; Broadley, M. R., Calcium in plants. *Annals of Botany* **2003,** *92* (4), 487-511.

[2] Malone, M.; Herron, M.; Morales, M. A., Continuous measurement of macronutrient ions in the transpiration stream of intact plants using the meadow spittlebug coupled with ion chromatography. *Plant Physiology* **2002,** *130* (3), 1436-1442.

[3] Bazzanella, A.; Lochmann, H.; Tomos, A. D.; Bachmann, K., Determination of inorganic cations and anions in single plant cells by capillary zone electrophoresis. *Journal of Chromatography A* **1998,** *809*, 231-239.

[4] Wei, Z. G.; Wong, J. W. C.; Zhao, H. Y.; Zhang, H. J.; Li, H. X.; Hu, F., Separation and determination of heavy metals associated with low molecular weight chelators in xylem saps of Indian mustard (Brassica juncea) by size exclusion chromatography and atomic absorption spectrometry. *Biological Trace Element Research* **2007,** *118*, 146-158.

[5] Filgueiras, A. V.; Lavilla, I.; Bendicho, C., Ultrasound-assisted solubilization of trace and minor metals from plant tissue using ethylenediaminetetraacetic acid in alkaline medium. *Fresenius Journal of Analytical Chemistry* **2001,** *369*, 451-456.

[6] Husted, S.; Hebbern, C. A.; Mattsson, M.; Schjoerring, J. K., A critical experimental evaluation of methods for determination of NH_4+ in plant tissue, xylem sap and apoplastic fluid. *Physiologia Plantarum* **2000,** *109*, 167-179.

[7] Eriksen, R. S.; Mackey, D. J.; van Dam, R.; Nowak, B., Copper speciation and toxicity in Macquarie Harbour, Tasmania: an investigation using a copper ion selective electrode. *Marine Chemistry* **2001,** *74*, 99-113.

[8] De Marco, R.; Shackleton, J., Calibration of the Hg chalcogenide glass membrane ion-selective electrode in seawater media. *Talanta* **1999,** *49*, 385-391.

[9] Ceresa, A.; Bakker, E.; Hattendorf, B.; Gunther, D.; Pretsch, E., Potentiometric polymeric membrane electrodes for measurement of environmental samples at trace levels: New requirements for selectivities and measuring protocols, and comparison with ICPMS. *Analytical Chemistry* **2001,** *73*, 343-351.

[10] Miller, A. J.; Cookson, S. J.; Smith, S. J.; Wells, D. M., The use of microelectrodes to investigate compartmentation and the transport of metabolized inorganic ions in plants. *Journal of Experimental Botany* **2001,** *52*, 541-549.

[11] Jain, A. K.; Raisoni, J.; Jain, S., Calcium(II)-selective potentiometric sensor based on p-isopropylcalix 6 arene in PVC matrix. *International Journal of Environmental Analytical Chemistry* **2008,** *88*, 209-221.

[12] Lindfors, T.; Ivaska, A., All-solid-state calcium-selective electrode prepared of soluble electrically conducting polyaniline and di(2-ethylhexyl)phosphate with ETH1001 as neutral carrier. *Analytica Chimica Acta* **2000,** *404*, 101-110.

[13] Michalska, A.; Konopka, A.; Maj-Zurawska, M., All-solid-state calcium solvent polymeric membrane electrode for low-level concentration measurements. *Analytical Chemistry* **2003,** *75*, 141-144.

[14] De Marco, R.; Clarke, G.; Pejcic, B., Ion-selective electrode potentiometry in environmental analysis. *Electroanalysis* **2007,** *19*, 1987-2001.

[15] Bakker, E.; Diamond, D.; Lewenstam, A.; Pretsch, E., Ion sensors: current limits and new trends. *Analytica Chimica Acta* **1999,** *393* , 11-18.

[16] Gyetvai, G.; Sundblom, S.; Nagy, L.; Ivaska, A.; Nagy, G., Solid contact micropipette ion selective electrode for potentiometric SECM. *Electroanalysis* **2007,** *19*, 1116-1122.

[17] Maksymiuk, K., Chemical reactivity of polypyrrole and its relevance to polypyrrole based electrochemical sensors. *Electroanalysis* **2006,** *18*, 1537-1551.

[18] Lai, C.-Z.; Joyer, M. M.; Fierke, M. A.; Petkovich, N. D.; Stein, A.; Buhlmann, P., Subnanomolar detection limit application of ion-selective electrodes with three-dimensionally ordered macroporous (3DOM) carbon solid contacts. *Journal of Solid State Electrochemistry* **2009,** *13*, 123-128.

[19] Fouskaki, M.; Chaniotakis, N., Fullerene-based electrochemical buffer layer for ion-selective electrodes. *Analyst* **2008,** *133*, 1072-1075.

[20] Zhu, Z.; Zhang, J.; Zhu, J.; Lu, W.; Zi, J., Fabrication and characterization of potassium ion-selective electrode based on porous silicon. *Ieee Sensors Journal* **2007,** *7*, 38-42.

[21] Crespo, G. A.; Macho, S.; Xavier Rius, F., Ion-selective electrodes using carbon nanotubes as ion-to-electron transducers. *Analytical Chemistry* **2008,** *80*, 1316-1322.

[22] Parra, E. J.; Crespo, G. A.; Riu, J.; Ruiz, A.; Rius, F. X., Ion-selective electrodes using multi-walled carbon nanotubes as ion-to-electron transducers for the detection of perchlorate. *Analyst* **2009,** *134*, 1905-1910.

[23] Collins, P. C.; Arnold, M. S.; Avouris, P., Engineering carbon nanotubes and nanotube circuits using electrical breakdown. *Science* **2001,** *292*, 706-709.

[24] Crespo, G. A.; Macho, S.; Bobacka, J.; Rius, F. X., Transduction Mechanism of Carbon Nanotubes in Solid-Contact Ion-Selective Electrodes. *Analytical Chemistry* **2009,** *81*, 676-681.

[25] Heng, L. Y.; Hall, E. A. H., Methacrylic-acrylic polymers in ion-selective membranes: achieving the right polymer recipe. *Analytica Chimica Acta* **2000,** *403*, 77-89.

[26] Qin, Y.; Peper, S.; Radu, A.; Ceresa, A.; Bakker, E., Plasticizer-free polymer containing a covalently immobilized Ca2+-selective Ionophore for potentiometric and optical sensors. *Analytical Chemistry* **2003,** *75*, 3038-3045.

[27] Lindner, E.; Umezawa, Y., Performance evaluation criteria for preparation and measurement of macro- and microfabricated ion-selective electrodes. *Pure and Applied Chemistry* **2008,** *80*, 85-104.

[28] Fibbioli, M.; Morf, W. E.; Badertscher, M.; de Rooij, N. F.; Pretsch, E., Potential drifts of solid-contacted ion-selective electrodes due to zero-current ion fluxes through the sensor membrane. *Electroanalysis* **2000,** *12*, 1286-1292.

[29] Sodergard, M.; Csoka, B.; Nagy, G.; Ivaska, A., Lowering the detection limit of solvent polymeric ion-selective membrane electrodes. An experimental study with calcium-selective micropipette electrodes. *Analytical Letters* **2003,** *36*, 2909-2923.

[30] Youden, W. J., Technique for testing the accuracy of analytical data. *Analytical Chemistry* **1947,** *19*, 946-950.

[31] Ampurdanes, J.; Crespo, G. A.; Maroto, A.; Angeles Sarmentero, M.; Ballester, P.; Xavier Rius, F., Determination of choline and derivatives with a solid-contact ion-selective electrode based on octaamide cavitand and carbon nanotubes. *Biosensors & Bioelectronics* **2009,** *25*, 344-349.

UNIVERSITAT ROVIRA I VIRGILI
SOLID CONTACT POTENTIOMETRIC SENSORS BASED ON CARBON NANOMATERIALS
Rafael Hernández Malo

UNIVERSITAT ROVIRA I VIRGILI
SOLID CONTACT POTENTIOMETRIC SENSORS BASED ON CARBON NANOMATERIALS
Rafael Hernández Malo

UNIVERSITAT ROVIRA I VIRGILI
SOLID CONTACT POTENTIOMETRIC SENSORS BASED ON CARBON NANOMATERIALS
Rafael Hernández Malo

5.1. Introduction.

The use of new materials as transducer elements in ion-selective electrodes has significantly varied since the first coated wire electrodes (where there was not a transducer element) to conducting polymers. This evolution has produced better electrodes, but with some drawbacks in the latest generation of ISEs based on conducting polymers, as these have certain sensitivity to light and other small molecules such as CO_2 and O_2. Our research group showed that SWCNTs could be used as transducers overcoming most of these drawbacks. Still, this type of ISEs could have some instability in the signal due to the presence of metals from the synthesis of SWCNTs.

The recent discovery of graphene could appear as a new solution to eliminate drawbacks from other transducers. Graphene was discorvered by Geim and Novoselov in 2004 and served them to obtain the Nobel Prize in phisycs. This material can be described as the basic monolayer present in graphite. Apparently this monolayer was unstable and very difficult to obtain but, Geim and Novoselow were able to isolate it in the simplest form using only a pencil and scotch tape. This incredible material reveals excellent thermal, optical and mechanical properties among others, but probably the most interesting one is its high electrical conductivity behaviour with huge electron mobility close to 15,000 $cm^2 \cdot V^{-1} \cdot s^{-1}$ (with theoretically potential limits of 200,000 $cm^2 \cdot V^{-1} \cdot s^{-1}$), which makes it the ideal candidate for use in ion-selective electrodes.

The aim of this chapter is to demonstrate that graphene can be used as transducer in the same way as SWCNTs, and we also tried to elucidate its working mechanism. As a proof of concept, a new calcium-selective electrode was been developed.

The Content of this chapter has-been published in the Journal of Physical Chemistry C, year 2012 volume 116, pages 22570-22578, and co-authored by Jordi Riu, Johan Bobacka, Cristina Vallés, Pablo Jiménez, Ana M. Benito, Wolfgang K. Maser and F. Xavier Rius.

5.2. Article

THE JOURNAL OF PHYSICAL CHEMISTRY C
Article
pubs.acs.org/JPCC

Reduced Graphene Oxide Films as Solid Transducers in Potentiometric All-Solid-State Ion-Selective Electrodes

Rafael Hernández,[†] Jordi Riu,[*,†] Johan Bobacka,[‡] Cristina Vallés,[§] Pablo Jiménez,[§] Ana M. Benito,[§] Wolfgang K. Maser,[§] and F. Xavier Rius[†]

[†]Department of Analytical and Organic Chemistry, Universitat Rovira i Virgili, Tarragona, Spain
[‡]Laboratory of Analytical Chemistry, Process Chemistry Centre, Åbo Akademi University, Turku-Åbo, Finland
[§]Department of Chemical Processes and Nanotechnology, Instituto de Carboquímica ICB-CSIC, Zaragoza, Spain

5.2.1. Abstract

The development of ion-selective electrodes (ISEs) a using solid-state transducer material is of great interest for advanced potentiometric detection systems. At present, conducting polymers are the most used solid-state transducing materials.

However, their reliability is strongly related to their chemical stability and the formation of internal water films. Here we report on the use of reduced graphene oxide (RGO) films of different thicknesses as transducer materials in potentiometric all-solidstate ISEs. First, the transduction mechanism is fully analyzed, revealing that RGO films act as asymmetric capacitors where their electron density is in contact with ions of the electrolyte solution, creating a capacitance due to the constant phase elements present in the system. Second, as a proof of concept, RGO films are used in calcium ISE showing highly reproducible sensing responses and outstanding increased signal-to-noise ratios with drifts of only 10 μV/h. These performance parameters are among the best compared to those of other ISE transducer materials so far. With its ease of fabrication and processing into reproducible films of controlled thickness and ease for further tailoring chemical composition and tailoring electrical properties, RGO offers great promise as a reliable high-performance transducer material for solid-state ISE sensors.

5.2.2. Introduction

Graphene is a one-atom-thick two-dimensional sheet of sp^2-hybridized carbon that has excellent and unique thermal **[1]**, optical **[2]**, mechanical **[3]**, electronic **[4]**, and electrochemical **[5-9]** properties. It is a promising candidate for next-generation devices such as transistors **[4]**, supercapacitors **[5]**, solar cells **[10]**, liquid crystal displays **[11]**, and biofuel cells **[12]**. Versatile and largescale assembly is offered by solution-based strategies **[13.14]**. While graphene itself is insoluble, chemically modified graphene (CMG) emerges as a valuable alternative **[14]**. To this end, graphene oxide (GO) is one of the most promising CMGs **[15]**. It can be described as a graphene sheet containing oxygen functional groups such as epoxides, alcohols, and carboxylic acids at its basal plane and edges **[16]**. It easily can be made from graphite oxide, which readily exfoliates as single GO sheets in water, forming stable aqueous dispersions **[15,17]**. These can be used to fabricate macroscopic assemblies, such as continuous GO films. While GO itself is insulating due to the numerous oxygen functional groups disrupting the sp^2 character of the carbon network, chemical reduction largely can restore the conductivity by several orders of magnitude by removal of oxygen and recovery of aromatic double-bonded carbons **[15]**.

The applied reduction step controls the conductivity and number of remaining oxygen groups in the resulting reduced graphene oxide (RGO). Being conducting and easily processable into thin films and not possessing any metallic impurities (as is the case for carbon nanotubes) renders RGO of great interest for the fabrication of transducers in different kinds of sensors **[18-21]**.

Electrochemical detection techniques have a series of advantages such as rapid response, ease of use, low cost, and small-sized commercial detectors. Amperometric sensing devices based on graphene have already been reported for the detection of NO_2, NH_3, 2,4-dinitrotoluene **[22,23]**, cadmium **[24]**, and dopamine **[25]**. Among the electrochemical techniques, potentiometry is one of the simplest, cost-efficient, and most available detection systems worldwide. Within potentiometric techniques, ion-selective electrodes (ISEs) are the most commonly used sensing devices.

Current ISEs have evolved from the first ISEs based on internal solutions to all-solid-state ISEs. Solid-state ISEs eliminate the internal solution, incorporating a solid

transducer between the ion-selective membrane and the conducting wire, paving the way for the development of a fully miniaturized device. One of the most used solid transducers in ISEs are conductive polymers **[26]**. Although these transducing materials showed benefits compared to those of classical electrodes using an internal solution, there were also some drawbacks such as the formation of internal water films **[27]**, sensitivity to light **[28]**, and sensitivity to oxygen, CO_2, and pH **[29]**.

These problems have encouraged the use of other transducing materials such as three-dimensionally ordered macroporous (3DOM) carbon **[30]**, single-walled carbon nanotubes (SWCNTs) **[31]**, or multiwalled carbon nanotubes (MWCNTs) **[32]** which offer a high potential stability in time, insensitivity to oxygen and light, and the absence of a layer of water because of the hydrophobicity of these materials. The availability of CMG with its processing advantages and the absence of additional metallic impurities affecting the device response put this material under scrutiny for improving the performance of ISEs. Very recently, Ping et al. **[33]** reported for the first time the use of RGO as an effective ion-to-electron transducer in potassium ISEs. They used a method of preparation of RGO similar to the one we use in this study (they obtained RGO prior to the deposition over a glassy carbon electrode, while in our case the reduction of GO to RGO is performed when the GO is already deposited on the glassy carbon electrode; see the Experimental Section), but using much lower volumes and concentrations of RGO, which may give rise to problems in homogeneously covering the surface of the glassy carbon electrode. Furthermore, the authors do not give information about the thickness of the RGO layer.

Li et al. **[34]** also presented a potassium ISE using GO as a solid transducer, but in this case it is not clear whether the authors reduced GO to form RGO, so the transducer they used may be different from the one we use in this study. Jaworska et al. **[35,36]** used carboxy-functionalized graphene in the construction of ISEs. They concluded that the analytical parameters of carboxyfunctionalized graphene ISEs are comparable to those of ISEs constructed with other solid-state transducers, but again, their carboxy-functionalized graphene was different from the RGO we use in this study since apparently the exfoliation procedure was not as thorough as the one we use (ultrasonication and centrifugation are not listed in their experimental procedure), and they did not seem to apply the reduction process with hydrazine vapors that we

perform to obtain RGO (see our detailed procedure in the section "Electrode Preparation" in the Experimental Section 5.2.3.3). All these ISEs made using different types of CMGs (which may have different chemical compositions and may also have different mechanisms of transduction) show the need of a deep and thorough characterization of these materials to be able to clearly and unambiguously compare the different sensors based on different CMGs.

In this paper we present the use of RGO films of well-defined thicknesses as transducers in potentiometric solid-state calcium ISEs. First, we thoroughly studied for the first time the transduction mechanism of RGO films of three different thicknesses by using cyclic voltammetry (CV), electrochemical impedance spectroscopy (EIS), and equivalent circuit analysis using five different electrolytes. Second, as a proof of concept, we fully characterized the sensing performance (time response, linear range, detection limit, stability, selectivity, water layer test) of the calcium ISE for six different electrodes and over a time window of more than 1 month. We show that RGO films with a homogeneous electrode coverage act as asymmetric capacitors offering a Nernstian response, high sensor sensitivity, and stability. Ease in the fabrication of RGO films with controlled thickness thus facilitates the fabrication of reliable and high-performance solid-state ISE sensors.

5.2.3. Experimental section

5.2.3.1. Reagents and Samples.

Fluka provided Ca^{2+}-selective ionophore N,N,N′,N′-tetracyclohexyl-3-oxapentane-diamide (ETH129), reagent-grade benzene, tetrahydrofuran (THF), potassium tetrakis[3,5-bis(trifluoromethyl)phenyl]borate (KTFPB), and azobisisobutyronitrile initiator (AIBN). Methyl methacrylate (MMA), n-butyl acrylate (nBA), dichloromethane (DCM), ethanol, acetone, petroleum ether with a high boiling point (high boiling point 80–100 °C), dimethylformamide (DMF), sodium nitrate ($NaNO_3$), sulfuric acid (H_2SO_4), potassium permanganate ($KMnO_4$), hydrazine monohydrate, and graphite powder were purchased from Sigma-Aldrich.

Aqueous solutions were prepared with freshly deionized water (18,2 MΩ·cm specific resistance) obtained with a Milli-Q PLUS reagent-grade water system (Millipore).

Abrasive papers and alumina were obtained from Buehler. Glassy carbon rods with a 3 mm diameter were purchased from HTW GmbH.

5.2.3.2. Apparatus and Procedures.

Environmental scanning electron microscopy (ESEM) images were taken with a Quanta 600 (FEI Co., Inc.) microscope. High-resolution transmission electron microscopy (HR-TEM) images were taken with an FEI Tecnai G2 20 microscope. Confocal microscopy LEICA dual-core 3D measuring equipment was used to control the thickness of RGO depositions. Scanning electron microscopy (SEM) images were obtained in a Hitachi S-3400N microscope, and the atomic force microscope used was a Multimode 8 microscope with control electronics Nanoscope V (Bruker). Xray photoelectron spectroscopy (XPS) was carried out on an ESCAPlus Omicron spectrometer using a monochromatized Mg X-ray source (1253,6 eV). XPS data were analyzed using the CasaXPS software. A high-input impedance electrometer 6514 from Keithley and an Autolab PGSTAT 128N from Eco Chemie were used for potentiometric and impedance measurements, respectively. All the experiments were done at room temperature (22,0 ± 0,1 °C) in a bath from Polyscience (ref 9106) with the same double-junction Ag/AgCl/3 M KCl reference electrode (type 6.0729.100, Methrom AG) containing a 1 M LiAcO electrolyte bridge. The same cell was used for the measurements in all the experiments to ensure that each experiment was carried out under the same conditions. The auxiliary electrode used in voltammetry, impedance, and chronopotentiometry measurements was a glassy carbon rod, and the reference electrode was a single-junction Ag/AgCl/3 M KCl reference electrode (type 6.0733.100, Methrom AG).

5.2.3.3. Electrode Preparation.

The solid-contact electrode was built on top of a glassy carbon (GC) rod (length 50 mm and diameter 3 mm) jacketed with a Teflon layer. The surface of the GC disk electrode was polished first with a sheet of abrasive paper (Buehler Carbimet 600/P1200) and then with different grain-sized alumina (30, 5, 1, and 0,5 μm). Graphite oxide was prepared using a modified Hummer method from graphite powder (Sigma-Aldrich) by oxidation with $NaNO_3$, H_2SO_4, and $KMnO_4$ in an ice bath as reported in detail elsewhere **[17,37]**. A suspension of GO sheets was obtained by sonication of the prepared graphite oxide powder in distilled water (1 mg/mL) for 2 h, followed by mild centrifugation of the

suspension at 4500 rpm for 60 min **[14,38]**. The resulting brown-colored water dispersion with a concentration of 0.3 mg/ml contained singleto few-layered GO sheets of 2–10 individual layers (see the appendix 8.2.1.2) **[38]**. GO films on GC electrodes were prepared as follows. Homogeneous aqueous GO dispersions of a controlled volume of 15 µl were drop-cast onto clean and polished surfaces of the GC electrodes and allowed to dry at room temperature. Once dried, the process was successively repeated to obtain GO films of controlled thickness between 125 and 1500 nm homogeneously covering the glassy carbon electrodes (see the appendix 8.2). Additionally, working with a highly diluted GO dispersion of 0.01 mg/ml, a 5 nm thick deposit was drop-cast on a GC electrode (see the appendix 8.2.1.2).

Reduction of deposited GO films was performed by a 24 h exposure of electrodes to hydrazine monohydrate vapors **[18]**. This reduction method efficiently removes various oxygen functional groups of the graphene oxide sheets and restores the aromaticity of the carbon network, even for films as thick as 1500 nm **[38]**. This procedure thus transforms the GO films into RGO films with remaining oxygen and nitrogen moieties of about 10 and 1.5 atom %, respectively (see the appendix 8.2). For comparison purposes the XPS results of the carboxy-functionalized graphene obtained by Jaworska et al. **[35]** present oxygen and nitrogen moieties of 22.6 and 1.2 atom %.

5.2.3.4. Preparation of the Ion-Selective Membrane for Calcium.

An acrylic matrix was used as the base for the ionselective membrane, the sensing part of the ISE. The acrylic matrix (methyl butyl acrylate, MBA, 1:10, 1 portion of methyl acrylate for 10 portions of butyl acrylate) was synthesized according to the procedure described by Heng et al. **[39]**. A suitable amount of ETH129 (ionophore) and of the lipophilic salt (KTFPB) were added to the acrylic matrix following the procedure reported by Qin et al. **[40]**. A total amount of 200 mg of cocktail (lipophilic salt, acrylic matrix, and ionophore) dissolved in 2 mL of dichloromethane was used (96.5 wt % acrylic matrix, 3 wt % ionophore, 0.05 wt % KTFPB). A 100 µL volume of the cocktail membrane was deposited by drop casting onto the glassy carbon electrode. The electrode was maintained under dry conditions for 1 day and was subsequently conditioned in the most appropriate solution depending on the measurement.

Electrode Conditioning. Conditioning the electrodes is a fundamental step for obtaining reliable results. In almost all the potentiometric measurements, freshly prepared electrodes were first conditioned in a 10^{-3} M solution of $CaCl_2$ for 1 day to exchange all the interfering ions of the membrane for the target ion (Ca^{2+}) and then conditioned for an additional 2 days in a 10^{-9} M solution of $CaCl_2$ to completely clean the membrane of any interfering ions **[41]**. To estimate the limit of detection, the electrodes were conditioned for 1 day in the same solution in which the measurements were taken (different initial solutions were tested according to the dilution method proposed by Lai et al. **[30]**). For the selectivity studies we used the separate solution method **[42]**, and the concentration of Ca^{2+} and of the interfering ions was 10^{-2} M in all cases.

5.2.4. Results and discussions

Three RGO films of different thicknesses (1500, 125, and 5 nm) drop-cast on GC electrodes were probed by electrochemical techniques to elucidate the transduction mechanism for this type of ISE.

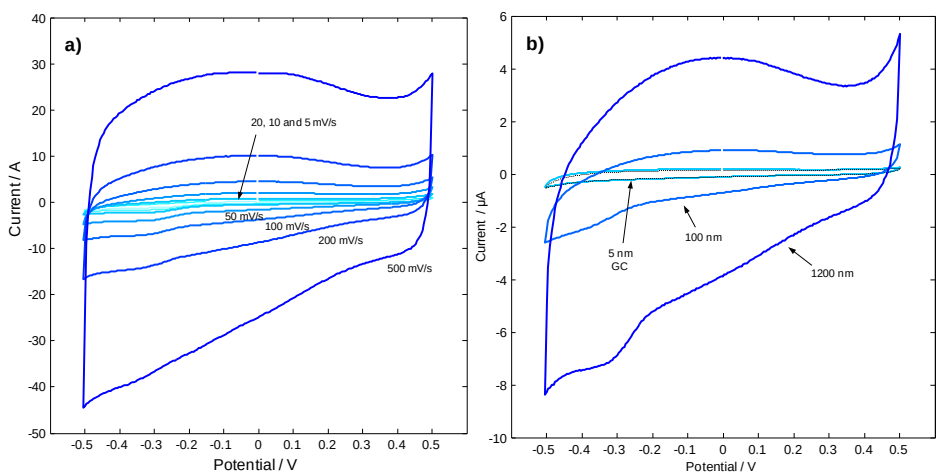

Figure 5.1. Cyclic voltammograms for GC/RGO electrodes in a 0.1 M KCl solution in the voltage window from −0.5 to +0.5 V: (a) for the 1500 nm thick RGO film at different scan rates (5, 10, 20, 50, 100, 200, and 500 mV/s); (b) for the 1500, 125, and 5 nm thick RGO films at a scan rate of 100 mV/s.

First, cyclic voltammograms in a 0,1 M KCl solution were recorded (Figure 5.1.a) at different scan rates to establish the most adequate values for this parameter in the following experiments.

All the scans were repeated five times per measurement. The voltage window of the measurements ranged from +0,5 to −0,5 V using in all cases a step potential of 0,005 V. Using a scan rate of 100 mV/s, cyclic voltammograms for the three different films were taken (figure 5.1.b). The electric current for the GC/RGO electrodes decreases with decreasing thickness of the RGO transducing layer, and the cyclic voltammogram of the GC/RGO electrode, which has a nominal thickness of only 5 nm, practically overlaps with that of the bare GC electrode. The behavior for the 5 nm deposit is explained by the fact that only some isolated GO flakes were drop-casted (instead of a 5 nm film covering the whole surface of the GC) while most of the GC electrode remained uncovered (see appendix 8.2). Underlining the impor tance of a full coverage of the GC electrode, the 5 nm thick deposit sample was not used anymore in the following experiments. Furthermore, the overall cyclic voltammograms are characterized by broad oxidation and reduction waves in addition to a small reduction peak at −0,3 V. Similar behaviour was observed for single-walled carbon nanotubes **[43,44]**. No significant differences were obtained when comparing the voltammograms in the presence and absence of oxygen in capacitive currents, leading to the conclusion that oxygen does not influence the electrochemical performance.

EIS measurements (figure 5.2) were performed in a working frequency range of 0.1 Hz to 10 kHz. Three different Edc potentials were applied to probe the behavior of the electrodes in currents in the redox zone and in the capacitive zone. The Edc voltages selected were 0.0 V, +0.2 V (in the range of capacitive currents), and −0.2 V (close to the reduction peak of oxygen). The amplitude of the measurements in all the cases was 10 mV, and all the solutions were bubbled with nitrogen in the same way as done for the cyclic voltammetry measurements.

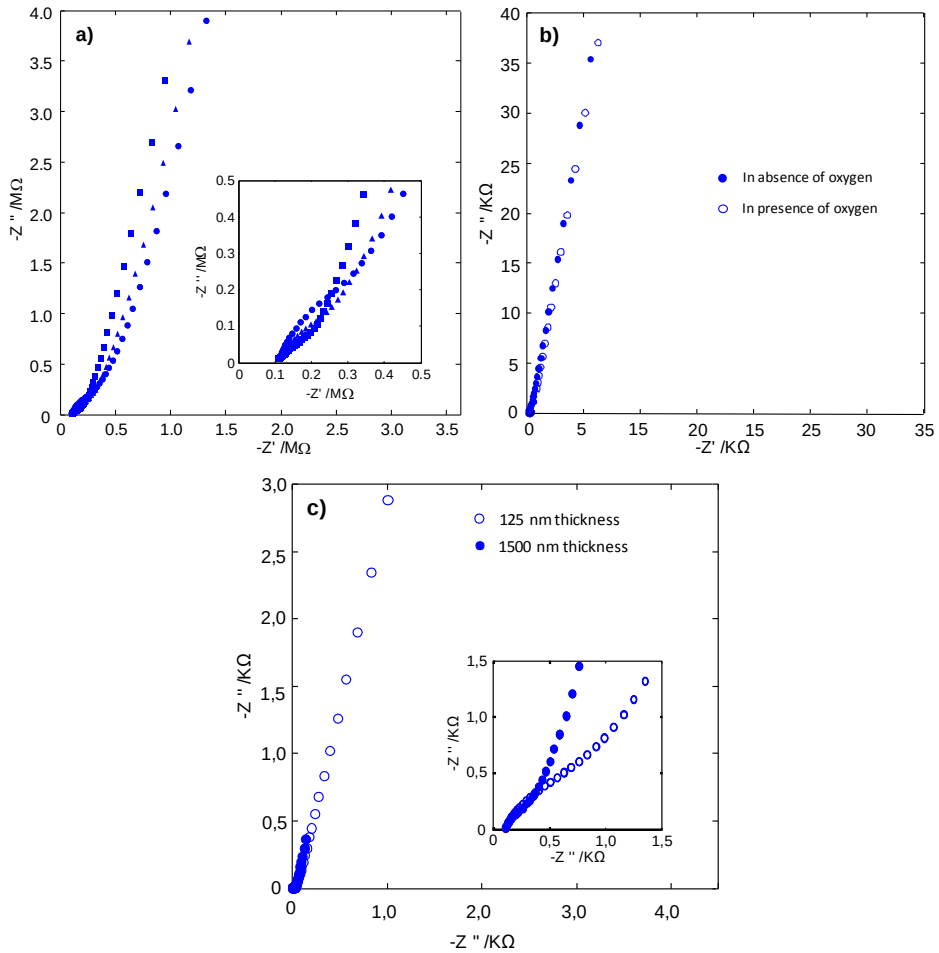

Figure 5.2. EIS spectra for the GC/RGO electrodes in 0,1 M KCl solution (frequency range 0,1 Hz to 10 kHz). (a) E_{dc} dependence for the 1500 nm thick RGO film: +0,2 V (squares), 0,0 V (triangles), and −0,2 V (circles). Inset: magnification of the high-frequency region showing the characteristic semicircle for Zarc circuits. (b) Oxygen dependence: EIS spectra for the 1500 nm thick RGO film before (filled circles) and after (empty circles) nitrogen bubbling (E_{dc} = +0,2 V). (c) Thickness dependence: EIS spectra for the 125 and 1500 nm thick RGO films for the 125 nm (circles) and 1500 nm (squares) thick RGO electrodes (E_{dc} = +0,2 V).

All impedance measurements were carried out at least three times for each GC/RGO electrode to ensure the reproducibility of all the data. Figure 5.2.a shows the EIS response of the 1500 nm thick RGO film tested at three different dc potentials (E_{dc}). At low frequencies we can observe a change in the behavior of the electrodes when the

potential is moved to negative values close to the reduction peak of oxygen. The presence of a semicircle in the high frequencies indicates a surface charge-transfer process followed by a capacitance phenomenon in the region of low frequencies with a phase angle of less than 90°. According to the previous cyclic voltammetry measurements, EIS analyses were recorded at positive potentials (E_{dc} = +0.2 V) to avoid any possible interference due to the redox reactions of oxygen **[43]**. As for the cyclic voltammetry, the presence of oxygen does not influence the EIS response (figure 5.2.b). Figure 5.2.c shows the impedance spectra for the GC/RGO electrodes of 125 and 1500 nm thickness. The dependence of the low-frequency line on the RGO film thickness indicates that it originates from a bulk process within the RGO film. The magnification of the high-frequency region (figure 5.2.c inset) reveals a depressed semicircle.

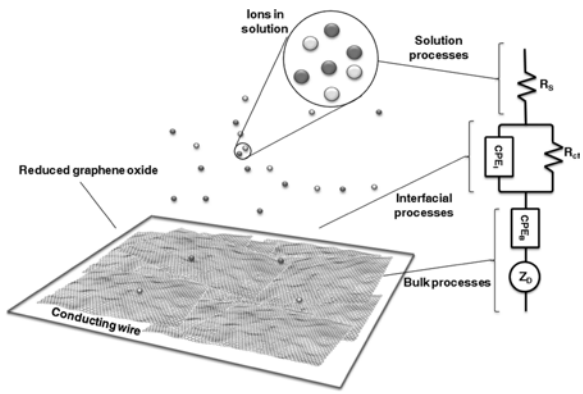

Figure 5.3. Proposed mechanism involved in the ion-to-electron RGO transduction and equivalent circuit for the GC/RGO electrodes. In the figure, the RGO flakes are much smaller than the area of the conducting wire beneath them and the flakes are interconnected.

To elucidate the mechanism of transduction, several equivalent electrical circuits were fitted to the experimental data by nonlinear least-squares fitting. The best equivalent circuit and the proposed transduction mechanism obtained are presented in figure 5.3. Our equivalent circuit is different from the one proposed by Li et al. **[34]**, but we have to take into account that apparently Li et al. did not perform the reduction process to form RGO from GO. In their case the proposed equivalent circuit was similar to the one using carbon nanotubes as solid transducers **[43]**. The average error (χ^2) of the fits for 121 different impedance spectra for different thicknesses of the graphene layer and different supporting electrolytes was around 1×10^{-4}. The equivalent circuit is composed

of the solution resistance (R_s), an interfacial constant phase element (CPE_I) in parallel with a charge-transfer resistance (R_{ct}), and the classical Warburg diffusion element (Z_D) in series with a bulk constant phase element (CPE_B). This equivalent circuit gives excellent agreement between experimental and calculated impedances, as illustrated by the Bode plot (figure 5.4).

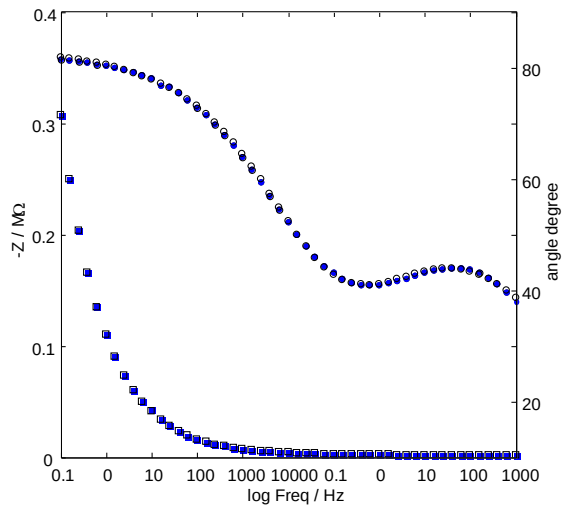

Figure 5.4. Bode plot of GC/RGO film electrodes in 0.1 M KCl solution (E_{dc} = +0.2 V, excitation amplitude of 10 mV, frequency range 0.1 Hz to 10 kHz, graphene film thickness 1500 nm). The empty symbols are the fitted values for the experimental data using the equivalent circuit from figure 5.3.

The influence of different electrolyte concentrations on the EIS spectra is shown in figure 5.5 for the 1500 nm thick film. The values of solution resistance, R_s, are independent of the RGO film thickness (and of E_{dc}), and R_s is inversely proportional to the supporting electrolyte concentration, as expected (Table 1). Opposite of R_s, the charge-transfer resistance, R_{ct}, is dependent on the RGO film thickness. The values for R_{ct} are significantly higher for the 125 nm films, compared with the 1500 nm thick films. This charge-transfer resistance is not related to any redox reaction because the measurements are recorded using supporting electrolytes without added redox couples at dc potentials where possible oxygen redox processes are not present. Therefore, R_{ct} could originate from electron transfer at the GC/RGO contact or from ion transfer at the RGO/electrolyte solution interface. Since Rct depends on the supporting electrolyte concentration, it presumably originates from ion transfer at the RGO/solution interface.

Two different capacitances (CPEs) are observed in the impedance spectra. One (CPE_I) is related to the RGO/solution interface, and the other one (CPE_B) is related to the bulk of the RGO film. The CPE parameters (Y_0 and n, frequency independent parameters) **[45]** for the interfacial and bulk capacitances are collected in Table 2. Five different electrolytes (KCl, NaCl, LiCl, $NaClO_4$, and $LiClO_4$) were used to show the different behaviors of the electrodes in different electrolytes and determine the values of the CPEs and Warburg element.

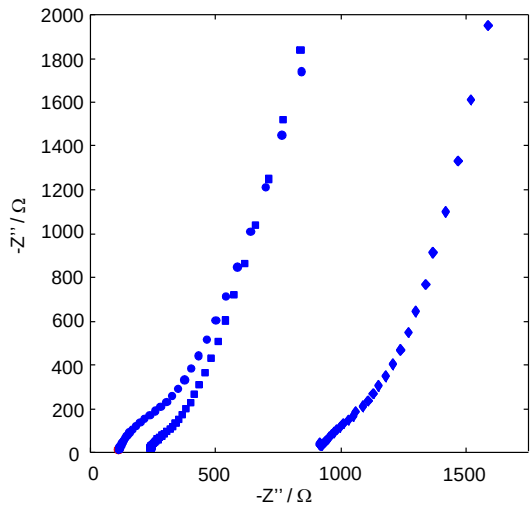

Figure 5.5. Electrochemical impedance spectra for GC/RGO 1500 nm film thickness electrodes in (circles) 0,1 M KCl, (squares) 0,05 M KCl, and (triangles) 0.01 M KCl (E_{dc} = +0,2 V, frequency range 0,1 Hz to 10 kHz).

Table 5.1. Solution resistance (R_s) and charge-transfer resistance (R_{ct}) obtained for two different RGO film thickness electrodes in three different electrolyte concentrations

Solution	*Film thickness (nm)*	R_s (Ω)	R_{ct} (Ω)
KCL, 0,01 M	1500	62,4 ± 0,4	35,5 ± 1,7
	125	64,2 ± 0,3	92,5 ± 0,3
KCL, 0,05 M	1500	15,1 ± 0,2	6,8 ± 0,4
	125	10,3 ± 1,5	13,5 ± 0,7
KCL, 0,1 M	1500	6,9 ± 0,0	8,7 ± 0,4
	125	4,8 ± 0,1	75,6 ± 3,1

The values of Y_o increase for both CPEs when the thickness of the RGO film increases. These Y_o values depend dramatically on the supporting electrolytes used in the impedance measurements. The n values give information about the deviation of CPE from a real capacitor. The possible values of n are between 0 and 1, where a value of 0 means that the CPE is acting as an ideal resistor and a value of 1 means that the CPE is acting as an ideal capacitor. The values observed are in the range of 0.5–1 for the interfacial process (CPE_I), and they are higher than 0.9 for the bulk process (CPE_B). The depressed semicircle in the inset of figure 5.2.c corresponds to the constant phase element (CPE_I) in parallel with the charge transfer resistance (R_{ct}). This system is also called the Zarc element and may be caused by, e.g., surface roughness, variation in the thickness, or nonuniform current distribution **[45]**. Its phase angle is confirmed in the Bode plot presented in figure 5.4. Such a constant phase element behavior has been observed for some other carbon-based electrodes due to the roughness of the electrodes interface **[46]**. This agrees with the microscopic characterization made by SEM and atomic force microscopy (AFM) (see the appendix 8.2.1.2).

The occurrence of CPE behavior (instead of ideal capacitors) can be related to the RGO material itself. RGO sheets are composed of basal and edge planes with different conductive and capacitive properties. These differences in the planes can cause time constant distributions and thus CPE behaviour associated with bulk (CPE_B) and interfacial (CPE_I) charging processes. Another reason for the appearance of CPEs instead of true capacitors could be the porosity and roughness of the RGO film. The dependence of the Warburg element on the film thickness (Table 2) indicates that Z_D is related to diffusion processes in the bulk of the RGO transducing layer. When SWCNTs are used as transducer layers in electrochemical measurements, **[43]** basically the sensing mechanism is produced by capacitance **[47]** or conductance depending on the kind of sensor where SWCNTs are used. Similar behavior can also be explained in the case of RGO in a similar way. Reduction processes transform insulating GO into conductive RGO by removing oxygen-containing functional groups at the basal plane and the edges and restoring the aromaticity of the carbon network, thus recovering conductivity in RGO. Since the degree of removal of oxygen functionalities and the restoration of the conductivity can be controlled by the applied reduction process **[48]**, in RGO both kinds of mechanisms, capacitive and conductive, are possible. For

instance, Robinson et al. **[18]** made a gas sensor device based on RGO where conductance was the transduction mechanism. In our case, RGO is acting as a capacitance-based transducer due to the double layer capacitance produced by both constant phase elements (CPE_I and CPE_B). There is no redox process as in the case of conducting polymers **[49],** but RGO acts as an asymmetric capacitor where one side is formed by the ions in the solution (or in the ion-selective membrane in the case of ISEs) and the other side is formed by the graphene sp^2 electrons.

Table 5.2. Interfacial constant phase element (CPE_I), bulk constant phase element (CPE_B), and warburg element (Z_D) values obtained for two electrodes with different RGO film thicknesses in different electrolytes

Solution (0.1 M)	*Film thickness (nm)*	*CPE_I*		*CPE_B*		*Z_D* [c]
		Y_0 [a]	n [b]	Y_0 [a]	n	
KCL	1500	0,00017	0,9839	0,00437	0,9436	0,004
	125	0,00009	0,6552	0,00014	0,9173	0,001
NaCL	1500	0,00282	0,5939	0,02150	0,9237	0,020
	125	0,00003	0,7631	0,00056	0,9296	0,0005
LiCL	1500	0,00426	0,5491	0,10062	0,9283	0,01
	125	0,00004	0,7006	0,00014	0,9020	0,0001
$NaClO_4$	1500	0,01481	0,5530	0,19865	0,9142	0,02
	125	0,00002	0,8368	0,00042	0,9432	0,004
$LiClO_4$	1500	0,00192	0,7500	0,01480	0,9340	0,01
	125	0,00003	0,7809	0,00057	0,9314	0,0005

[a] Values of Yo are given in $S{\cdot}s^{0.5}/cm^2$.

[b] Adimensional.

[c] Values for the Warburg element are given in S·so.5/cm2.

With this transduction mechanism, it is preferable to have a solid contact with a high capacitive value as long as the adhesion and the coverage of the glassy carbon rod remain good. Since the capacitance of RGO increases with the film thickness (Table 2), the thicker RGO film (1500 nm) is preferable (compared to the 125 nm film) as an ion-to-electron transducer in solid-contact ISEs.

Once we have completely characterized RGO films as transducing elements in potentiometric measurements, we place on the top of the GC/RGO electrode an ion-selective membrane (ISM) for the detection of calcium ions (see the section "Preparation of the Ion-Selective Membrane for Calcium" in the Experimental Section

5.2.3.4). Therefore, as a proof of concept, the ISE for the selective detection of calcium is formed by the GC/RGO/ISM electrode. The sensitivity and linear range of the electrode were calculated on the basis of 30 calibration curves with 6 different electrodes (5 measurements for each electrode) measured over more than 1 month, which shows the performance of these ISEs over time (figure 5.6).

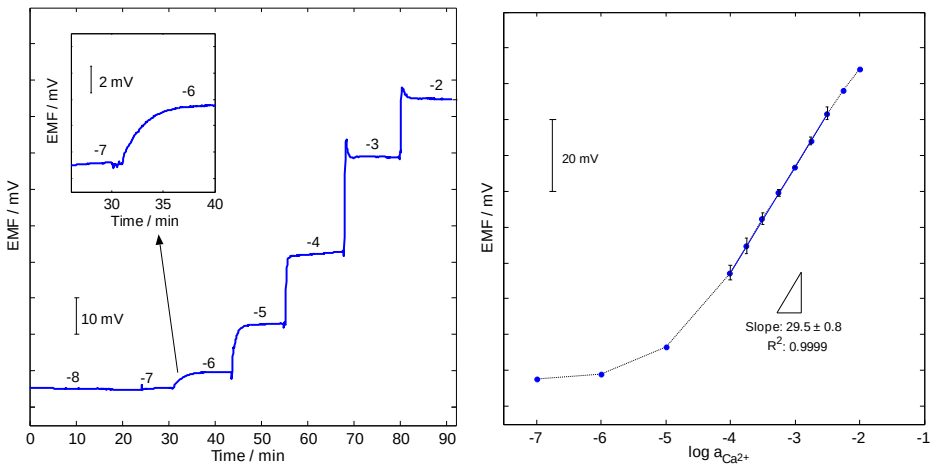

Figure 5.6. GC/RGO/ISM as the ISE for Ca^{2+} detection. (a) Potentiometric time response of an RGO Ca^{2+}-selective electrode for different Ca^{2+} activities. Inset: time response for low concentrations (10–6 M). (b) Nernstian slope of RGO-based Ca^{2+}-selective electrodes. The bars indicate standard deviations

The variation of electromotive force (EMF) versus time is shown in figure 5.6.a. Time responses of approximately 5 min are observed for very low concentrations of Ca^{2+}. This response time decreases to a few seconds for higher concentrations of Ca^{2+}.

Figure 5.6.b shows the typical potentiometric calibration curve with an excellent Nernstian slope with values of 29,5 mV/decade (n = 30, SD = 0,8 mV/decade, R^2=0,9999) and with a linear range from 10^{-5} to $10^{-2.5}$ M. The vertical bars in figure 5.6.b for each level of Ca^{2+} activity represent the standard deviation obtained with 30 experimental values (6 different electrodes and 5 measurements for each electrode). The maximum of these standard deviations in the linear range is 2,32 mV, almost half that obtained by Jaworska et al. **[35]** in their carboxy-functionalized graphene-based ISE. Medium-term stability of the electrodes was evaluated by recording the potentiometric signal for 24 h using a $10^{-2.4}$ M concentration of $CaCl_2$ (figure 5.7).

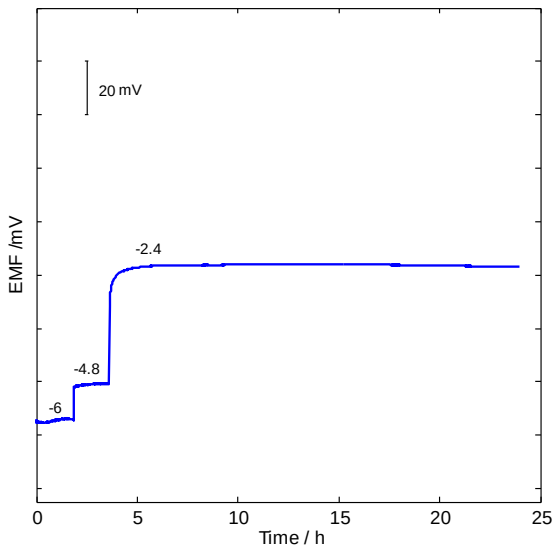

Figure 5.7. Medium-term potential stability of the Ca^{2+}-selective electrode over 24 h for a $10^{-2.4}$ M solution of $CaCl_2$.

The initial conditioning solution was 10^{-6} M before addition of a medium concentration ($10^{-4.8}$ M) to achieve the final concentration of $10^{-2.4}$ M. We observed a very minor and stable drift of the potentiometric signal (10 μV/h) compared with that of ISEs based on other nanostructured materials, **[31,32,50]** a drift that is slightly better than that presented by Ping et al. **[33]** in their RGO-based ISE. A much higher drift has been observed in a previous work using the same membrane and SWCNTs as the transducer (493 μV/h) **[51]**. RGO seems to add more stability to the signal, avoiding drifts at short and medium time responses. The increase in the signal/noise ratio is a clear advantage to obtain reliable analyte concentrations. A limit of detection of $10^{-6.2}$ M was estimated with the newly developed ISE. The limit of detection obtained in this paper is similar for other solid-contact calcium ISEs and the same as that obtained in a previous work using SWCNTs since the limit of detection and the selectivity values are slightly influenced by the transducer layer and depend strongly on the composition of the ion-selective membrane **[52]**. The selectivity of the RGO-based electrodes has been compared with that of similar solid-contact electrodes based on different conducting polymers **[53]**. The results are shown in figure 5.8, and the comparison of the values is collected in

Table 3, where selectivity coefficients have been obtained using the separated solution method **[42]**.

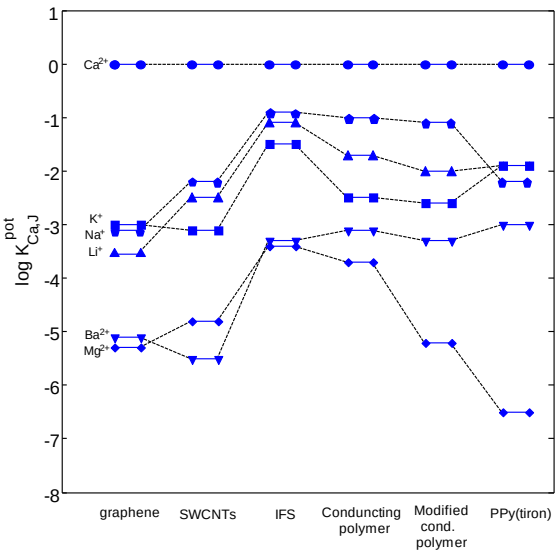

Figure 5.8. Comparison of the different selective coefficients for ISEs based on RGO, SWCNTs, and conducting polymers

To determine the presence of an aqueous layer between the RGO transducing layer and the ion-selective membrane that could influence the instrumental signal, we performed the water layer test proposed by Fibbioli et al. **[27]** The formation of this thin aqueous layer could cause chemical hysteresis and also mechanical failures due to the presence of ions or CO_2 in the water layer. The water layer test consists of observing the behavior of the ISE when a solution of the primary ion ($CaCl_2$, 0.1 M, in our case) is exchanged for a solution of an interfering ion ($MgCl_2$, 0.1 M, in our case) and then exchanged again for the initial solution of $CaCl_2$. Potential drifts observed in any part of the changing solution procedure indicate the presence of a thin aqueous layer, which causes new equilibria due to diffusion of ions to the aqueous layer. Electrodes were conditioned in a $CaCl_2$ (0.1 M) solution for 24 h and then replaced with a fresh solution of $MgCl_2$.

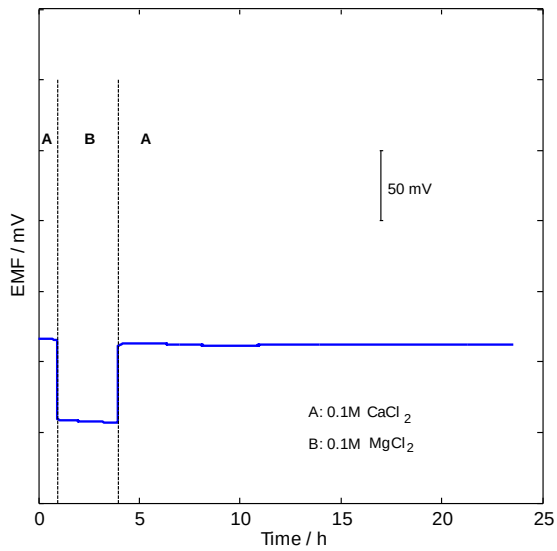

Figure 5.9. Potentiometric response of ISE in the water layer test. (A) At t = 1 h, the 0.1 $CaCl_2$ fresh solution of primary ion was replaced with the interfering 0.1 M $MgCl_2$ solution. (B) At t = 4 h, the interfering solution was exchanged with the initial solution, observing a very stable signal to 24 h.

Figure 5.9 shows a verystable response testing all three different zones. Very fast shifts are observed when the primary ion (zone A) is replaced with an interfering ion (zone B) and also when this ion is replaced with the initial solution (zone A). This fact suggests that the calcium is rapidly replaced by magnesium in the membrane. The water layer is presumed to be absent because there are no appreciable drifts in zone B due to the quilibrium of the interfering ion in the aqueous layer.

In a previous work using a nanostructured material (3DOM) **[30]** as the transducer, Lai et al. observed a positive drift when a solution of the primary ion was exchanged with an interfering ion, probably due to the leaching of the primary ion from the poly(vinyl chloride) (PVC) membranes, but this effect has not been shown in our ISE, obtaining a very fast replacement of primary ions without any drift. Similar results were obtained using SWCNTs with the same membrane in a previous work **[51]**. Both graphene- and SWCNT-based ISEs display a highly hydrophobic behavior that probably prevents the formation of an aqueous layer in the electrodes **[54]**.

5.2.5. Conclusions

In this work we presented the use of RGO films as transducer materials in potentiometric all-solid-state ISEs. Good adhesion to the underlying glassy carbon electrode, homogeneous coverage, and high capacitive values were obtained for RGO films with thicknesses of 125 and 1500 nm. The transduction mechanism revealed that RGO films act as asymmetric capacitors with high capacitive values. As a proof of concept, the GC/RGO film electrodes were used in the construction of an ISE for calcium. Highly reproducible sensing responses over time with an outstanding increased signal-to-noise ratio with drifts of only 10 μV/h were obtained. This provides RGO films with advantages over other types of transducer materials such as conducting polymers and carbon nanotubes. Combined with the ease of fabrication of RGO films with controlled thickness on GC electrodes, reliable ISE sensors with improved performance can be envisaged.

5.2.6. Acknowledgements

This study has been supported by the Spanish Ministry of Science and Innovation (MICINN) through Project Grants CTQ2010-18717 and MAT2010-15026, CSIC under Project 201080E124, and the Government of Aragon and the European Social Fund under Project DGA-FSE-T66 CNN. C.V. thanks MICINN and the European Social Fund for a postdoctoral contract under the Juan de la Cierva Programme. P.J. is grateful for a Ph.D. grant from Fundación Ramón Areces.

5.2.7. References

[1] Yu, A.; Ramesh, P.; Itkis, M. E.; Bekyarova, E.; Haddon, R. C., Graphite nanoplatelet-epoxy composite thermal interface materials. *Journal of Physical Chemistry C* **2007,** *111*, 7565-7569.

[2] Nair, R. R.; Blake, P.; Grigorenko, A. N.; Novoselov, K. S.; Booth, T. J.; Stauber, T.; Peres, N. M. R.; Geim, A. K., Fine structure constant defines visual transparency of graphene. *Science* **2008,** *320*, 1308-1308.

[3] Bunch, J. S.; van der Zande, A. M.; Verbridge, S. S.; Frank, I. W.; Tanenbaum, D. M.; Parpia, J. M.; Craighead, H. G.; McEuen, P. L., Electromechanical resonators from graphene sheets. *Science* **2007,** *315*, 490-493.

[4] Novoselov, K. S.; Geim, A. K.; Morozov, S. V.; Jiang, D.; Zhang, Y.; Dubonos, S. V.; Grigorieva, I. V.; Firsov, A. A., Electric field effect in atomically thin carbon films. *Science* **2004,** *306*, 666-669.

[5] Stoller, M. D.; Park, S.; Zhu, Y.; An, J.; Ruoff, R. S., Graphene-Based Ultracapacitors. *Nano Letters* **2008,** *8*, 3498-3502.

[6] Pumera, M., Graphene-based nanomaterials and their electrochemistry. *Chemical Society Reviews* **2010,** *39*, 4146-4157.

[7] Alwarappan, S.; Liu, C.; Kumar, A.; Li, C.-Z., Enzyme-Doped Graphene Nanosheets for Enhanced Glucose Biosensing. *Journal of Physical Chemistry C* **2010,** *114*, 12920-12924.

[8] Alwarappan, S.; Boyapalle, S.; Kumar, A.; Li, C.-Z.; Mohapatra, S., Comparative Study of Single-, Few-, and Multi layered Graphene toward Enzyme Conjugation and Electrochemical Response. *Journal of Physical Chemistry C* **2012,** *116*, 6556-6559.

[9] Alwarappan, S.; Joshi, R. K.; Ram, M. K.; Kumar, A., Electron transfer mechanism of cytochrome c at graphene electrode. *Applied Physics Letters* **2010,** *96*, 1-3.

[10] Wang, Y.; Li, Y.; Tang, L.; Lu, J.; Li, J., Application of graphene-modified electrode for selective detection of dopamine. *Electrochemistry Communications* **2009,** *11*, 889-892.

[11] Blake, P.; Brimicombe, P. D.; Nair, R. R.; Booth, T. J.; Jiang, D.; Schedin, F.; Ponomarenko, L. A.; Morozov, S. V.; Gleeson, H. F.; Hill, E. W.; Geim, A. K.; Novoselov, K. S., Graphene-based liquid crystal device. *Nano Letters* **2008,** *8*, 1704-1708.

[12] Liu, C.; Alwarappan, S.; Chen, Z.; Kong, X.; Li, C.-Z., Membraneless enzymatic biofuel cells based on graphene nanosheets. *Biosensors & Bioelectronics* **2010,** *25*, 1829-1833.

[13] Ruoff, R., Calling all chemists. *Nature Nanotechnology* **2008,** *3*, 10-11.

[14] Li, D.; Mueller, M. B.; Gilje, S.; Kaner, R. B.; Wallace, G. G., Processable aqueous dispersions of graphene nanosheets. *Nature Nanotechnology* **2008,** *3*, 101-105.

[15] Stankovich, S.; Dikin, D. A.; Piner, R. D.; Kohlhaas, K. A.; Kleinhammes, A.; Jia, Y.; Wu, Y.; Nguyen, S. T.; Ruoff, R. S., Synthesis of graphene-based nanosheets via chemical reduction of exfoliated graphite oxide. *Carbon* **2007,** *45*, 1558-1565.

[16] Dreyer, D. R.; Park, S.; Bielawski, C. W.; Ruoff, R. S., The chemistry of graphene oxide. *Chemical Society Reviews* **2010,** *39*, 228-240.

[17] Hummers, W. S.; Offeman, R. E., Preparation of graphitic oxide. *Journal of the American Chemical Society* **1958,** *80*, 1339-1339.

[18] Robinson, J. T.; Perkins, F. K.; Snow, E. S.; Wei, Z.; Sheehan, P. E., Reduced Graphene Oxide Molecular Sensors. *Nano Letters* **2008,** *8*, 3137-3140.

[19] Shao, Y.; Wang, J.; Wu, H.; Liu, J.; Aksay, I. A.; Lin, Y., Graphene Based Electrochemical Sensors and Biosensors: A Review. *Electroanalysis* **2010,** *22*, 1027-1036.

[20] Pumera, M., Graphene in biosensing. *Materials Today* **2011,** *14*, 308-315.

[21] Banks, C. E.; Crossley, A.; Salter, C.; Wilkins, S. J.; Compton, R. G., Carbon nanotubes contain metal impurities which are responsible for the "electrocatalysis" seen at some nanotube-modified electrodes. *Angewandte Chemie-International Edition* **2006,** *45*, 2533-2537.

[22] Fowler, J. D.; Allen, M. J.; Tung, V. C.; Yang, Y.; Kaner, R. B.; Weiller, B. H., Practical Chemical Sensors from Chemically Derived Graphene. *Acs Nano* **2009,** *3*, 301-306.

[23] Lu, G.; Ocola, L. E.; Chen, J., Gas detection using low-temperature reduced graphene oxide sheets. *Applied Physics Letters* **2009,** *94*, 1-3.

[24] Li, J.; Guo, S.; Zhai, Y.; Wang, E., Nafion-graphene nanocomposite film as enhanced sensing platform for ultrasensitive determination of cadmium. *Electrochemistry Communications* **2009,** *11*, 1085-1088.

[25] Alwarappan, S.; Erdem, A.; Liu, C.; Li, C.-Z., Probing the Electrochemical Properties of Graphene Nanosheets for Biosensing Applications. *Journal of Physical Chemistry C* **2009,** *113*, 8853-8857.

[26] Bobacka, J., Potential stability of all-solid-state ion-selective electrodes using conducting polymers as ion-to-electron transducers. *Analytical Chemistry* **1999,** *71*, 4932-4937.

[27] Fibbioli, M.; Morf, W. E.; Badertscher, M.; de Rooij, N. F.; Pretsch, E., Potential drifts of solid-contacted ion-selective electrodes due to zero-current ion fluxes through the sensor membrane. *Electroanalysis* **2000,** *12* , 1286-1292.

[28] Lindfors, T., Light sensitivity and potential stability of electrically conducting polymers commonly used in solid contact ion-selective electrodes. *Journal of Solid State Electrochemistry* **2009,** *13*, 77-89.

[29] Vazquez, M.; Bobacka, J.; Ivaska, A.; Lewenstam, A., Influence of oxygen and carbon dioxide on the electrochemical stability of poly(3,4-ethylenedioxythiophene) used as ion-to-electron transducer in all-solid-state ion-selective electrodes. *Sensors and Actuators B-Chemical* **2002,** *82*, 7-13.

[30] Lai, C.-Z.; Joyer, M. M.; Fierke, M. A.; Petkovich, N. D.; Stein, A.; Buhlmann, P., Subnanomolar detection limit application of ion-selective electrodes with three-dimensionally ordered macroporous (3DOM) carbon solid contacts. *Journal of Solid State Electrochemistry* **2009,** *13*, 123-128.

[31] Crespo, G. A.; Macho, S.; Xavier Rius, F., Ion-selective electrodes using carbon nanotubes as ion-to-electron transducers. *Analytical Chemistry* **2008,** *80*, 1316-1322.

[32] Parra, E. J.; Crespo, G. A.; Riu, J.; Ruiz, A.; Rius, F. X., Ion-selective electrodes using multi-walled carbon nanotubes as ion-to-electron transducers for the detection of perchlorate. *Analyst* **2009,** *134*, 1905-1910.

[33] Ping, J.; Wang, Y.; Wu, J.; Ying, Y., Development of an all-solid-state potassium ion-selective electrode using graphene as the solid-contact transducer. *Electrochemistry Communications* **2011,** *13*, 1529-1532.

[34] Li, F.; Ye, J.; Zhou, M.; Gan, S.; Zhang, Q.; Han, D.; Niu, L., All-solid-state potassium-selective electrode using graphene as the solid contact. *Analyst* **2012,** *137*, 618-623.

[35] Jaworska, E.; Lewandowski, W.; Mieczkowski, J.; Maksymiuk, K.; Michalska, A., Critical assessment of graphene as ion-to-electron transducer for all-solid-state potentiometric sensors. *Talanta* **2012,** *97*, 414-419.

[36] Jaworska, E.; Lewandowski, W.; Mieczkowski, J.; Maksymiuk, K.; Michalska, A., Non-covalently functionalized graphene for the potentiometric sensing of zinc ions. *Analyst* **2012,** *137*, 1895-1898.

[37] Valles, C.; Jimenez, P.; Munoz, E.; Benito, A. M.; Maser, W. K., Simultaneous Reduction of Graphene Oxide and Polyaniline: Doping-Assisted Formation of a Solid-State Charge-Transfer Complex. *Journal of Physical Chemistry C* **2011,** *115*, 10468-10474.

[38] Valles, C.; David Nunez, J.; Benito, A. M.; Maser, W. K., Flexible conductive graphene paper obtained by direct and gentle annealing of graphene oxide paper. *Carbon* **2012,** *50*, 835-844.

[39] Heng, L. Y.; Hall, E. A. H., Methacrylic-acrylic polymers in ion-selective membranes: achieving the right polymer recipe. *Analytica Chimica Acta* **2000,** *403*, 77-89.

[40] Qin, Y.; Peper, S.; Radu, A.; Ceresa, A.; Bakker, E., Plasticizer-free polymer containing a covalently immobilized Ca2+-selective Ionophore for potentiometric and optical sensors. *Analytical Chemistry* **2003,** *75*, 3038-3045.

[41] Lindner, E.; Umezawa, Y., Performance evaluation criteria for preparation and measurement of macro- and microfabricated ion-selective electrodes. *Pure and Applied Chemistry* **2008,** *80*, 85-104.

[42] Bakker, E.; Pretsch, E.; Buhlmann, P., Selectivity of potentiometric ion sensors. *Analytical Chemistry* **2000,** *72*, 1127-1133.

[43] Crespo, G. A.; Macho, S.; Bobacka, J.; Rius, F. X., Transduction Mechanism of Carbon Nanotubes in Solid-Contact Ion-Selective Electrodes. *Analytical Chemistry* **2009,** *81*, 676-681.

[44] Tang, L.; Wang, Y.; Li, Y.; Feng, H.; Lu, J.; Li, J., Preparation, Structure, and Electrochemical Properties of Reduced Graphene Sheet Films. *Advanced Functional Materials* **2009,** *19*, 2782-2789.

[45] MacDonald, J. R.; Barsoukov, E., *Impedance Spectroscopy*. John Wiley & Sons,: Hoboken, New Jersey, **2005**.

[46] Kim, C. H.; Pyun, S.; Kim, J. H., An investigation of the capacitance dispersion on the fractal carbon electrode with edge and basal orientations. *Electrochimica Acta* **2003,** *48*, 3455-3463.

[47] Snow, E. S.; Perkins, F. K.; Houser, E. J.; Badescu, S. C.; Reinecke, T. L., Chemical detection with a single-walled carbon nanotube capacitor. *Science* **2005,** *307*, 1942-1945.

[48] Gilje, S.; Han, S.; Wang, M.; Wang, K. L.; Kaner, R. B., A chemical route to graphene for device applications. *Nano Letters* **2007,** *7*, 3394-3398.

[49] Bobacka, J., Conducting polymer-based solid-state ion-selective electrodes. *Electroanalysis* **2006,** *18*, 7-18.

[50] Ampurdanes, J.; Crespo, G. A.; Maroto, A.; Angeles Sarmentero, M.; Ballester, P.; Xavier Rius, F., Determination of choline and derivatives with a solid-contact ion-selective electrode based on octaamide cavitand and carbon nanotubes. *Biosensors & Bioelectronics* **2009,** *25*, 344-349.

[51] Hernandez, R.; Riu, J.; Xavier Rius, F., Determination of calcium ion in sap using carbon nanotube-based ion-selective electrodes. *Analyst* **2010,** *135*, 1979-1985.

[52] Mousavi, Z.; Bobacka, J.; Lewenstam, A.; Ivaska, A., Poly(3,4-ethylenedioxythiophene) (PEDOT) doped with carbon nanotubes as ion-to-electron transducer in polymer membrane-based potassium ion-selective electrodes. *Journal of Electroanalytical Chemistry* **2009,** *633*, 246-252.

[53] Michalska, A.; Konopka, A.; Maj-Zurawska, M., All-solid-state calcium solvent polymeric membrane electrode for low-level concentration measurements. *Analytical Chemistry* **2003,** *75*, 141-144.

[54] Sun, Y. P.; Fu, K. F.; Lin, Y.; Huang, W. J., Functionalized carbon nanotubes: Properties and applications. *Accounts of Chemical Research* **2002,** *35*, 1096-1104.

UNIVERSITAT ROVIRA I VIRGILI
SOLID CONTACT POTENTIOMETRIC SENSORS BASED ON CARBON NANOMATERIALS
Rafael Hernández Malo

UNIVERSITAT ROVIRA I VIRGILI
SOLID CONTACT POTENTIOMETRIC SENSORS BASED ON CARBON NANOMATERIALS
Rafael Hernández Malo

UNIVERSITAT ROVIRA I VIRGILI
SOLID CONTACT POTENTIOMETRIC SENSORS BASED ON CARBON NANOMATERIALS
Rafael Hernández Malo

6.1. Introduction

In the previous chapters we have demonstrated the efficient use of carbon-based nanomaterials in ion-selective electrodes for the detection of calcium. Recently, our research group also showed that SWCNTs can be used in aptasensors for selectively detecting ultralow concentrations of bacteria in real time.

To date, the detection of bacteria can be performed by simple culture samples in specific nutrients, but this method is very time-consuming, and time is often crucial for the treatment of certain diseases. Other methods such as polymerase chain reaction (PCR) are much faster, since detection can be performed in a few minutes, but these methods are expensive and they often require sample pretreatment.

The aim of this chapter is using graphene-based materials for the construction of an aptasensor for the selective and ultralow detection of *Staphylococcus aureus*. We covalenty and non-covalently attached the aptamer to the graphene-based material in two different versions of the aptasensor.

The Content of this chapter has-been published in the Journal, Biosensors & Bioelectronics, year 2014, volume 54, pages 553-557, and co-authored by Cristina Vallés, Ana M. Benito, Wolfgang K. Maser, F. Xavier Rius and Jordi Riu.

6.2. Article

Biosensors and Bioelectronics 54 (2014) 553–557

Contents lists available at ScienceDirect

Biosensors and Bioelectronics

journal homepage: www.elsevier.com/locate/bios

Short communication

Graphene-based potentiometric biosensor for the immediate detection of living bacteria.

Rafael Hernández [a], Cristina Vallés [b], Ana M. Benito [b], Wolfgang K.Maser [b], F.Xavier Rius [a], Jordi Riu [a],*

a Department of Analytical and Organic Chemistry, Universitat Rovira I Virgili, Campus Sescelades, c/Marcel·lí Domingo s/n, 43007 - Tarragona, Spain
b Department of Chemical Processes and Nanotechnology, Instituto de Carboquímica ICB-CSIC, Zaragoza, Spain

6.2.1. Abstract

In this communication we present a potentiometric aptasensor based on chemically modified graphene (transducer layer of the aptasensor) and aptamers (sensing layer). Graphene oxide (GO) and reduced graphene oxide (RGO) are the basis for the construction of two versions of the aptasensor for the detection of a challenging living organism such as *Staphylococcus aureus*. In these two versions, DNA aptamers are either covalently (in the GO case) or non-covalently (in the RGO case) attached to the transducer layer. In both cases we are able to selectively detect a single CFU/mL of *S. aureus* in anassay close to real time, although the noise level associated to the aptasensors made with RGO is lower than the ones made with GO. These new aptasensors, that show a high selectivity, are characterized by the simplicity of the technique and the materials used for their construction while offering ultra-low detection limits in very short time responses in the detection of microorganisms.

6.2.2. Introduction

In this communication we report for the first time a potentiometric biosensor based on chemically modified graphene and aptamers for the rapid, selective and ultrasensitive detection of *Staphylococcus aureus* (*S. aureus*).

Without need for tedious pretreatment procedures, such as DNA extraction, and with a detection limit of only one colony-forming unit (CFU)/ml on a time scale of a few seconds this biosensor largely out performs existing detection methods insimplicity and performance parameters thus demonstrating a high potential for the detection of challenging microorganisms.

Effective prevention of infectious diseases caused by bacteriais one of the major public concerns. Standard methods used to assess the presence of microbiological threats consist of specific enrichment media to separate, identify, and count bacterial cells. Depending on the specific microorganism to detect, one day to several weeks might be necessary to determine its presence. Current research efforts led to rapid detection of ultra-low amounts of microorganisms. For instance methods based on ultrafast polymerase chain reaction (PCR) **[1]** can detect bacteria in a few minutes with limits of detection of a few CFU. However, the techniques based on nucleic acid sequences detection usually require preprocessing steps for DNA extraction, amplification and detection, what makes the overall procedure expensive and complicated. Other recent strategies are based on the use of functionalized gold nanoparticles that bind to the bacterial surface for colorimetric detection **[2]**, positron emission tomography (PET) imaging **[3]** or bacteriophage amplification coupled with mass spectrometry **[4]**. Again, in all cases this is achieved by employing tedious pretreatment steps or requires expensive equipments.

Electrochemical techniques are usually much simpler and non-expensive, and a few amperometric techniques for *S. aureus* detection have been reported so far but with detection limits ranging between 10^6 CFU/ml in 3h **[5]** or 10^3 CFU/ml in 50 min **[6]**. We recently presented carbon nanotube and aptamer-based potentiometric biosensors in which we took benefit of the excellent recognition ability of aptamers towards a specific target and of the outstanding transducer abilities of carbon nanotubes. Taking benefit of the simplicity and low-cost instrumentation of potentiometric techniques, these biosensors based on aptamers (also known as aptasensors) and carbon nanotubes are able to detect, with inter and intra-strain selectivity 1 CFU of *Salmonella Typhi* in 5ml of buffered sample in less than 1 min **[7]**, or 12 CFU of *Escherichia coli* (*E. coli*) in 2 ml of milk in a couple of minutes **[8]**. Using these carbon nanotube-based

aptasensors in case of challenging microorganisms such as *S. aureus* we were able to detect $8x10^2$ CFU/ml of living *S. aureus* in a couple of minutes **[9]**.

This value is very high compared to the cases of *Salmonella Typhi* or *E. coli*. However, taking into account the inherent difficulty for the detectionof *S.aureus* due to the presence of a thick polysaccharide layer of poly-N-acetylglucosamine on its surface and the low abundance of antigens externally exposed the value of $8x10^2$ CFU/ml represents a benchmark for thedirect detection of *S.aureus* employing electrochemical biosensing systems. Herein we report the construction of a new generation of potentiometric aptasensors with significantly enhanced performance exploiting for the first time the excellent electrochemical **[10]** and transduction **[11]** properties of chemically modified graphene. Using both, graphene oxide (GO) and reduced graphene oxide (RGO) as transduction layer subsequently functionalized with a DNA aptamer able to recognize epitopes on the surface of *S.aureus* **[12]** we demonstrate that the resulting aptasensor s are able to selectively detect just one single CFU/ml of the challenging *S.aureus* in 1-2 min. The ultra-sensitive performance of this potentiometric aptasensor not only outperforms results obtained with carbon nanotubes as transduction layer but represents an important breakthrough towards rapid zero-tolerance microbiological detection systems.

6.2.3. Experimental part

6.2.3.1. Construction of the biosensor

The biosensor was built on top of a glassy carbon (GC) rod (length 50 mm and diameter 3 mm) jacketed with a teflon layer. The surface of the GC rod was polished first with a sheet of abrasive paper (BuehlerCarbimet600/P1200) and then with different grain-sized alumina (30, 5, 1 and 0.5 µm).

Graphite oxide was prepared using a modified Hummer´s method from graphite powder (Sigma-Aldrich) by oxidation with $NaNO_3$, $H2SO_4$ and $KMnO_4$ in an ice bath as reported in detail elsewhere **[13]**. A suspension of GO sheets was obtained by sonication of the prepared graphite oxide powder in distilled water (1 mg/mL) for 2h, followed by mild centrifugation of the suspension at 4500 rpm for 60min **[14]**. The resulting brown-coloured water dispersion with a concentration of 0.3mg/ml contained

single to few-layered GO sheets of 2 to 10 individual layers. GO films on glassy carbon (GC) electrodes were prepared as follows.

Homogeneous aqueous GO dispersions of a controlled volume of 15 mL were drop-casted onto clean and polished surfaces of the GC electrodes and allowed to dry at room temperature. The deposition process was repeated other 9 times until the final thickness obtained for 10 depositions was 1460 nm (thicknesses measured by confocal microscopy). A set of GO electrodes was kept for later covalent functionalization and in another set GO was reduced to RGO for further non-covalent functionalization. Reduction of deposited GO films was performed by a 24 h exposure of electrodes to hydrazine monohydrate vapours **[15]**. This reduction method efficiently removes various oxygen functional groups of the graphene oxide sheets and restores the aromaticity of the carbon network, even for films as thick as 1500 nm **[14]**. This procedure thus transforms the GO films into reduced graphene oxide (RGO) films with remaining oxygen and nitrogen moieties of about 10 and 1.5%, respectively.

Finally, both sets of electrodes (GO and RGO electrodes) were properly functionalized with the corresponding aptamers. GO electrodes were introduced in a solution of 100 nmol of N-(3-dimethylaminopropyl)-N′-ethyl- carbodiimide hydrochloride (EDC) and 25 nmol of N-hydroxysuccinimide (NHS) in a 50 mM 2-(N-morpholino) ethanesulfonic acid (MES) buffer at pH 5 for 30 min to activate the carboxylic groups present at the edge planes and defects of the deposited graphene oxide. After this step, electrodes were immersed overnight into 0.5 mL of a 1 µM *S. aureus* SA20 binding aptamer solution dispersed in PBS pH 7.4 (1mM). In the case of the RGO electrodes, non-covalent functionalization of the *S. aureus* SA31 binding aptamer was done depositing a drop of the 1 µM aptamer dispersed in PBS pH 7.4 (1 mM) and leaving overnight in a wet atmosphere. Both 88-mer aptamers (SA20 and SA31) have similar affinities for *S. aureus* **[12]**.

6.2.3.2. Potentiometric measurements

Potentiometric analysis was performed by real-time measurements of the electromotive force (EMF) between the terminals of a two-electrode system consisting of the GO/RGO aptasensor as the working electrode, and a double junction reference electrode (Ag/ AgCl/KCl 3M containing a 1 M LiAcO electrolyte bridge, type 6.0729.100,

MetrohmAG, Herisau, Switzerland) as the reference electrode at isothermal conditions (22±0.5 ºC) in a water-jacketed glass cell under constant stirring conditions (300 rpm). A high-input impedance voltmeter (10^{15} Ω, model EMF16, Lawson Laboratories Inc, Malvern, PA, USA) was used in all the cases to measure the difference in electromotive force. The changes on EMF were automatically measured at periods of 10s. The electrolyte used in the cell was 5ml of PBS 1.7m M pH 7.4. The EMF value was recorded automatically with the software provided by the company. In all cases, the amount of bacteria detected by the potentiometric measurements was simultaneously standardized in quintuplicate using the agar plate count technique.

Details about materials, aptamers, culture conditions and characterization of GO and RGO films can be found in the Annexe 8.3.

6.2.4. Results and discussions

The basis of the aptasensor is the transduction layer formed by GO that is deposited onto the polished surface of a GC rod. For comparison purposes, and in order to look for the best strategy of detection, two different methods of functionalization were used to attach the aptamers to this transduction layer: a covalent approach and a non-covalent one (figure. 6.1.a and b). The covalent approach consisted of chemically linking the aptamers to GO by amide bonds formed between the carboxylic groups present on the deposited GO flakes and an amine moiety introduced at the 3′-end of the aptamer by well-known carbodiimide mediated chemistry **[16]**. The flexibility of the aptamer chains then facilitates their flat arrangement on the GO surface (comparable to DNA wrapping on carbon nanotubes) **[17]**. In the non-covalent approach we first reduced GO to RGO to remove the unnecessary presence of the various functional oxygen moieties located on the basal and edge plane of GO.

Subsequently, pyrenil moieties previously introduced at the 3′-end of the aptamer were non-covalently physisorbed onto the RGO surface. Effective π–π interactions between pyrene and graphene also facilitate a flat organization of the aptamer to the RGO surface **[18]**. In presence of the target bacteria, for both the covalent and the non-covalent functionalization, the aptamer prefers to bind to the bacteria rather than remaining attached onto the GO/RGO surface. It thus overcomes the strong π–π interactions and tends to separate its negatively ionized phosphodiester groups at a pH

value of 7.4 from the underlying GO/RGO surface. Since the GO/RGO films act as asymmetric capacitors **[11]** this separation of charges provokes a subsequent change of the recorded potential.

Consecutive additions of increasing amounts of living *S. aureus* in phosphate buffer solutions (PBS 1.7 mM, pH 7.4) were performed to test the response of the covalent and the non-covalent functionalized aptasensors. Figure 6.1.c shows a transmission electron microscopy (TEM) image of a single *S. aureus* cell captured on the graphene–aptamer layer. The amount of bacteria in each addition was simultaneously checked by five independent measurements using the agar plate count technique. Figure 6.2.a reveals that the non-covalent functionalized aptasensors are able to detect 1 CFU/ml in a few minutes and that an immediate change was observed after the addition of *S. aureus* for the whole working range.

For the covalent functionalized aptasensors the potentiometric response exhibits a (somewhat) higher noise level although the aptasensor is also able to respond to low additions of *S. aureus*. The difference in noise can be observed in the instrumental limit of detection (defined as three times the standard deviation of the noise), which corresponds to 29 mV for the non-covalent functionalization and 76 mV for the covalent functionalization. Both values are significantly better than the instrumental limit of detection of 240 mV obtained for carbon nanotube-based aptasensors **[7]**. The lower noise and therefore the lower instrumental limit of detection for the non-covalent functionalization may be attributed to the lower number of defects in the RGO layers after hydrazine reduction (compared to the defects in the GO layers used in the covalent functionalization). This positively affects the charge-separation mechanism and favours the asymmetric capacitor-like behaviour of the transducer layer **[11]** thus resulting in an overall enhanced transducer efficiency.

Surprisingly, and despite a higher noise level, the precision associated with the determination of *S. aureus* using different aptasensors is better in case of the covalent functionalization approach. Figure. 6.2.b and c clearly showth at the construction of a set of covalently functionalized aptasensors offers a higher reproducibility compared to the non-covalently functionalized ones.

The fact that in the case of the non-covalent functionalization an additional reduction step is required (to convert GO into RGO) may negatively impact on the reproducibility because of the inherent experimental variability due to this extra step.

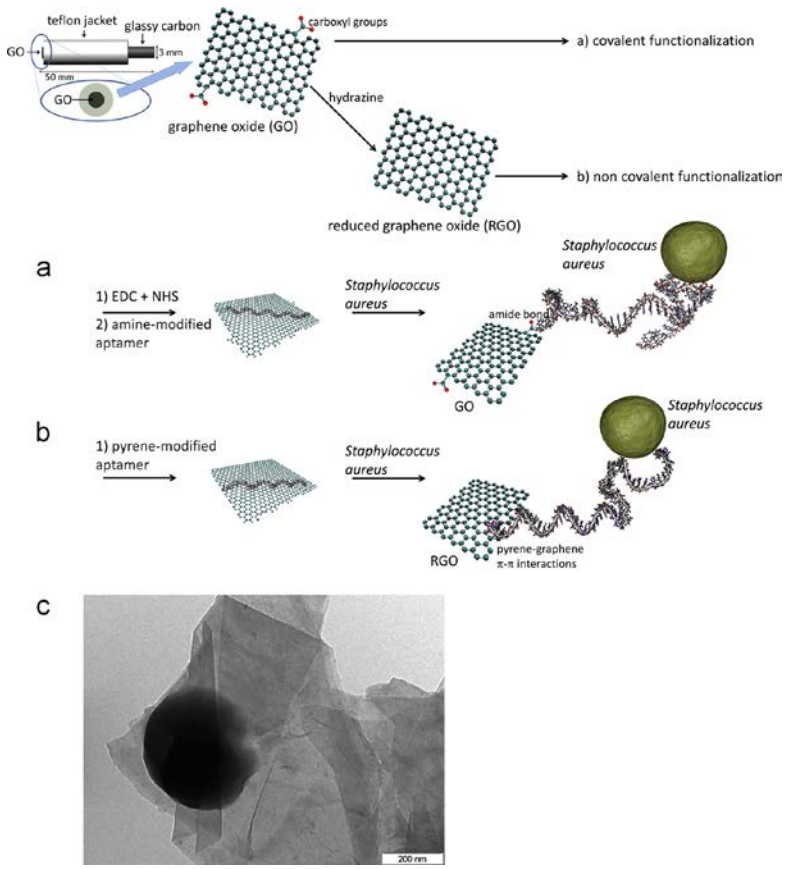

Figure 6.1. Scheme of the overall process of functionalization and detection of *S. aureus* (the different parts are not to scale). Top: Schematic illustration of the potentiometric aptasensor. Forsake of clarity the GO layer only presents a few carboxyl groups and other functional defects (e.g. alcohols, ethers, ketones…) are not shown. (a) The covalent functionalization of GO with the *S. aureus* aptamer following carbodiimide-mediated chemistry facilitates a flat stacking of the aptamer to the GO surface. (b) The non-covalent functionalization of GO with the *S. aureus* aptamer resultsin π–π stacking between RGO and pyrene moieties and also facilitates a flat stacking of the aptamer to the RGO surface. (c) TEM image of a single *S. aureus* cell captured on agraphene–aptamer layer

In any case, thick layers of transducer films (i.e. 146onm) help to overcome this problem **[1]**. At higher amounts of bacteria, each EMF increase was less prominent, demonstrating progressive saturation of the available binding sites. Although the noise level may hinder in some cases (especially in the non-covalent functionalization) a precise quantification of *S. aureus* until a better reproducibility in the home-made construction of the biosensor is attained, the biosensor can also be used for semiquantitative purposes or to decide the presence/absence of *S. aureus* below or above a threshold value (even if this threshold is aslo was a few CFU/ml). It is important to remark that the apparent low values of the sensitivities (figure. 6.2) are due to the particular sensing mechanism, different from the classical Nernstian model, in which the change in the electromotiveforce results from a rearrangement of the electrical charges at the surface of GO/RGO during the recognition event. Therefore, no Nernstian responses are expected in these aptasensors.

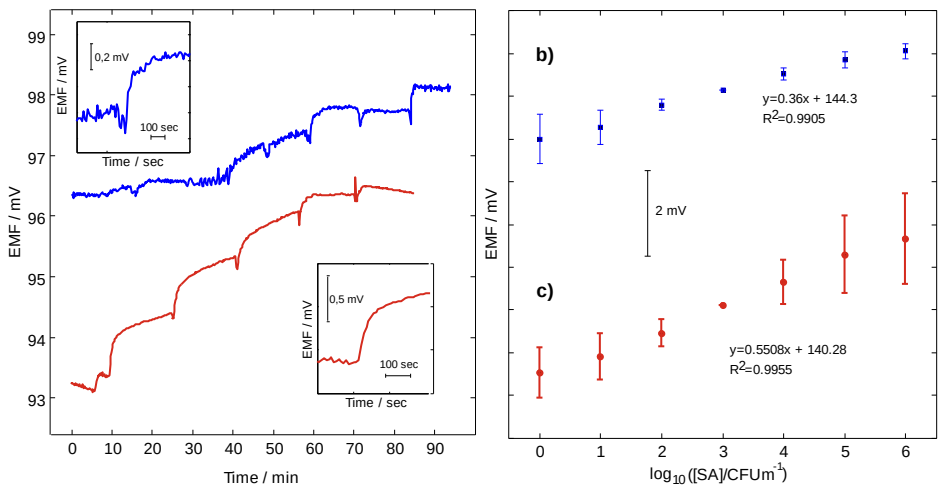

Figure. 6.2. (a) Aptamer-functionalized aptasensor exposed to stepwise increases of *S. aureus* concentration and the corresponding potentiometric response; numbers above each potentiometric jump represent the final concentration of bacteria. Insets show the detail of two inoculation steps for the covalent and non-covalent functionalization. (b) EMF response versus log of concentration of *S. aureus* for the covalent functionalization. (c) EMF response versus log of concentrationof *S. aureus* for the non-covalent functionalization. In (b) and (c) error bars are standard deviation of the response obtained at a given concentration for six different sensors. The sensitivities of the aptasensors are 0.34 mV/decade (covalent functionalization) and 0.55 mV/decade (non-covalent functionalization).

Interestingly, when using carbon nanotubes as the transducer material [7] for the detection of the same microorganism the differences between the covalent and the non- covalent functionalization are tremendous: the best results (a high detection value of 8x102 CFU/ml of *S. aureus*) are obtained with the covalent functionalization, obtaining a very poor detection ability with the non-covalent strategy (concentrations above 107 CFU/ml). This effect most likely is related to the surface properties of the aptasensor. While the entangled network of carbon nanotubes forming the transducer layer sterically reduces the interaction possibilities with the pyrene molecules, the bidimensional graphene sheets provides a large surface area to favour π–π stacking between RGO and pyrene moieties. This also directly influences the transducing properties and leads to significantly improved responses for graphene-based aptasensors, independently if covalently or non-covalently functionalized.

The new aptasensors show a high degree of selectivity since no response was obtained for experiments using either *E. coli* as a Gram-negative bacteria or *Lactobacillus casei* (L. casei) as a Gram-positive microorganism (figure. 6.3.a–d). Control experiments (figure. 6.3.e–i) confirmed that the responses are solely caused by the binding event between *S. aureus* and the aptamer and the subsequent transduction of the GO or RGO layer. We tested glassy carbon electrodes without transduction and recognition layer (figure. 6.3.e) and glassy carbon (without transduction layer) both covalently and non-covalently functionalized (figure. 6.3.f and g). We also examined the potentiometric response without recognition layer (figure. 6.3.h) and using a non-covalently functionalized aptasensor but without pyrenil moieties (figure. 6.3.i). There was no potentiometric response under any of these conditions, showing that the EMF changeis only generated when aptamers attached to GO/RGO interact with *S. aureus*. Therefore, the two elements, aptamer (as recognition layer) and GO or RGO (as transduction layer), are essential to successfully detect *S. aureus*.

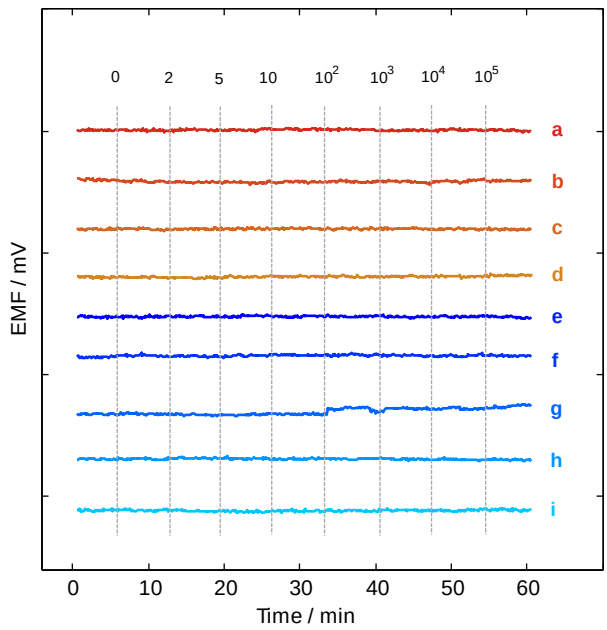

Figure 6.3. Selectivity ((a)–(d)) and control ((e)–(i)) assays. EMF response versus time for different concentrations of bacteria. Vertical lines represent inoculation with increasing amounts of bacteria (in CFU/ml). From top to bottom: (a) and (b) Covalently functionalized biosensor exposed to *Escherichia coli* and *L. casei*, respectively; (c) and (d) Non-covalently functionalized biosensor exposed to *E. coli* and *L. casei*, respectively; (e) Glassy carbon electrode exposed to *S. aureus*; (f) and (g) Glassy carbon without GO/RGO covalently and non-covalently functionalized with aptamer exposed to *S. aureus*; (h) Glassy carbon with a layer of GO/RGO and without aptamer exposed to *S. aureus*; (i) Non-covalently functionalized aptasensor without pyrenil moieties in the aptamer exposed to *S. aureus*.

The aptasensors can be easily regenerated after each set of measurements by dissociating the aptamers from the bacteria in 2 M NaCl solution for 1h. Inpresence of 2 M NaCl, the tertiary structure of the aptamer changes so that *S. aureus* dissociate from aptamers. After regeneration, all the electrodes were washed gently with MilliQ water and stored in sterile PBS solution (1.7 mM, pH 7.4) for new measurements. All the electrodes were reused at least three times during around one month without any change in sensitivity or instrumental noise.

6.2.5. Conclusions

In this communication we present a graphene-based aptasensor that is able to selectively detect a single CFU/ml in an assay close to real time of a challenging living organism such as *S. aureus*.

Two different strategies were followed to attach the aptamer to the GO or RGO layer. Both, the outperforming results obtained, as well as the simplicity of the technique and the materials used for the construction of the aptasensors may pave the way towards a new generation of microbiological analysis systems characterized by construction simplicity while offering ultra-low detection limits and close to real-time responses.

To use this aptasensor in real samples with complex matrices, we would probably need to use a filtration protocol **[12]** to remove the undesired electroactive species within the original matrix, which other wise may lead to inaccurate results in biosensing experiments. These experiments with real biological samples are foreseen and they will show the final viability of our concept. In any case it is important to remark that this filtration protocol is carried out using standard commercial cellulose acetate filters and that the total time of this step is only of 1–2 min.

6.2.6. Acknowledgements

The authors acknowledge the financial support from the Spanish Ministry of Science and Innovation (MICINN) through project grants CTQ2010-18717, MAT2010-15026, CSIC under project 201080 E124 and the Government of Aragon and the European Social Fund under project DGA-FSE-T66CNN.

6.2.7. References

[1] Banada, P. P.; Chakravorty, S.; Shah, D.; Burday, M.; Mazzella, F. M.; Alland, D., Highly Sensitive Detection of *Staphylococcus aureus* Directly from Patient Blood. *Plos One* **2012,** 7, 1-7.

[2] Wang, J.; Gao, J.; Liu, D.; Han, D.; Wang, Z., Phenylboronic acid functionalized gold nanoparticles for highly sensitive detection of *Staphylococcus aureus*. *Nanoscale* **2012,** 4, 451-454.

[3] Panizzi, P.; Nahrendorf, M.; Figueiredo, J.-L.; Panizzi, J.; Marinelli, B.; Iwamoto, Y.; Keliher, E.; Maddur, A. A.; Waterman, P.; Kroh, H. K.; Leuschner, F.; Aikawa, E.; Swirski, F. K.; Pittet, M. J.; Hackeng, T. M.; Fuentes-Prior, P.; Schneewind, O.; Bock, P. E.; Weissleder, R., In vivo detection of *Staphylococcus aureus* endocarditis by targeting pathogen-specific prothrombin activation. *Nature Medicine* **2011,** *17*, 1142-U153.

[4] Pierce, C. L.; Rees, J. C.; Fernandez, F. M.; Barr, J. R., Detection of *Staphylococcus aureus* Using N-15-Labeled Bacteriophage Amplification Coupled with Matrix-Assisted Laser Desorption/Ionization-Time-of-Flight Mass Spectrometry. *Analytical Chemistry* **2011,** *83*, 2286-2293.

[5] Dolores Morales, M.; Serra, B.; Guzman-Vazquez de Prada, A.; Julio Reviejo, A.; Manuel Pingarron, J., An electrochemical method for simultaneous detection and identification of *Escherichia coli*, *Staphylococcus aureus* and *Salmonella choleraesuis* using a glucose oxidase-peroxidase composite biosensor. *Analyst* **2007,** *132*, 572-578.

[6] Escamilla-Gomez, V.; Campuzano, S.; Pedrero, M.; Pingarron, J. M., Immunosensor for the determination of *Staphylococcus aureus* using a tyrosinase-mercaptopropionic acid modified electrode as an amperometric transducer. *Analytical and Bioanalytical Chemistry* **2008,** *391*, 837-845.

[7] Zelada-Guillen, G. A.; Riu, J.; Duezguen, A.; Rius, F. X., Immediate Detection of Living Bacteria at Ultralow Concentrations Using a Carbon Nanotube Based Potentiometric Aptasensor. *Angewandte Chemie-International Edition* **2009,** *48* (40), 7334-7337.

[8] Zelada-Guillen, G. A.; Bhosale, S. V.; Riu, J.; Xavier Rius, F., Real-Time Potentiometric Detection of Bacteria in Complex Samples. *Analytical Chemistry* **2010,** *82*, 9254-9260.

[9] Zelada-Guillen, G. A.; Luis Sebastian-Avila, J.; Blondeau, P.; Riu, J.; Xavier Rius, F., Label-free detection of *Staphylococcus aureus* in skin using real-time potentiometric biosensors based on carbon nanotubes and aptamers. *Biosensors & Bioelectronics* **2012,** *31*, 226-232.

[10] Ambrosi, A.; Bonanni, A.; Sofer, Z.; Cross, J. S.; Pumera, M., Electrochemistry at Chemically Modified Graphenes. *Chemistry-a European Journal* **2011,** *17*, 10763-10770.

[11] Hernandez, R.; Riu, J.; Bobacka, J.; Valles, C.; Jimenez, P.; Benito, A. M.; Maser, W. K.; Xavier Rius, F., Reduced Graphene Oxide Films as Solid Transducers in Potentiometric

All-Solid-State Ion-Selective Electrodes. *Journal of Physical Chemistry C* **2012,** *116*, 22570-22578.

[12] Cao, X.; Li, S.; Chen, L.; Ding, H.; Xu, H.; Huang, Y.; Li, J.; Liu, N.; Cao, W.; Zhu, Y.; Shen, B.; Shao, N., Combining use of a panel of ssDNA aptamers in the detection of *Staphylococcus aureus*. *Nucleic Acids Research* **2009,** *37*, 4621-4628.

[13] Hummers, W. S.; Offeman, R. E., Preparation of graphitic oxide. *Journal of the American Chemical Society* **1958,** *80*, 1339-1339.

[14] Valles, C.; David Nunez, J.; Benito, A. M.; Maser, W. K., Flexible conductive graphene paper obtained by direct and gentle annealing of graphene oxide paper. *Carbon* **2012,** *50*, 835-844.

[15] Robinson, J. T.; Perkins, F. K.; Snow, E. S.; Wei, Z.; Sheehan, P. E., Reduced Graphene Oxide Molecular Sensors. *Nano Letters* **2008,** *8*, 3137-3140.

[16] Jung, D. H.; Kim, B. H.; Ko, Y. K.; Jung, M. S.; Jung, S.; Lee, S. Y.; Jung, H. T., Covalent attachment and hybridization of DNA oligonucleotides on patterned single-walled carbon nanotube films. *Langmuir* **2004,** *20*, 8886-8891.

[17] Liu, J.; Li, Y.; Li, Y.; Li, J.; Deng, Z., Noncovalent DNA decorations of graphene oxide and reduced graphene oxide toward water-soluble metal-carbon hybrid nanostructures via self-assembly. *Journal of Materials Chemistry* **2010,** *20*, 900-906.

[18] Liang, Y.; Wu, D.; Feng, X.; Muellen, K., Dispersion of Graphene Sheets in Organic Solvent Supported by Ionic Interactions. *Advanced Materials* **2009,** *21*, 1679-1683.

UNIVERSITAT ROVIRA I VIRGILI
SOLID CONTACT POTENTIOMETRIC SENSORS BASED ON CARBON NANOMATERIALS
Rafael Hernández Malo

UNIVERSITAT ROVIRA I VIRGILI
SOLID CONTACT POTENTIOMETRIC SENSORS BASED ON CARBON NANOMATERIALS
Rafael Hernández Malo

The main conclusion of this thesis is the feasibility of using carbon-based nanostructured materials in solid state potentiometric electrodes. We report in this thesis the use of single-walled carbon nanotubes and chemically modified graphene for the detection of different types of analytes.

This main conclusion can be broken down into a set of specific conclusions from each of the items that make up this thesis.

The use of cyclic voltammetry and electrochemical impedance spectroscocy has demonstrated the mechanism used graphene-based materials in ISEs. Both carbon nanotubes and graphene-based materials have demonstrated a clear capacitive character (double layer capacitance) which agrees well with the structure and properties of these materials.

The rapid ion-to-electron transduction of carbon nanotubes and graphene-based materials in ISEs allows us to have close to real-time responses as we have shown in this thesis.

The easy use of carbon nanotubes and graphene-based materials allows a high reproducibility in ion-selective electrodes. Deposition methods used in this thesis are easy costless and allow highly reproducible series of electrodes. This process can be improved if the process is mechanised, avoiding thereby the different exposure times obtained by spray deposition, therefore avoiding a variation in the thicknesses of the transducer layer. For graphene-based materials deposition it has been found that drop casting offers an easy and highly reproducible deposition, thereby obtaining very thin layers of a few nanometers..

The applicability and versatility of carbon nanotubes is shown in the construction of a ISE for the detection os calcium in plant sap. The use of copper wire as conductive substrate, and the absence of redox reactions, reinforces the absence of the formation of a water layer between the conductive substrate and the transducer layer.

The use of graphene-based materials in potentiometric sensors improves the stability of the potentiometric signal. This is because the excellent electrochemical properties of graphene-based materials and also probably to the absence of metallic nanoparticles from the process of synthesis.

Classical ion-selective membranes used in ion-selective electrodes can be removed thereby creating membraneless potentiometric sensors for determining large analytes such as bacteria. In these sensors the sensing layer is directly attached (either in a covalent or in a non-covalent way) to the transducer layer.

The use of specific aptamers for *Staphylococcus aureus* has allowed the ultra-low detection of only one colony forming unit (CFU) in a very short time, largely improving the results of the aptasensors based on carbon nanotubes.

UNIVERSITAT ROVIRA I VIRGILI
SOLID CONTACT POTENTIOMETRIC SENSORS BASED ON CARBON NANOMATERIALS
Rafael Hernández Malo

UNIVERSITAT ROVIRA I VIRGILI
SOLID CONTACT POTENTIOMETRIC SENSORS BASED ON CARBON NANOMATERIALS
Rafael Hernández Malo

8.1. Glossary

Term used	Definition
3DOM	Three-dimensionally ordered macroporous carbon
ºC	Celsius degree
β_{IL}	Formation constant between ligand *L* and ion *i*
Ω	Ohm
ϑ	Chiral angle
Ø	Electrical potential
μ_i	Mobility of the specie i
µV	MicroVolt
µm	Micrometer (10^{-6} m)
µl	Microlitre
µF	MicroFarad
X^2	Average error
A	Adenine, Amper, Counter electrode
a_1, a_2	Unitary hexagonal cell lattice vectors
a_i	Activity of the specie i
a_i^{org}	Activity of the specie *i* in the organic phase
a_i^{aq}	Activity of the specie *i* in the aqueous phase
AAS	Atomic absorption spectroscopy
AFM	Atomic force microscopy
Ag	Silver element
AgCl	Silver chloride
AIBN	2,2-Azobis(2-methylpropionitrile)
C	Citosine, Capacitance (Farad, F), Coulomb
$C_{60, 540, 70}$	Buckminsterfullerene notation (70, 540 and 70 carbon atoms)
C_h	Chiral vector (Hamada vector)
Ca^{2+}	Calcium ion
$CaCl_2$	Calcium chloride
CECT	Colección Española de Cultivos Tipo
CFU	Colony forming unit
CGRE	Combined glass reference electrode
cm	Centimiter (10^{-2} m)
CMG	Chemically modified graphene

CNT	Carbon nanotube
CO_2	Carbon dioxide
CP	Conducting polymer
CPE_I	Interfacial constant phase element
CPE_B	Bulk constant phase element
Cu	Copper element
CV	Cyclic voltammetry
CWE	Coated wire electrode
DCM	Dichloromethane
dE	Potential differential
dec	Decade
DOS	Bis(2-ethylhexyl sebacate)
DMA	Decyl methacrylate
DMF	Dimethylformamide
DNA	Desoxiribonucleic acid
dt	Time differential
E^o	Standard potential
E_{const}	Sum of all sample-independent potential contributions
E_{dc}	Direct current potential
E_D	Diffusion potential
E_i^{EMF}	Measured potential for the specie i
E_J	Liquid junction potential
E_M	Membrane optential
E_{PB}	Boundary potential between inner solid contact and membrane
$E_{PB'}$	Boundary potential between membrane and sample
EDC	N-(3-dimethylaminopropyl)-N′-ethyl-carbodiimide hydrochloride
EIS	Electrochemical impedance spectroscopy
EMF	Electromotive force
ESEM	Environmental scanning electron microscopy
ETH129	N,N,N′,N′-Tetracyclohexyl-3-oxapentanediamide
eV	ElectronVolt
F	Faraday constant (96485 C·mol-1)
G	Guanine, gram
GC	Glassy carbon
GICs	Graphite intercalated compounds
GO	Graphene oxide

h	Hour
H_2O_2	Hydrogen peroxide
H_2SO_4	*Sulfuric acid*
HCl	*Chloridic acid*
HR-TEM	*High resolution transmission electron microscopy*
I	*Intensity (Amper, A)*
IDA	Isodecyl acrylate
IE	Indicator electrode
IUPAC	International Union of Pure and Applied Chemistry
ISE	Ion-selective electrode
ISM	Ion-selective membrane
IS-ISE	Internal solution ion-selective electrode
J	Joule
K	Kelvin degree
KCl	Potassium chloride
$KMnO_4$	Potassium permanganate
KTpClPB	Potassium tetrakis(p-chlorophenyl)borate
KTFPB	Potassium tetrakis[3,5-bis(trifluoromethyl)phenyl]borate
K_{ij}^{pot}	Selectivity coefficient
KHz	KiloHertz
kV	KiloVolt
L	Ionophore, litre
LiAcO	Lithium acetate
LOD	Limit of detection
M	Molar (mols/litre)
MΩ	MegaOhm
MES	2-(N-morpholino) ethane sulfonic acid
mg	Miligram (10^{-3} g)
$MgCl_2$	Magnesium chloride
MBA	Methyl butyl acrylate
mHz	MiliHertz
min	Minute
ml	Mililiter
mm	Milimiter (10^{-3} m)
mM	Milimolar
MMA	Methyl methacrylate

mV	millivolt (10^{-3} V)
MWCNTs	Multi-walled carbon nanotubes
n	Length of ssDNA/RNA chain (number of nucleic acids)
n,m	Integers for the determination of chirality and diameter of CNT
nA	NanoAmper
NaCl	Sodium chloride
$NaNO_3$	Sodium nitrate
NaHFPB	Sodium tetrakis[3,5-bis(1,1,1,3,3,3-hexafluoro-2-methoxy-2-propyl)-phenyl] borate trihydrate
NaTPB	Sodium tetraphenylborate
nBA	n-butyl acrylate
NH_3	Amonia
NHS	N-hydroxysuccinimide
nm	Nanometer (10^{-9} m)
NO_2	Nitrogen dioxide
O_2	Oxygen
o-NPOE	o-nitrophenyl octyl ether
P	Lipophilicity
PAHs	Polycyclic aromatic compunds
PANI	Polyaniline
PBS	Phosphate buffered saline
PCR	Reaction chain polymerasa
PEDOT	Poly(3,4-ethylenedioxithiophene)
PET	Positron emission tomography
pH	Decimal logarithm of the reciprocal hydrogen ion activity
POT	Poly(3-octylthiophene)
PPy	Polypyrrole
PVC	Poly(vinyl) chloride
R	Universal gas constant (8.314 J·K-1·mol-1), Resistance (Ohm, Ω)
R^+	Lipophilic cationic salt
R-	Lipophilic anionic salt
R_1, R_2	Ramifications
R^2	Correlation coefficient
R_S	Solution resistance
R_{ct}	Charge-transfer resistance
RE	Reference electrode

RGO	Reduced graphene oxide
RNA	Ribonucleic acid
rpm	Revolutions per minute
s	Second, standard deviation
sccm	square cubic centimetre (cm^3)
SCE	Solic contact electrode
SC-ISE	Solid contact ion-selective electrode
SELEX	Systematic evolution of ligands by exponential enrichment
SEM	Scanning electron microscopy
SD_{Noise}	Standard deviation of instrumentation noise
ssDNA	Single-stranted desoxiribonucleic acid
SWCNT	Single-walled carbon nanotubes
T	Absolute temperature - Timine
TDDMACl	tridodecylmethylammonium
TDDACl	tetradodecylammonium chloride
TEM	Transmission electron microscopy
T_g	Transition temperature
THF	Tetrahydrofuran
TSA	Tryptic soy agar
TSB	Tryptic soy broth
TYB	total Youden blank
V	Volt
W	Working electrode
XPS	X-ray photoelectron spectroscopy
XRD	R-ray difraction
z_i	Charge of the specie i

UNIVERSITAT ROVIRA I VIRGILI
SOLID CONTACT POTENTIOMETRIC SENSORS BASED ON CARBON NANOMATERIALS
Rafael Hernández Malo

8.2.Complementary information of chapter 5

8.2.1. Characterization of GO and RGO films

8.2.1.1. Graphene Oxide

Water dispersions of graphene oxide (GO) with a concentration of 0.3 mg/mL contain GO flakes comprised of few-layered GO sheets with 2 to 10 individual graphene layers with a majority of 4. Flake sizes typically range from 200 nm to 800 nm **[1]**.

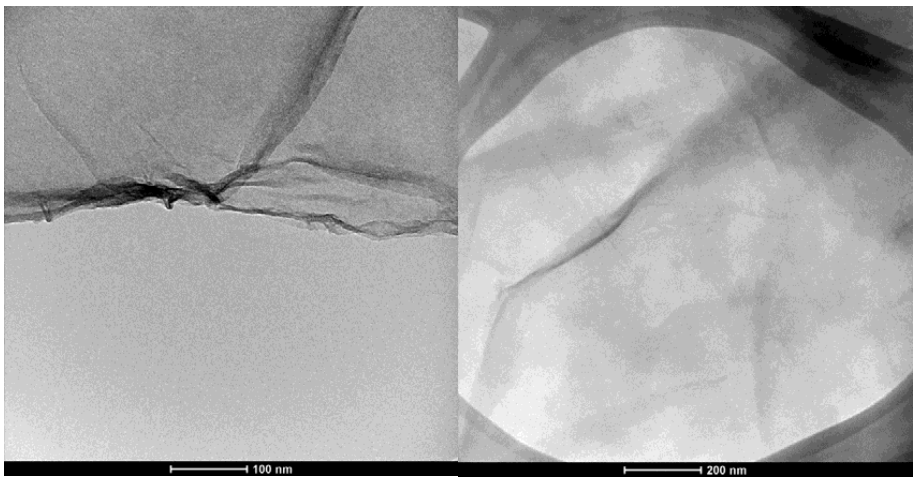

Figure 8.2.1. HRTEM images of graphene oxide

8.2.1.2. Aqueous graphene oxide dispersions

Homogeneous aqueous GO dispersions of a concentration of 0.3 mg/mL were dropcasted (controlled volumes of 15 µL) onto clean and polished glassy carbon (GC) surface electrodes. Once dried, the process is successively repeated to obtain films of controlled thickness. Thicknesses of the resulting GO films were measured by confocal microscopy. Values are summarized in Table 8.2.1. Film thickness scales well with the deposited volume as shown in Figure 8.2.1. This underlines the important processing advantage of GO for fabricating in a reproducible way films of defined thickness covering homogeneously the underlying GC electrode.

Table 8.2.1. Thicknesses of deposited GO films for different volumes of drop-casted aqueous GO dispersions as measured by confocal microscopy.

Drop-casted volume (µl)	*Thickness of drop-casted GO films (nm)*
15	125
60	460
150	1460

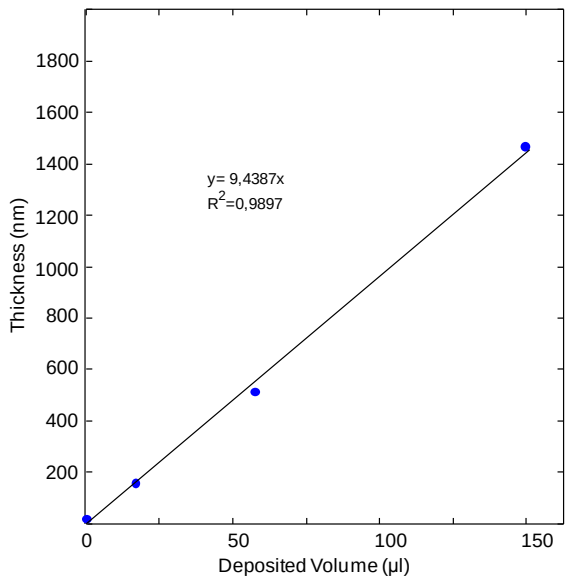

Figure 8.2.2. Film thickness calibration curve

It also can be seen that in order to obtain films with thickness of a few nm only, either very small volumes in the range of 0,5 µL, or highly diluted GO dispersions of concentrations in the range of 0.01 mg/mL (maintaining minimum deposited volume of 15 µL) have to be used.

A corresponding deposition experiment was additionally carried out using 15 µL of a highly diluted GO dispersion with a concentration of 0,01 mg/mL. This should lead to GO films of nominal thickness of 5 nm. However, only deposits comprised of a few isolated GO islands on GC were obtained. A continuous coverage of the glassy carbon electrode at such diluted concentrations could not be obtained, thus leaving large parts

of the underlying GC electrode uncovered. Thus, in order assure homogeneous coverage of the 3 mm diameter GC electrode concentrations of GO dispersion in the order of 0.3 mg/mL deposited in volumes of 15 4L should be used. When successively drop-casted, films of defined thicknesses are obtained, underlining the ease for a reliable film fabrication.

Figure 8.2.3 shows SEM images for the GO films of (a) 125 nm , (b) 460 nm and (c) 1460 nm thickness drop-casted on GC electrodes. For all cases, the GC electrodes are fully covered. However, the thicker the films, the smoother the surface and less agglomerates are visible.

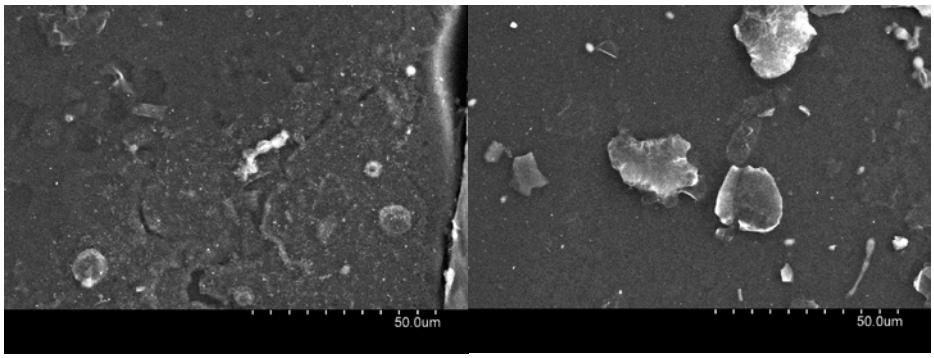

Figure 8.2.3 (a). SEM images for GO films of 125 nm thickness. Top: Coating near the border of the GC electrode. Bottom: coating in the middle of the GC electrode. Visible flakes are larger agglomerates on top of the GO coating.

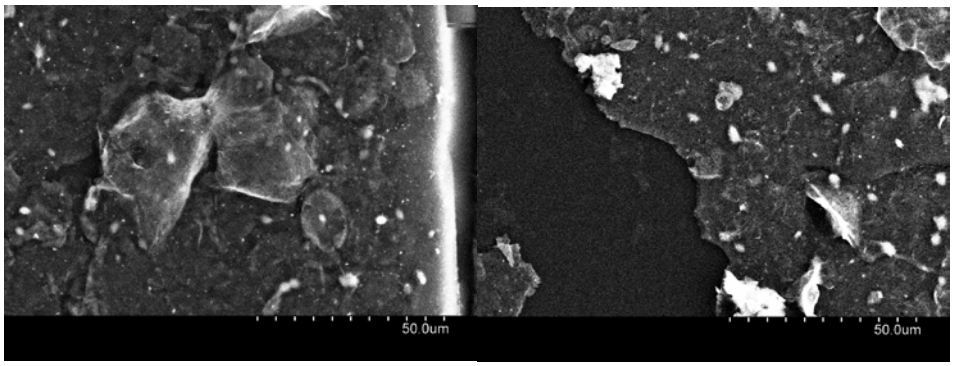

Figure 8.2.3 (b). SEM images for GO films of 460 nm thickness. Top: Coating near the border of the GC electrode. Bottom: Coating in the middle of the GC electrode near an artificial scratch. Larger agglomerates still visible, but surface smoother than for 100 nm thick films

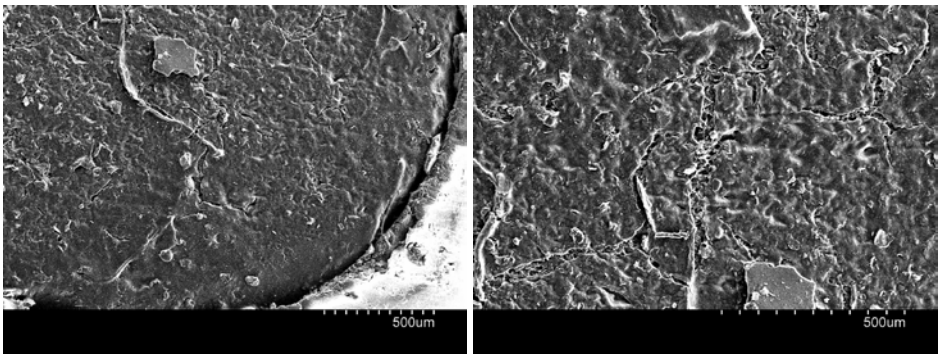

Figure 8.2.3 (c). SEM images for GO films of 1460 nm thickness. Top: Coating near the border of the GC electrode. Bottom: Coating in the middle of the GC electrode. Only very few agglomerates are visible on top of a smooth and homogeneous coating.

Figure 8.2.4 shows AFM images for RGO films (GO films after applying the reduction process) on GC electrode. Again, it can be seen, that the films with a thickness of 127 nm is characterized by a larger number of agglomerates on top of the GC electrode coverage than the thicker films, where almost no agglomerates are visible and which produce a more homogeneous and smoother coating. The surface roughness for the 1460 nm thick film is about 30 nm.

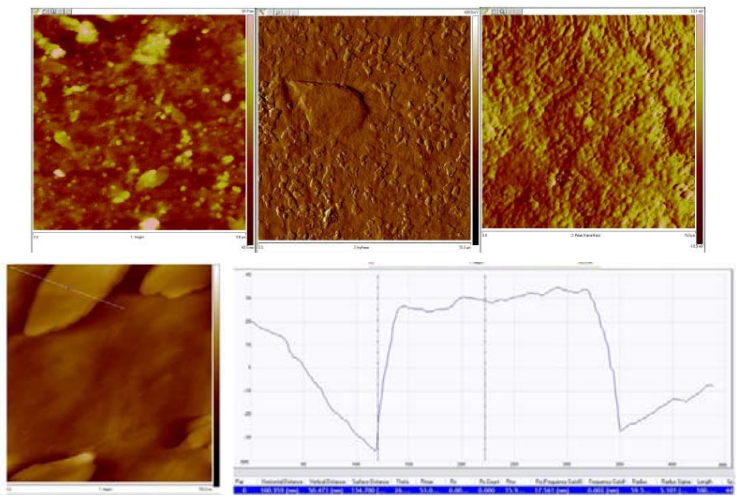

Figure 8.2.4. AFM images of RGO films on glassy carbon electrodes. Top Films with thicknesses of 125 nm, 460 nm and 1460 nm (from left to right). Bottom. Height profile taken for the 1460 nm film exhibiting a surface roughness of about 30 nm.

8.2.1.3. X-ray photoelectron spectroscopy (XPS) of RGO

The chemical composition of the prepared RGO material was analyzed by XPS. The resulting C1s core electron spectrum is depicted in Figure 8.2.5. Deconvolution reveals the presence of C-C bounds at 288,2 eV, various types of oxygen functionalities C-O, C=O and O-C=O moieties at 285,8 eV, 287,5 eV and 289,5 eV, respectively. Additionally, CN functional moieties are observed at 284.6 eV. The quantified atomic percentages for C, O and N correspond to 88,36 at. %, 10,19 at. % and 1,45 at. % as listed in Table 8.2.2.

The oxygen functional groups in RGO are remaining from the starting GO material, while nitrogen groups originate from both, the use of $NaNO_3$ in the preparation of GO as well as the use of hydrazine monohydrate vapors in the reduction process. Similar nitrogenated carbon signals in hydrazine treated GO have been previously observed by Stankovich et al **[2]** from their analysis of GO reduced in hydrazine solutions. Most interestingly, the appearance of the π-π contribution in the XPS spectrum at 291.6 eV, not observable in the starting GO material, indicates first hints for the restoration of carbon sp2 character upon reducing GO to RGO. This opens new conducting pathways which are characteristic for the recovery of the electrical conductivity in RGO **[1-3]**.

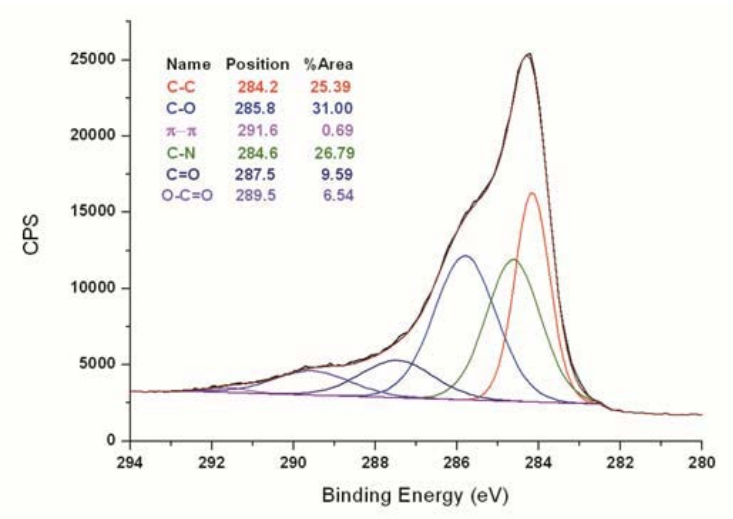

Figure 8.2.5. C1s core electron XPS of as prepared RGO

Table S1. Results of XPS analysis of as prepared RGO

Element	*Atomic %*
C	88.36
O	10.19
N	1.45

8.2.2. Characterization of GO and RGO films

[1] Valles, C.; David Nunez, J.; Benito, A. M.; Maser, W. K., Flexible conductive graphene paper obtained by direct and gentle annealing of graphene oxide paper. *Carbon* **2012,** *50* (3), 835-844.

[2] Stankovich, S.; Dikin, D. A.; Piner, R. D.; Kohlhaas, K. A.; Kleinhammes, A.; Jia, Y.; Wu, Y.; Nguyen, S. T.; Ruoff, R. S., Synthesis of graphene-based nanosheets via chemical reduction of exfoliated graphite oxide. *Carbon* **2007,** *45* (7), 1558-1565.

[3] C. Mattevi, G. Eda, S. Agnoli, S. Miller, K.A. Mkhoyan, O. Celik et al., Adv. Func. Mater. 2009, **19,** 2577.

8.3. Complementary information of chapter 6

8.3.1. Reagents and apparatus

Graphene powder, sodium nitrate, sulphuric acid, potassic permanganate, hydrazine hydrate, N-hydroxysuccinimide (NHS), 2-(N-morpholino) ethanesulfonic acid (MES) and N-(3-dimethylaminopropyl)-N′-ethylcarbodiimide hydrochloride (EDC) were purchased from Sigma-Aldrich. Aqueous solutions were prepared with freshly deionized water (18,2 MΩ·cm specific resistance) obtained with a Milli-Q PLUS reagent-grade water system (Millipore). Sand papers and alumina were obtained from Buehler. Glassy carbon rods 3 mm diameter was purchased from HTW GmbH. *Staphylococcus aureus* binding aptamer SA20 with the sequence 5'-GCAAT GGTAC GGTAC TTCCG CGCCC TCTCA CGTGG CACTC AGAGT GCCGG AAGTT CTGCG TTATC AAAAG TGCAC GCTAC TTTGC TAA-3' modified in the 3′ end with a 3C spacer followed by a pyrene cap phosphoramidite was purchased from Eurogenetec (London, UK). The same company provide the *Staphylococcus aureus* binding aptamer SA31 with the sequence 5'-GCAAT GGTAC GGTAC TTCCT CCCAC GATCT CATTA GTCTG TGGAT AAGCG TGGGA CGTCT ATGAC AAAAG TGCAC GCTAC TTTGC TAA-3′ modified in the 3′ end with a 6C spacer and an amine moiety (-$(CH2)_6$-NH_2). Aliquots of aptamers were obtained and stored in the refrigerator at -80ºC until use.

Lyophilized strains of *Staphylococcus aureus* (CECT 4630), *Lactobacillus casei* subsp. *Casei* (CECT 4180) and *Escherichia coli* (CECT 4558) were purchased from Colección Española de Cultivos Tipo (Valencia, Spain). All the potentiometric measurements were done using a Keithley high imput impedance voltmeter M6514 (London, UK) in a thermostatized 20 ml flask (22,0 ± 0,5ºC). High-resolution transmission electronic (HR-TEM) images were taken on a FEI Tecnai G2 20 microscope. Confocal microscopy LEICA Dual Core 3D measuring Microscope 3D equipment was used to control the thickness of graphene depositions. Atomic force microscope (AFM) images were obtained with a Multimode8 microscope with control electronics Nanoscope V (Bruker). A high input impedance electrometer 6514 from Keithley was used for potentiometric measurements. All the experiments were done at room temperature (22,0±0,1ºC) in a bath from Polyscience (ref.9106) with the same double-junction Ag/AgCl/ 3 M KCl reference electrode (type 6.0729.100, Methrom AG) containing a 1 M LiAcO electrolyte bridge.

The same cell was used for the measurements in all the experiments in order to ensure that each experiment was carried out under the same conditions. X-Ray photoelectron spectroscopy (XPS) was carried out on an ESCAPlus Omicron spectrometer using a monochromatized Mg X-ray source (1253.6 eV). XPS data were analyzed using the CasaXPS software.

8.3.2. Culture conditions

All bacteria strains were cultivated under the same experimental conditions, including incubation time and temperature. The bacteria lyophiles were stored at -20 °C in glycerol/TSB medium (10% v/v) and reactivated by incubating the bacteria in 10 mL of sterile TSB at 37 °C for 24 h. The bacteria samples were then centrifuged at 6000 rpm for 15 minutes and the supernatant was discarded. The precipitate was successively washed with PBS 1.7 mM pH 7.4 following the same centrifugation conditions previously mentioned. The pellet was finally resuspended in sterile PBS 1.7 mM pH 7.4. The resulting solution (namely 100 solution) was sixth-fold 1:10 diluted serially to give a series of 10-1 to 10-6 stock solutions of bacteria. The stock solutions were quantified in quintuplicate using the standard plate count method (Gerhardt et al., 1981) in TSA and the same procedure was also applied to the standardization of the variable aliquots of stock solutions that were used to inoculate the samples to be analyzed. The bacteria concentration was measured in colony-forming units (CFU)/mL.

8.3.3. Characterization of GO and RGO films

Water dispersions of graphene oxide (GO) with a concentration of 0.3 mg/mL contain GO flakes comprised of few-layered GO sheets with 2 to 10 individual graphene layers with a majority of 4. Flake sizes typically range from 200 nm to 800 nm (figure 8.3.1).

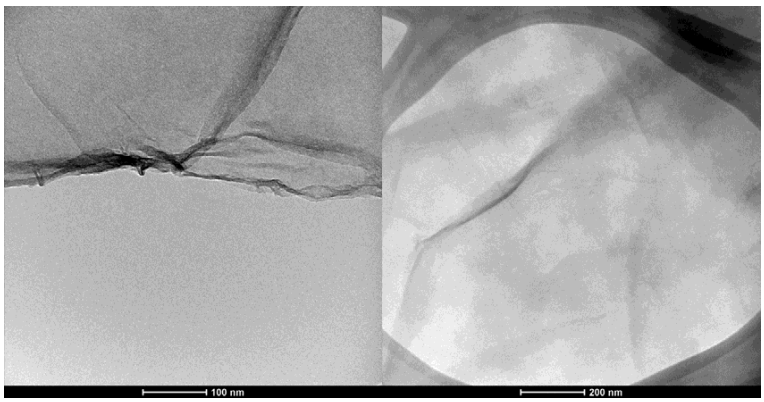

Figure 8.3.1. HRTEM images of graphene oxide

Figure 8.3.2 shows AFM images for RGO films over the GC electrode. The films present almost no agglomerates with a homogeneous and smooth coating. The surface roughness is about 30 nm.

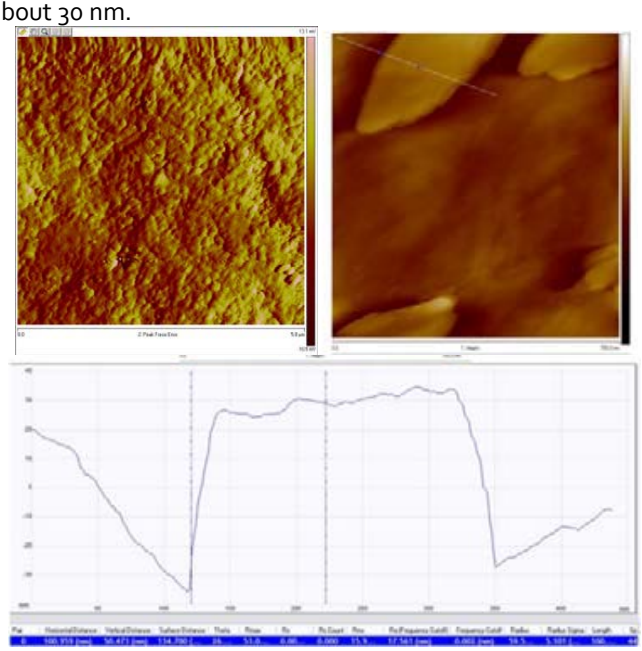

Figure 8.3.2. AFM images of RGO films on glassy carbon electrodes (left). Height profile taken exhibiting a surface roughness of about 30 nm (right).

8.3.4. X-ray photoelectron spectroscopy (XPS) of RGO

The chemical composition of the prepared RGO material was analyzed by XPS. The resulting C1s core electron spectrum is depicted in figure 8.3.3. Deconvolution reveals the presence of C-C bounds at 288,2 eV, various types of oxygen functionalities C-O, C=O and O-C=O moieties at 285,8 eV, 287,5 eV and 289,5 eV, respectively. Additionally, C-N functional moieties are observed at 284.6 eV. The quantified atomic percentages for C, O and N correspond to 88,36 at. %, 10,19 at. % and 1,45 at. %. The oxygen functional groups in RGO are remaining from the starting GO material, while nitrogen groups originate from both, the use of $NaNO_3$ in the preparation of GO as well as the use of hydrazine monohydrate vapors in the reduction process Most interestingly, the appearance of the π-π contribution in the XPS spectrum at 291,6 eV, not observable in the starting GO material, indicates first hints for the restoration of carbon sp^2 character upon reducing GO to RGO.

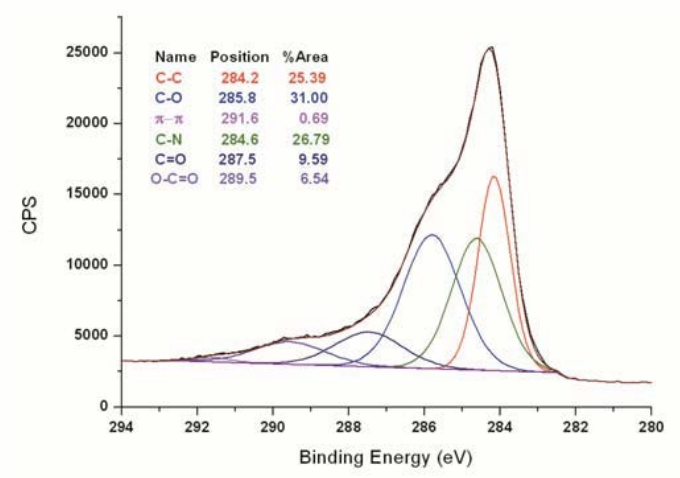

Figure 8.3.3. C1s core electron XPS of as prepared RGO

8.3.5. References

[1] Gerhardt, P.; Murray, R. G. E.; Costillow, R. N.; Nester, E. W.; Wood, W. A.; Krieg, G. B., *Manual of methods for general bacteriology*. **1981**.

8.4. Scientific contributions

8.4.1. Journal articles

- *Determination of calcium ion in sap using carbon nanotube-based ion-selective electrodes*. Hernández, R.; Riu, J.; Rius, F.X. **Analyst,** 2010, 135, 1979-1985.

- *Reduced Graphene Oxide Films as Solid Transducers in Potentiometric All-Solid-State Ion-Selective Electrodes.* Hernández, R.; Riu, J.; Bobacka, J.; Valles, C.; Jimenez, P.; Benito, A. M.; Maser, W. K.; Rius, F.X.**Journal of Physical Chemistry C,** 2012, 116, 22570-22578.

- *Graphene-based potentiometric biosensor for the immediate detection of living bacteria.* Hernandez, R.; Vallés C.; Benito A. M.; Maser W. K. M.; Rius, F.X.; Riu J. **Biosensors & Bioelectronics,** 2014, 54, 553-557.

8.4.2. Congress contributions

- *"Investigation of Casimir/van der Waals forces between CNTs/NWs and a patterned Si/SiO_2 substrate"*. Aline Ribayrol, Gabriela Conache, Rafael Hernández, Jordi Riu, Linus Fröberg, Ralf Jede, Ulrich Schmucker, Mikhail Zubtsov, Michael Bordag, Hakan Pettersson, Lars Montelius. **Oral communication at the International Conference on Nanoscience and Nanotechnology (ICN+T) 2006**. Abstracts book ICN+T 2006. Basel (Switzerland). 2006

- *"An optoelectronic device based on photoresistive proteins attached to vertically aligned carbon nanotubes"*. Rafael Hernandez Malo, Jordi Riu Rusell, F. Xavier Rius Ferrús. **Poster at the 1st Workshop Nanociencia y Nanotecnología Analíticas**. Abstracts book 1st NyNA. Cordoba (Spain). 2007.

- *"Determinación in-situ de calcio en savia de plantas"*. Rafael Hernandez Malo, Jordi Riu Rusell, F. Xavier Rius Ferrús. **Poster at the 2nd Workshop Nanociencia y Nanotecnología Analíticas**. Abstracts book 2nd NyNA. Tarragona (Spain). 2008.

UNIVERSITAT ROVIRA I VIRGILI
SOLID CONTACT POTENTIOMETRIC SENSORS BASED ON CARBON NANOMATERIALS
Rafael Hernández Malo

Þú munt ná áfangastað þó ferðast rólega
-You will reach your destination, although travel slowly-
(Icelandic proverb)